N O T I C E

THIS DOCUMENT HAS BEEN REPRODUCED FROM
MICROFICHE. ALTHOUGH IT IS RECOGNIZED THAT
CERTAIN PORTIONS ARE ILLEGIBLE, IT IS BEING RELEASED
IN THE INTEREST OF MAKING AVAILABLE AS MUCH
INFORMATION AS POSSIBLE

✦SPERRY
FLIGHT SYSTEMS

NASA CR- 166796

PRELIMINARY DESIGN FOR
A ZERO GRAVITY
TEST FACILITY (ZGTF)

VOLUME I   TECHNICAL

SPERRY
FLIGHT SYSTEMS

PRELIMINARY DESIGN FOR A ZERO GRAVITY TEST FACILITY (ZGTF)

VOLUME I TECHNICAL

PREPARED BY

AL GERMAIN
SPERRY FLIGHT SYSTEMS
21111 N. 19TH AVE
PHOENIX, ARIZONA 85027

PREPARED FOR

GODDARD SPACE FLIGHT CENTER
GREENBELT, MARYLAND 20771

PREFACE

This report describes the preliminary design of a Zero Gravity Test Facility (ZGTF) for testing High-Gain Antenna Systems (HGAS). The work was done at Sperry Flight Systems, Phoenix, Arizona, under the supervision of Mr. Richard Van Riper, Space Pointing Systems Department Head and Mr. Mike Maurice, System and Software Development Section Head. Messrs. George Stocking, Crockett Ellis, Jim Wilson, Bob Touchberry, and Dr. George Wilson provided valuable guidance in the design. The work was performed between February and July 1981 in fulfillment of the Contract No. NAS5-26479.

The report is presented in two parts: Volume I, Technical, and Volume II, Development Plan and Cost Estimate (proprietary).

TABLE OF CONTENTS

TABLE OF CONTENTS (cont)

LIST OF ILLUSTRATIONS

LIST OF ILLUSTRATIONS (cont)

LIST OF TABLES

SECTION 1.0

INTRODUCTION

SECTION 1.0

INTRODUCTION

SECTION 1.0

INTRODUCTION

1.1 GENERAL

This report describes the work done for the preliminary design of a Zero Gravity Test Facility (ZGTF), NASA Contract No. NAS5-26479. The major project objectives were to define the functional requirements and develop the best conceptual design for a test facility that simulates weightless operating conditions for a High-Gain Antenna Systems (HGAS), that will broadcast to the Tracking Data Relay Satellites (TDRSS). The typical HGAS defined for this project is mounted on a low earth-orbiting satellite, and consists of an antenna with a double-gimbal pointing system mounted on a 13-foot-long mast. Typically, the gimbals are driven by pulse-modulated dc motors or stepper motors. These drivers produce torques on the mast, with jitter that excites the satellite and may cause disturbances to sensitive experiments.

The facility objectives as defined by the Statement of Work are:

- Verification of the dynamic properties of the antenna support structure (mast), including flexible mode characteristics.

- A good practical estimate of the torque profile induced on the spacecraft by motion of the high-gain antenna.

- Verification of gain and phase margins of the servo control loop of the gimbal drive electronics.

- An indication of tracking performance (pointing verification).

The facility proposed in this report should meet all of these objectives.

Although this facility was designed specifically for testing High-Gain Antenna Systems, it can also be used for testing other satellite mechanisms under simulated weightlessness. Examples of such mechanisms are telescope mirrors, solar panels, or deployed antennas. The major requirements are that the supported mechanism operates within the weight and speed limitations of the facility, and that the mechanism can be supported from above at a single point.

1.2 SYSTEM REQUIREMENTS

Part of the preliminary design effort was to define the performance requirements and test item parameters for the ZGTF. This involved gathering data representative of high-gain antenna systems expected to be tested on the ZGTF, and listing their worst-case parameters. The test facility performance requirements were derived from the type of tests to be performed, the test item parameters, and the allowable error to be introduced by the facility on the test item during testing.

Two antenna pointing systems that represented the expected test design extremes were used to define the requirements. These were the Landsat high-gain antenna and the Space Telescope (ST) antenna system. The ST antenna system is a lightweight approach that uses the antenna mast as a waveguide tube to send the RF signals between the electronics at the base of the mast and the antenna and gimbals at the top of the mast. The gimbal drives use brushless dc motors to rotate the antenna in two directions perpendicular to the axis of the mast.

The Landsat antenna system is a heavy system with the radio and gimbal control electronics located at the top of the mast. The gimbals are driven by stepper motors around the axis of the mast, and up and down in elevation. The pertinent parameters for these antenna systems are listed in Table 1-1. The facility requirements for testing these antenna systems are listed in Table 1-2.

There was some question whether the Wide-Angle Test Fixture (WATF) built at Sperry for testing the ASPS Gimbal System (AGS) would be practical or available for testing the HGASs. The WATF is not high enough to allow testing with a 13-foot mast on the test item. The drive mechanisms on the WATF do not possess the required positional accuracy to meet the applied torque error requirement (1 ounce-inch). Finally, the WATF will be committed almost full time to testing the AGS once the test program is started and will therefore be unavailable to other programs during that time.

TABLE 1-1
ZERO GRAVITY TEST FACILITY ITEM PARAMETERS

Pointing system gimbal loop bandwidth - 1 Hz maximum

Payload gimbal weight - 200 pounds maximum (45 pounds typical)

Mast weight - 0 to 150 pounds

Gimbal - payload cg offset - 2 feet, maximum

Gimbal travel arc - ±115 degrees

Mast length - 13.5 feet maximum

Gimbal slew rate - 30 degrees per minute (8.7×10^{-3} radians per second, maximum

Dummy payload cg travel rate - .21 inches per second, maximum

Mast bending mode - 5 to 6 hertz (typically very rigid)

TABLE 1-2
ZERO GRAVITY TEST FACILITY REQUIREMENTS

● Simulate zero gravity operation for gimbals and antenna mass

● Allow verification of the structural and control dynamics of the pointing system

● Allow gimbal angles as large as possible with a goal of 90 degrees

● Measure all forces and torques at the base of the pointing system mast to 1 percent accuracy

● Apply less than 1 oz-in. of torque to the gimbals (or 5 percent of maximum gimbal torque)

● Allow no Facility structural modes or control loop resonances that interfere with pointing system measurements

SECTION 2.0

TRADEOFF

SECTION 2.0

TRADEOFF

Several candidate methods for meeting the test requirements were considered for the ZGTF. All of the best candidates were based on tests that were conducted at Sperry for antenna pointing systems over the past several years.

2.1 COUNTERBALANCE METHOD

A sketch of the ZGTF counterbalance method is shown in Figure 2-1. The antenna system is suspended upside down from a test structure. The antenna mass is simulated by a set of counterweights attached to the gimbals. The counterweights reproduce the antenna moments of inertia, with the center of mass of the gimbal-counterweight combination going through each gimbal. To avoid overloading the mast, the weight of the gimbals and counterweights is suspended by cables driven by servomotors at a constant force. As in all of the methods, the mast is bolted to an instrumented base for measuring forces and torques transmitted by the antenna system during operation. This method introduces inaccuracies in the antenna system from the mass of the suspension cables, which interfere with the mast dynamics and the counterbalance weights. The counterbalance weights produce high loads on the gimbal bearings, and do not model the effect of the offset center of mass of the real antenna on gimbal dynamics. The counterweights interfere with each other and the gimbals, over a range of gimbal angles, preventing full gimbal rotation to all locations. Sperry's experience has shown that locating the counterweights for balancing during test setup is a tedious process.

The major advantage of this method is that it is relatively inexpensive.
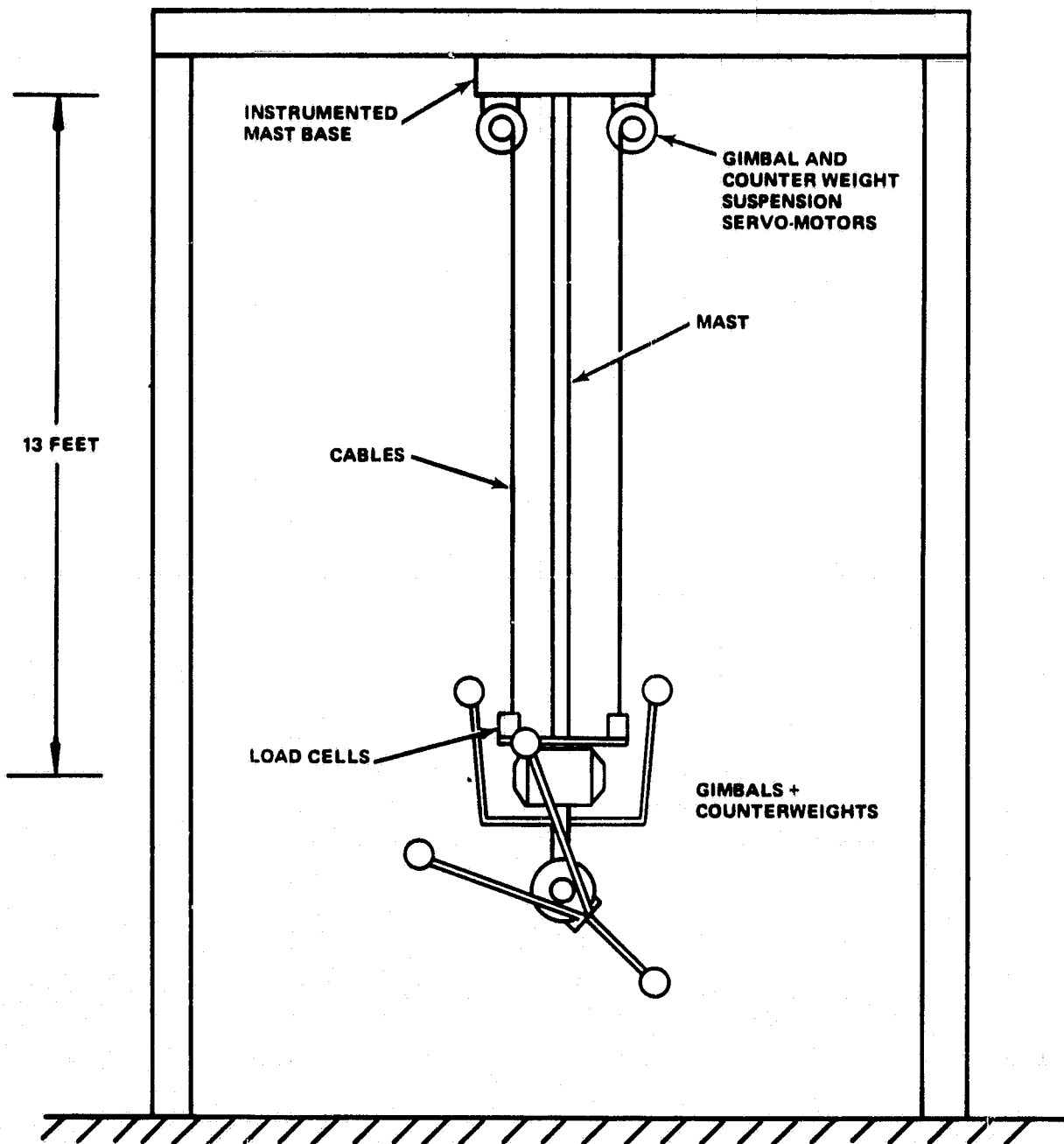
Figure 2-1
ZGTF Counterbalance Method

2.2 WATF DERIVATIVE METHOD

This concept (Figure 2-2) is based on Sperry's Wide-Angle Test Fixture (WATF) used for testing the ASPS Gimbal System (AGS) to be used for Shuttle Orbiter pointing missions.

The antenna system is mounted upright, with the dummy antenna and upper gimbal supported by a cable that is controlled at a constant force level, but is free to wind and unwind on its spool. The cable drive is mounted on a carriage which moves in two perpendicular directions horizontally (X and Y), and is controlled to stay directly above the antenna suspension point. The cable remains vertical at all times. A tower supports the X-Y drive carriage 8 to 10 feet above the antenna gimbals to provide enough cable length to reduce the errors induced by the suspension to a negligible amount. The method requires very precise position and force sensors for the X, Y, and Z control loops. The ZGTF control loops must also have bandwidths that are higher than the pointing system control bandwidths.

Gimbal angle travel is limited to less than 90 degrees. For reference, the WATF gimbal angle limit is 60 degrees. This concept allows functional testing of the antenna system structure under simulated zero-gravity conditions at any allowable gimbal angle. It produces near-zero torque about each of the three gimbal axes. Some radial load remains on the gimbal bearings. The tower for the WATF derivative is the tallest of the four concepts, requiring higher than normal laboratory ceiling height and careful design to ensure that the tower modal frequencies are higher than the test item frequencies.
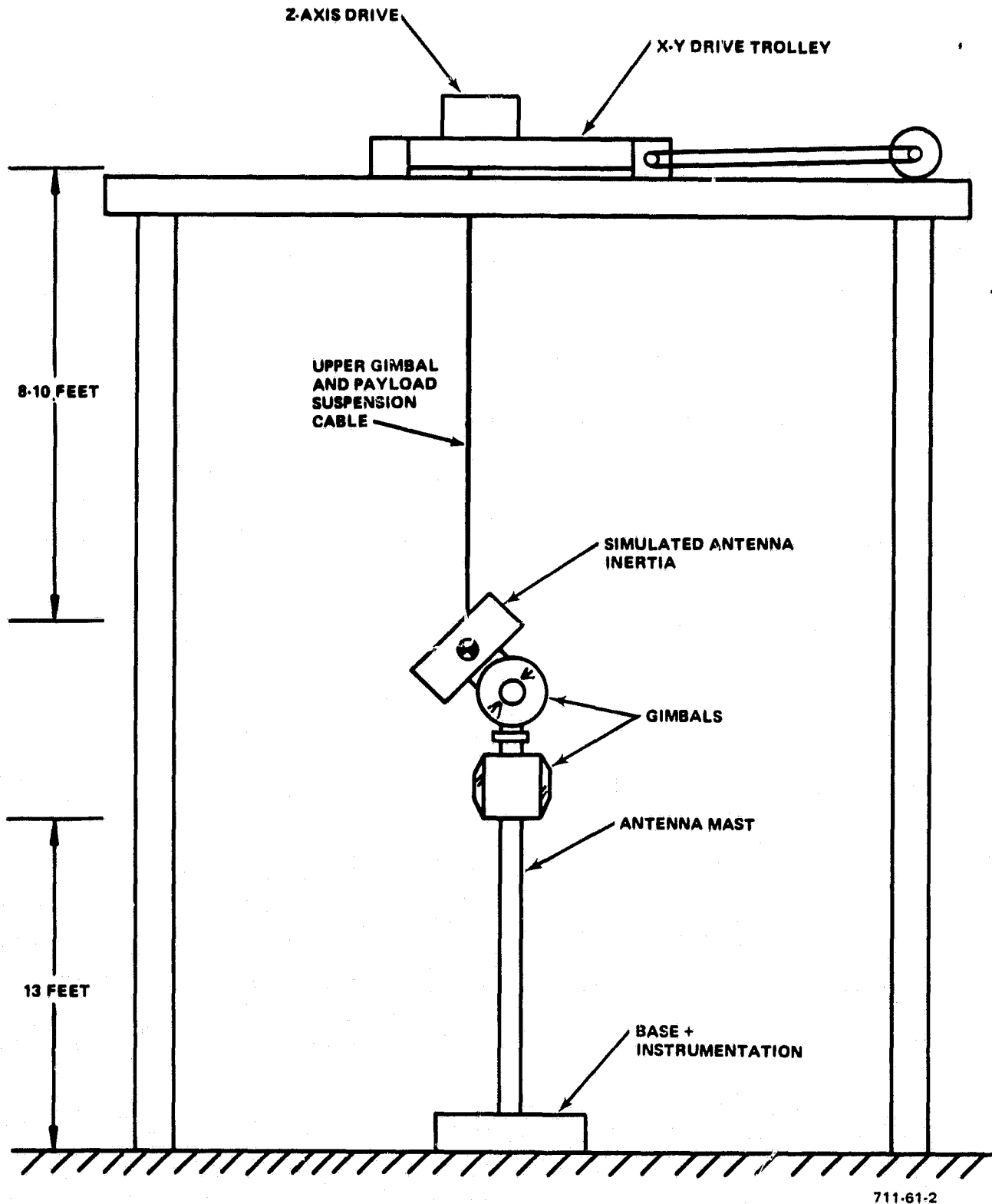
Figure 2-2
Wide-Angle Test Fixture Concept for a Zero Gravity Test Facility

2.3 UPSIDE-DOWN WATF DERIVATIVE

Another WATF derivative concept (Figure 2-3) places the X, Y, and Z drives at the base of the tower, with the antenna system mounted upside down. The constant vertical force is transmitted through a pivoting link from a linear actuator on the drive carriage to the dummy antenna mass, with the link remaining vertical at all times. The description of the WATF derivative concept also applies to this concept except that the tower for the upside down WATF is shorter. A major problem with this method is ·the inherent instability of the control loops for the dummy mass suspension. The problem is analogous to balancing a weight on the tip of a pencil on the palm of your hand while another person pushes on the weight (Figure 2-4). This test method was expected to be the most expensive.

2.4 AIR-BEARING SUSPENSION

A concept that uses an air bearing to support the weight of the dummy antenna and gimbals was developed, based on a test run at Sperry on the Solar Max Mission High-Gain Antenna System. A sketch of the concept is shown in Figure 2-5.

The mast base is clamped to a track on a concrete pillar, allowing the mast to be tilted to any angle up to 90 degrees from horizontal. The dummy antenna weight is floated on an air bearing, which allows it to pivot about one gimbal axis in the horizontal plane only. The surface plate is mounted on rollers to allow it to be positioned closer to the concrete pillar as the mast is tilted up from horizontal.

Theoretically, the air bearing should allow nearly frictionless motion about one gimbal axis and produce no load on the gimbal bearings. However, closer analysis shows that errors are introduced to the structural dynamics tests in the form of extraneous forces on the mast and torques on .the gimbals. Because of the frictionless nature of the air bearings, the surface plate must be very level to avoid torques on the gimbals caused by the dummy mass and bearing "sliding downhill" around the gimbal axis.
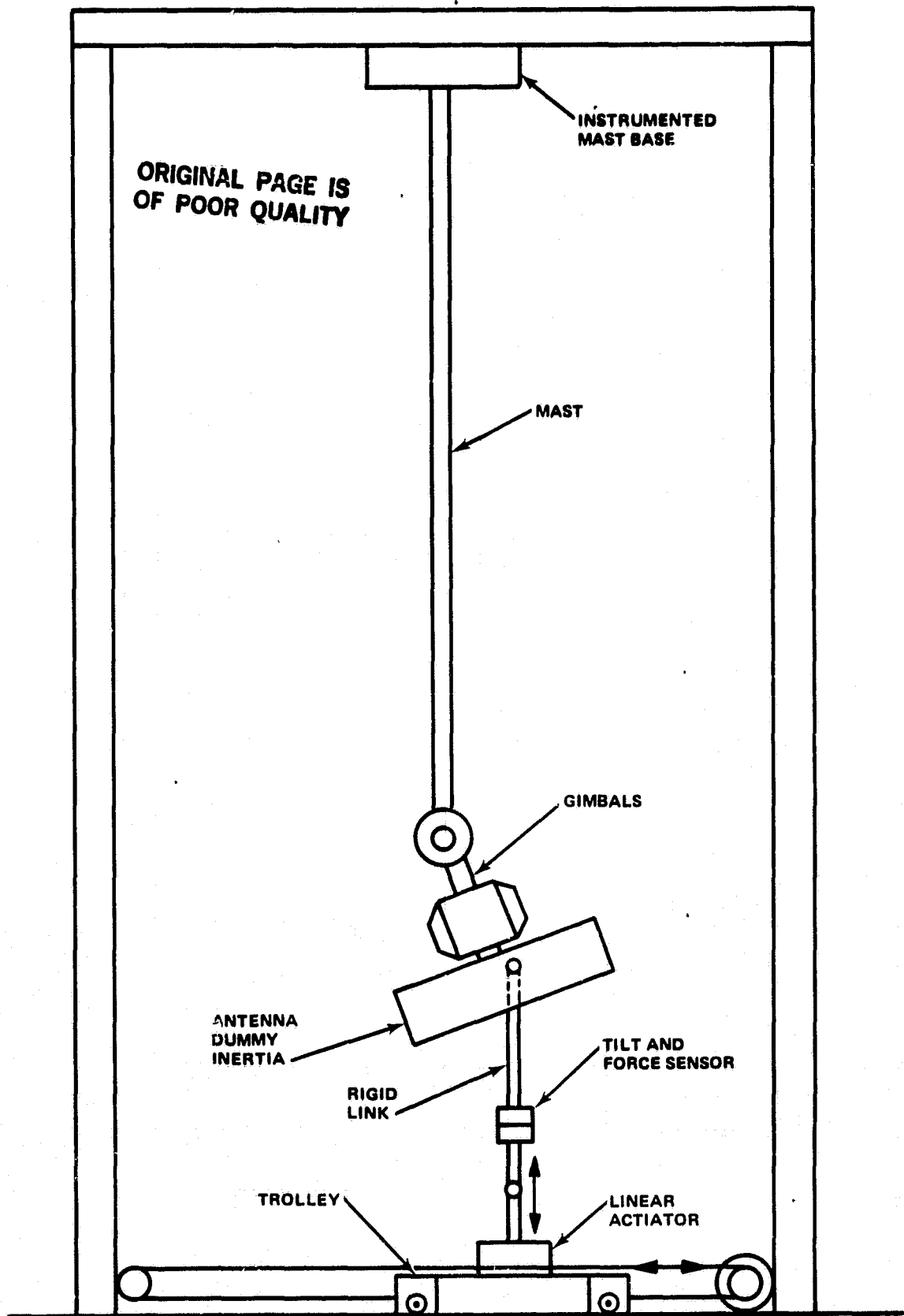
Figure 2-3
Upside-Down Wide-Angle Test Fixture

2-6
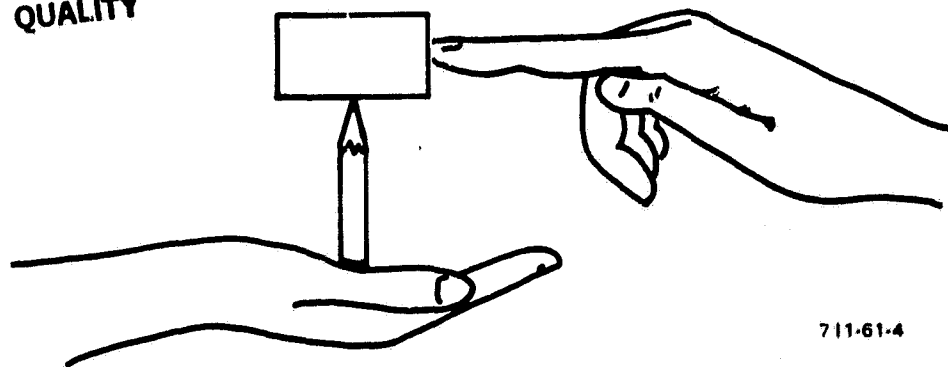
711-61-4

Figure 2-4
Upside-Down WATF Problem

Calculations for the Space Telescope (ST) antenna pointing system (the least stringent case) indicate the table has to be leveled to within 32 arc seconds (1 degree/112) from horizontal to produce less than 1 oz-in. of torque on the gimbals. Since the surface plate must be moved for each gimbal angle tested, it must also be leveled again for each test.

Another problem is the fact that the air bearing acts as a nonlinear spring suspension in the vertical direction. During tests where the mast angle is other than horizontal, the reaction forces and torques from the gimbal are coupled into the mast in such a way as to cause mast bounce in the vertical plane. The air-bearing spring adds an unwanted force to this degree of freedom, and interferes with the ability to measure reaction forces at the mast base.

This method also tends to be dependent on operator technique for proper operation of the air bearing and leveling of the surface plate.

The major advantages of this concept are: 1) a large test structure is not required, and 2) control systems for force or position are not required.

HOIST

CONCRETE PILLAR
WITH TRACK FOR
MAST BASE

INSTRUMENTED
MAST BASE

22 FT
TO CEILING

MAST

AIR SUPPLY
HOSE

DUMMY
ANTENNA
MASS

GIMBALS

SURFACE
PLATE
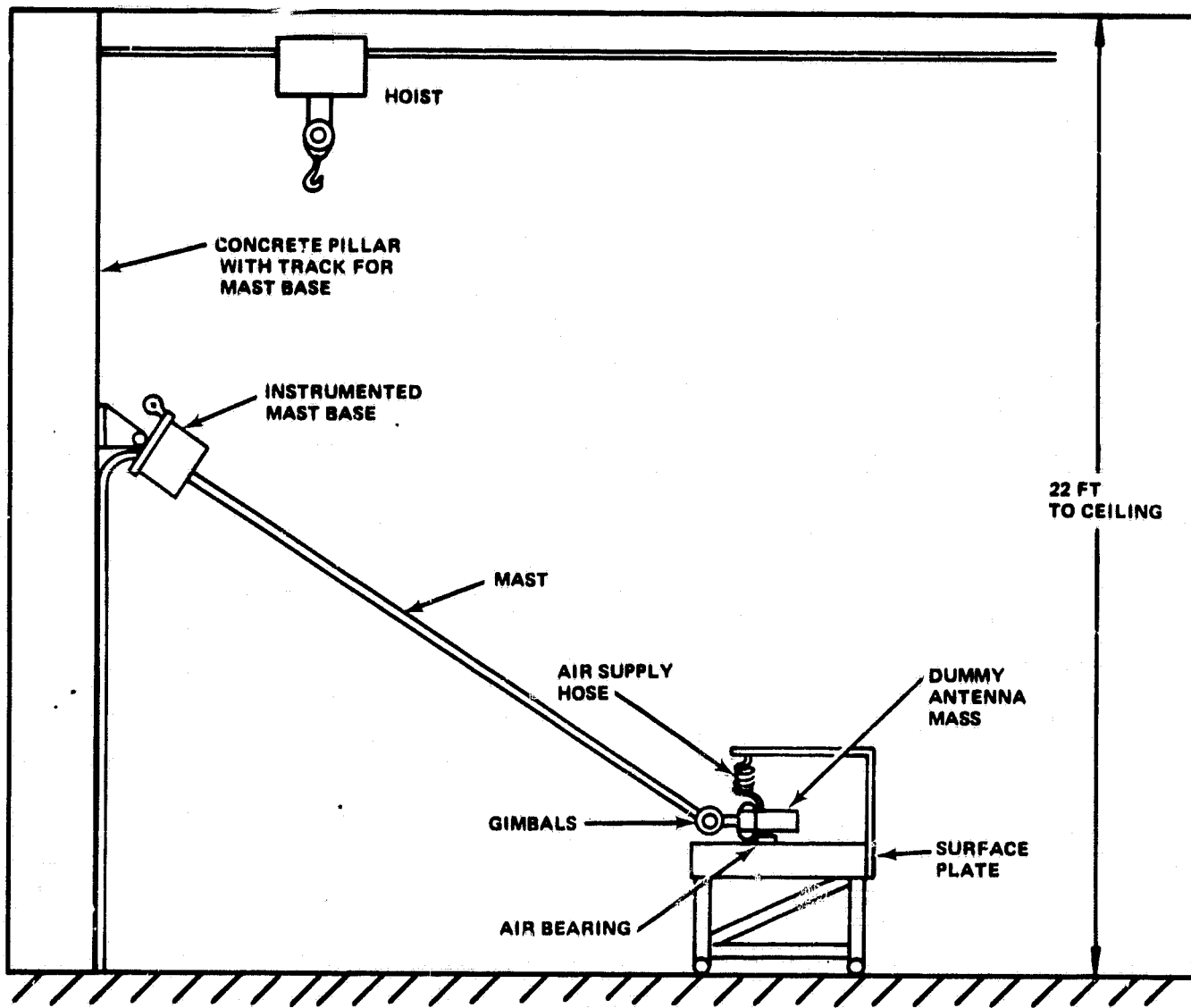
AIR BEARING

711-61-5

Figure 2-5
ZGTF Air-Bearing Method

2.5 TEST METHOD COMPARISON

A table qualitatively comparing the different test methods is presented in Table 2-1, which shows that the counterbalance and air-bearing method can be built with the least front-end design and fabrication effort. The two WATF derivative designs are more complex, and require more mechanical and electronic components. This complexity, however, buys greater accuracy for force and torque measurements on the mast as well as decreased time to run the tests once the setup is completed.

Several forces and torques to be measured at the mast base are missing in the counterbalance method. The gimbal loads are high and the mast suspension affects the mast dynamics adversely.

For the air-bearing method, the air-bearing suspension interferes with the vertical axis dynamics, and there is the possibility of high gimbal torque error if the surface plate is not leveled properly before each test sequence. The requirement for a new test setup and surface plate releveling for each gimbal angle increases the time required to run a test series, and perhaps forces the tester to reduce the number of tests to meet a time constraint.

The upside-down WATF offers no real advantages over the WATF derivative method because of the inherent instability and sensitivity to error of the antenna mass suspension.

These factors leave the WATF derivative as the test method which best meets the reqirements for the Zero Gravity Test Facility. The preliminary facility design is therefore based on the WATF concept, and the term ZGTF will be interpreted as the WATF-derivative design for the rest of this report.

TABLE 2-1

TEST METHOD COMPARISON

	Counterbalance	WATF	Upside Down WATF	Air Bearing
Limits on Gimbal Angle	Up to 110° in a limited envelope	60° any direction envelope to 90	same as WATF	110° planar only
Residual Torque on Gimbals	None	None	None	Potentially High
Load on Gimbals	High	Small or None	Small or None	Small or None
Mechanical Complexity	Low	High	High	Low
Electronic Complexity	Moderate	High	High	Moderate
Design Complexity	Low	High	High	Low
Test Setup Time	Moderate	Long	Long	Repetitively Long
Time to Run Tests	Moderate	Moderate	Moderate	Long
Chance of Equipment Breakdown	Low	Moderate-High High	Moderate-High	Low - Moderate
Structure Size (with 13 ft mast)	Medium	Large	Medium	Medium
Initial Cost	Low	High	High	Low-Medium
Quality of Ug Simulation for the:				
Gimbal Bearings	Fair	Good	Good	Good (limited to plane)
Mast	Fair	Good	Good	Poor-Fair
Inherent Errors Introduced by Test Method to Mast Forces	Antenna cg offset force plus Torques Missing	None	None	Vertical Axis Force plus Torques plus possible Gimbal Torque Error
Sensitivity to Errors (noise, vibration, etc)	Medium-Low	Low	High	Medium

SECTION 3.0
PRELIMINARY DESIGN

SECTION 3.0

PRELIMINARY DESIGN

3.1 TEST FACILITY PERFORMANCE REQUIREMENTS

Once the type of test facility was selected, the detailed performance requirements for the facility could be defined. For the WATF-derivative facility, the requirements are that the X, Y, and Z control loops respond swiftly and accurately enough to follow the motion of dummy antennas, and that the structural resonances not be in the same frequency range as those of the test article. Table 3-1 defines the ZGTF performance requirements.

TABLE 3-1
ZGTF PERFORMANCE REQUIREMENTS

Structural resonance	20 to 30 hertz minimum
X,Y, and Z-axis loop bandwidths	10 hertz minimum
Z-axis cable resonance	10 hertz minimum
Z-axis load cell ranges	0 to 75 pounds, 0 to 250 pounds
Allowable Z-axis force error	$\sim$.02 percent of payload weight
Z-axis travel during test	-2 feet
X-Y axis position loop allowable error	.020 inch with 8 feet of cable
X-Y axis travel during test	±2 feet

The structural and cable resonance frequencies are above the maximum test item mast frequency of 5 to 6 hertz, and the 1-hertz gimbal-loop bandwidth. The X, Y, and Z control-loop bandwidths are also set higher than the test-item frequencies to ensure adequate response. The X, Y, and Z allowable errors are based on calculations for the maximum torque error allowed from the test facility to the test item. The X, Y, and Z axis travel distances were sized to accommodate any projected high-gain antenna system presently foreseen. The Z-axis load cell ranges were specified to provide the proper amount of sensitivity for the whole range of antenna system weights. A ZGTF that meets these requirements will be flexible enough to handle any high-gain antenna system now proposed.

3.2 GENERAL DESIGN DESCRIPTION

A sketch of the ZGTF is shown in Figure 3-1. The most prominent feature is the 24-foot tower which supports the X, Y, and Z drives at the top. The X, Y, and Z drives have been copied from the WATF as much as possible to keep new-design costs down. The X- and Y-axis position control has been changed from the WATF's open-loop position command to a closed-loop system which minimizes the carriage position error with respect to the cable attachment point on the antenna mass. An optical position sensor was added to measure this error. The Z-axis force loop remains unchanged from the WATF design. A high-accuracy load cell at the base of the Z-drive cable has been specified to allow the loop to meet the low error requirement. The instrumented mast base will probably utilize a 6-component force and torque transducer, normally used for wind-tunnel testing, which allows all force components at the mast base to be measured simultaneously.

The electronics for the ZGTF have also been based on WATF electronics as much as possible. The motor-drive electronics are similar to the current WATF drivers except that they will have higher current capability. The WATF is being updated to include this change. The motor electronic safety interlocks and inhibits are the same for both facilities.

The ZGTF control electronics use the same microprocessor architecture as the WATF, but the software will be different to reflect the different control philosophies. Sensor electronics have been added, to handle the additional force and position transducers used in the ZGTF.

The following sections give a more detailed description of the components of the ZGTF.
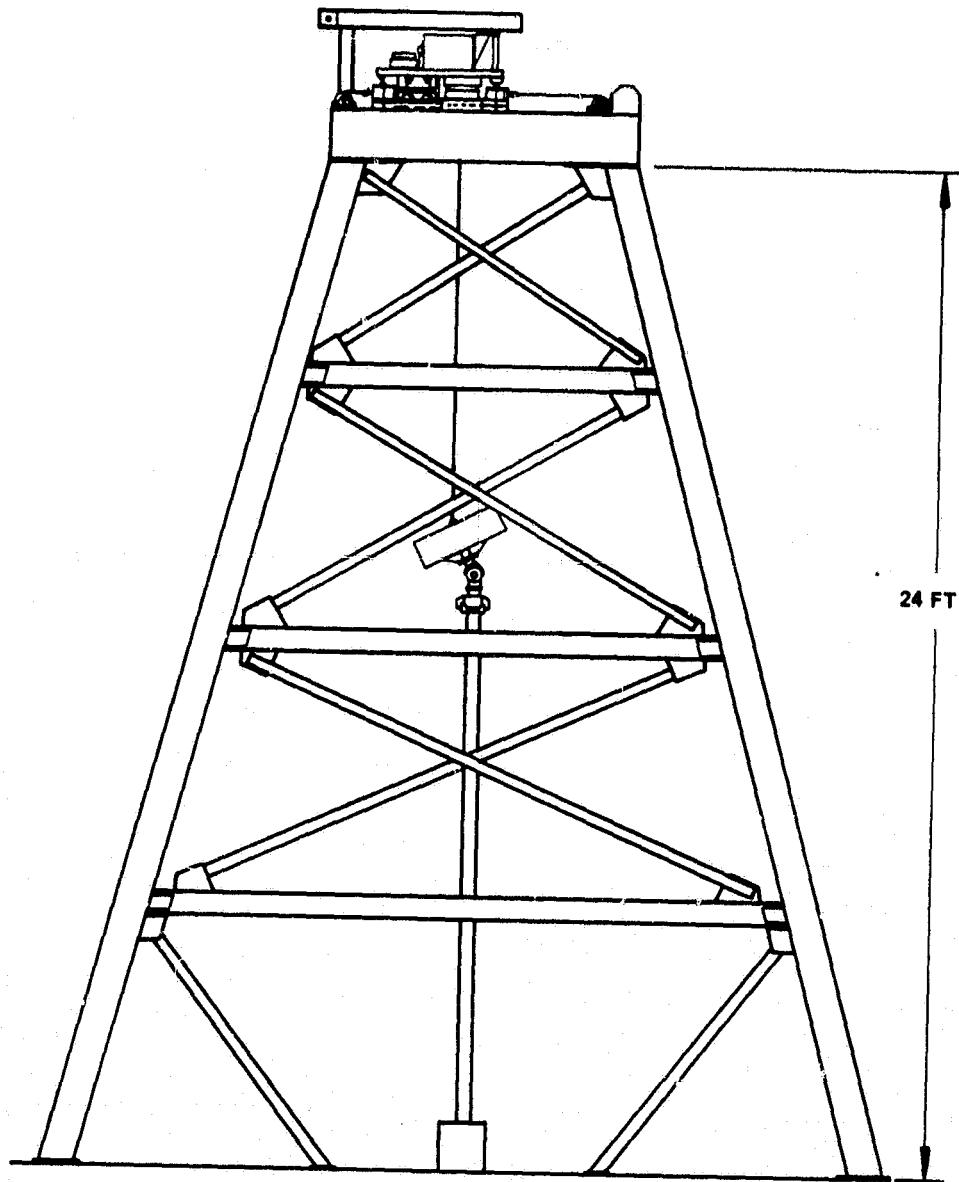
711-61-6 R1

Figure 3-1
Zero Gravity Test Facility

3.3 MECHANICAL COMPONENTS

3.3.1 Tower

The tower design for the ZGTF differs markedly from the WATF tower. Originally, a scaled-up WATF tower was considered for the ZGTF. However, a computer analysis of that design showed a first mode bending frequency of only about 15 hertz, too low for the ZGTF. The proposed design (Figure 3.1) is much stiffer and has a calculated first mode frequency of about 22 hertz. The tower is all steel, and all joints are welded for rigidity. The legs are 8-inch schedule 40 pipe as in the WATF design. The horizontal beams are 6-inch, wide flange, I-beams and the diagonal braces are 3-inch angle iron. The structure will be bolted together during construction and then welded.

At the second level (12 feet above floor level), a floor is built of I-beams covered with catwalk grating. A 5-foot square hole is left at the center of this level for clearance for the test item. With a 13-foot mast and a 1-foot allowance for the mast base, the gimbals for the test item should be at approximately waist level for a person standing on the second level. Removable gratings or plates can be used to cover the 5-foot hole during set up of the antenna system to allow easy access during assembly. Access to the second level will be by removable ladders. As yet, no OSHA safety requirements for the tower have been identified, but fall protection can be provided for people working on the second level by using safety belts with a strap or cable attached to the tower third-level horizontal beam.

Construction of the tower requires cranes to lift the tower parts to their positions. The building enclosing the ZGTF must have enough clearance for this machinery to move around during construction. The minimum ceiling height for the building should be about 30 feet.

3.3.2 X and Y Drive Mechanism

The X and Y drives move the suspension point for the Z-axis (vertical) cable in the two horizontal directions. The X-Y drive is based as much as possible on the WATF X-Y drive shown in Figures 3-2 and 3-3. The major mechanical components of the X-Y drive are the bridge (X direction), the trolley (Y direction), power boom, and the drive trains.

The bridge rests on rails on top of the 14-inch I-beam frame at the top of the tower. The bridge is pulled back and forth on the rails by a pair of drive cables at each end of the bridge. A single electric motor drives both cables through a long drive shaft at one end of the frame.

The trolley rides on rails on top of the bridge, pulling itself along a single cable which runs through the center of the trolley. A single motor drives the trolley. The drive cable runs across two idler pulleys on each side of the motor to allow the cable to wrap around the motor drive gear. The power boom supports the electrical cables that supply power to the trolley. The two sections of the boom are counterbalanced about their vertical pivots on the trolley and the frame.

Both X and Y drives have limit switches which shut off motor power when the bridge or trolley reaches the limit of travel. The optical position sensor and electronics for the X, Y, and Z drives are discussed in a separate section of this report.

3.3.3 Z-Axis Drive Mechanization

The Z-axis drive keeps a constant force that is equal to the dummy antenna weight, on the Z-axis cable. The mechanical portion of the drive consists of a brush-type dc torquer motor which drives a cable drum through reduction gearing. A load cell at the bottom of the cable senses the force applied by the drive, and signals adjustments to be made by the control electronics. The drive applies constant force for static conditions and when the cable is reeling or unreeling from the drum. The mechanism is based on

POWER BOOM

TROLLEY

TROLLE
AND BEA

14" I BEAM AT
TOP OF TOWER

SAFETY LIGHT

5¾"

139½"

96"

BRIDGE

38"

Z DRIVE MOTOR

Z CABLE

102"

FOLDOUT FRAME

SECTION X-X

TROLLEY RAIL
AND BEARING

X DRIVE
CABLE

X DRIVE MOTOR

SAFETY LIGHT

139½"

7¾"

96"

5½"

SECTION Y-Y

Z DRIVE MOTOR

Z CABLE

BRIDGE RAIL
AND BEARING

102"

711-61-7 R1
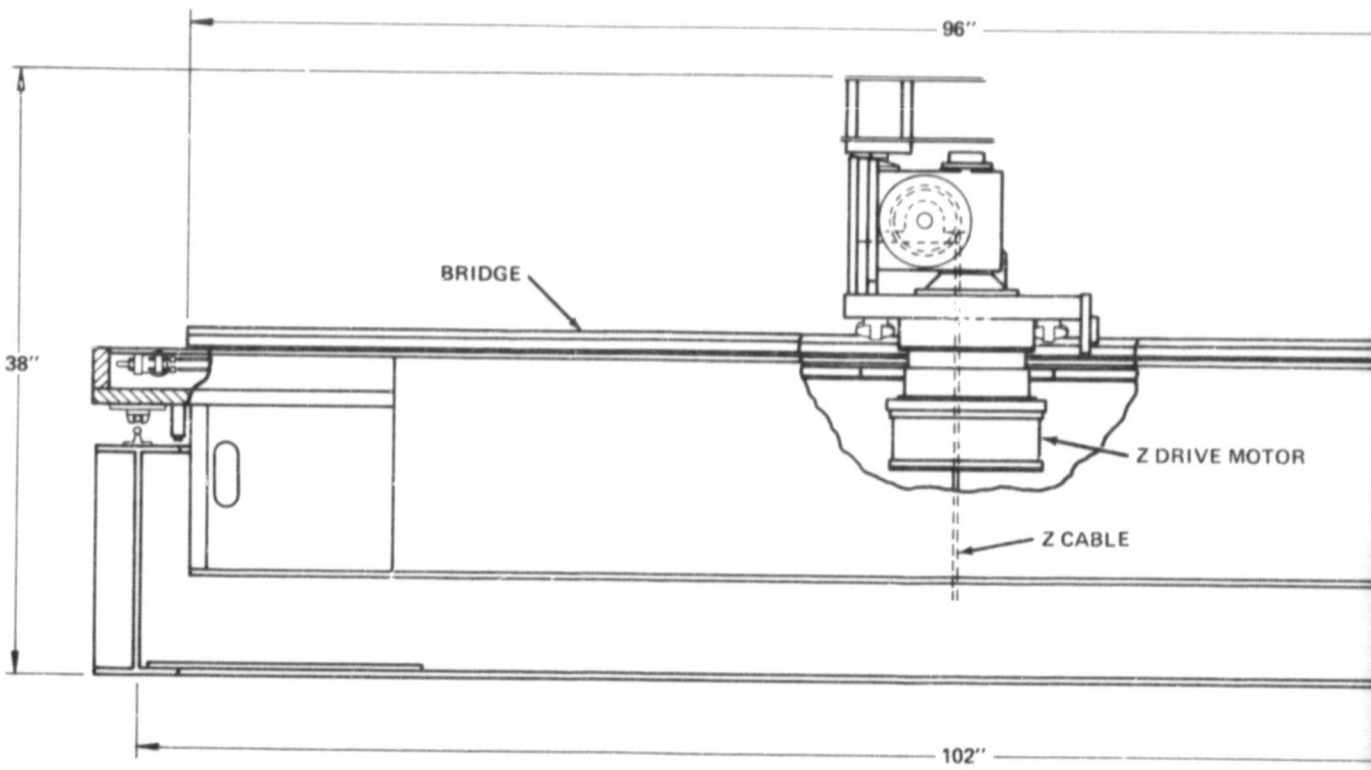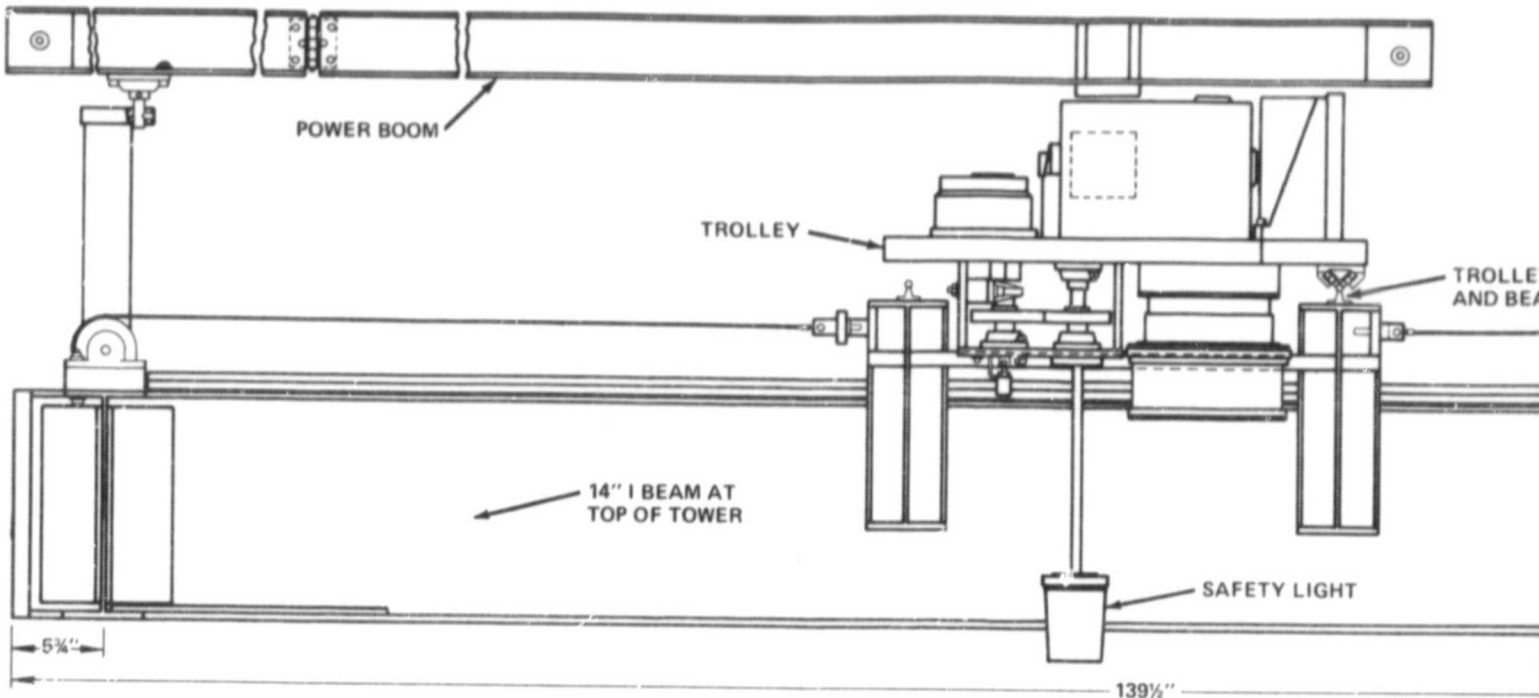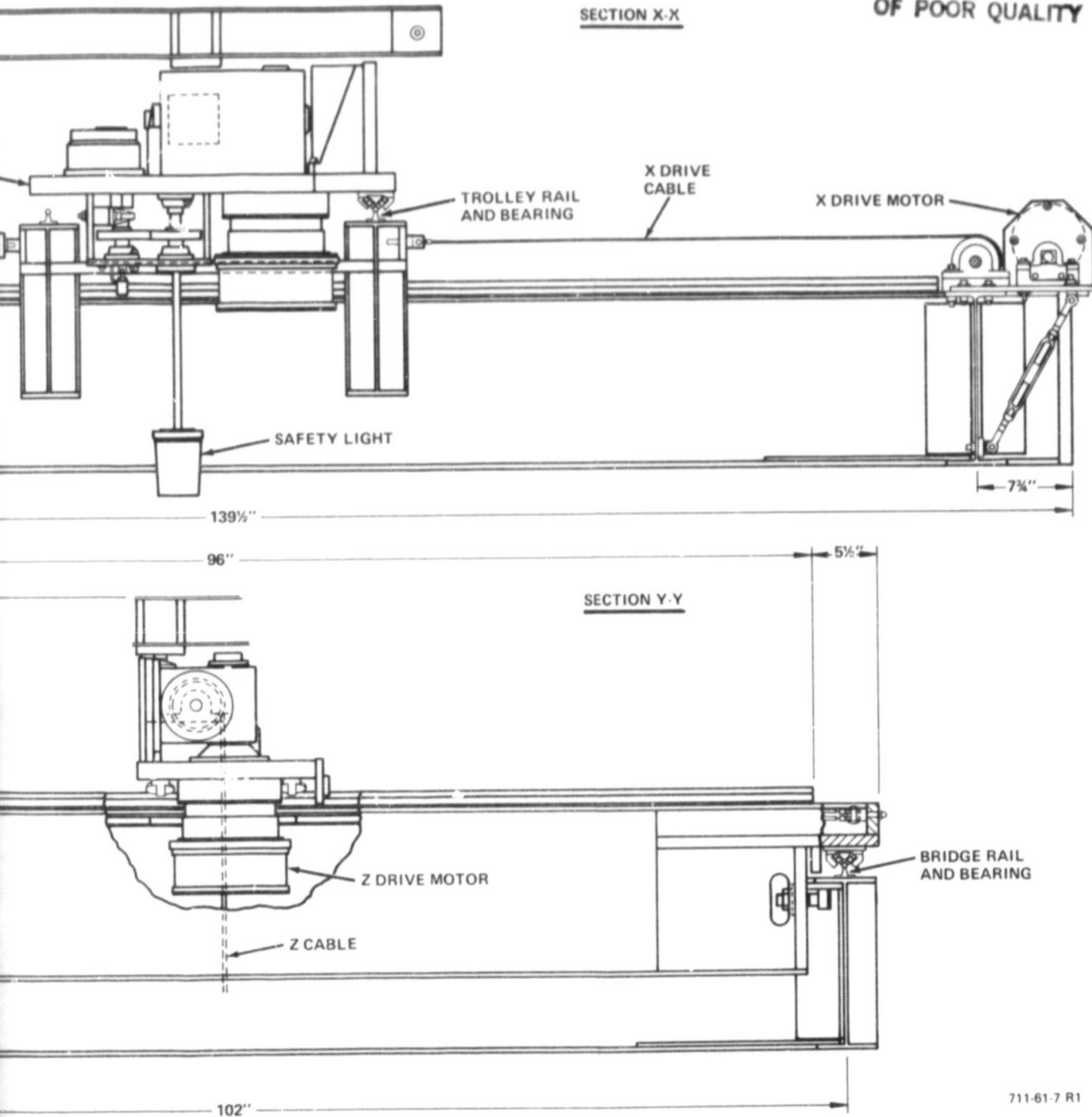
Figure 3-2
ZGTF X, Y, and Z Drives
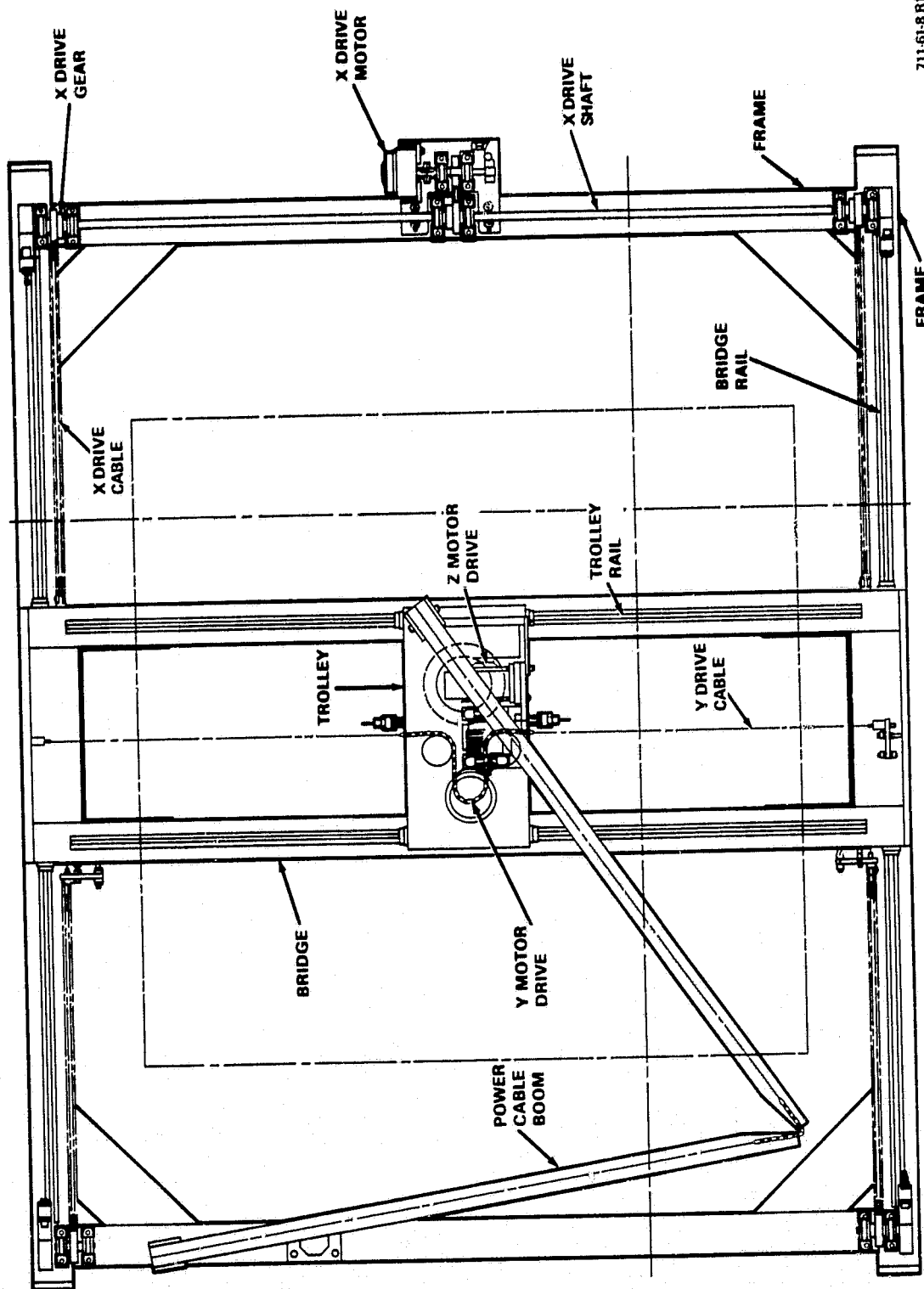
Figure 3-3
ZGTF X, Y, and Z Drives

the WATF Z-drive, but several changes were required to adapt it for use on the ZGTF. The WATF Z-drive motor is a surplus control-moment-gyro torquer that was available when the WATF was built, which will be replaced in the ZGTF by a brush-type dc motor. The load cell at the base of the cable was respecified to a high-accuracy transducer that is capable of meeting the ZGTF error requirements. Changes to the cable spool were also necessary. As the WATF Z-cable unreels, the location of the point at which the cable comes off the drum moves along the drum, and depends upon how much cable has been payed out. The ZGTF design will either allow the drum to move axially so that the cable reels off at the same point relative to the trolley, or the cable will pass over a pulley after coming off the drum, thus constraining it's horizontal position.

One bandwidth limitation of the ZGTF is due to the resonant frequency of the Z-cable. This resonance modulates the vertical tension produced by the Z-axis drive. The frequency depends on the cable force, cable length, the length of the load cell at the base of the cable, and its inertia. The WATF cable frequency was 10 hertz, which is also the goal for the ZGTF cable frequency.

The worst condition occurs with a light load and the cable unreeled to its maximum length. Using high-gain antenna system parameters and an unmodified WATF Z-cable, the resonant frequency will be about 3 hertz, so some redesign of the ZGTF is also necessary in this area. Modifications may include lightening and shortening the load cell link at the base of the Z-cable.

3.3.4 Mast Base

The mast base provides an interface for bolting the antenna mast to the floor, and the base also acts as a transducer to measure six components of force and torque transmitted by the antenna system to the spacecraft. The forces and torques will be measured by either a wind-tunnel sting transducer or by a Sperry custom-designed transducer. The tradeoff between the two choices involves the cost of the wind-tunnel transducer against the technical risk and cost involved in developing the custom-designed transducer. A brochure describing the wind-tunnel transducer is included in the Appendix.

3-8

The custom transducer would utilize six off-the-shelf load cells arranged in an array described in Figure 3-4.

CUSTOM 6-COMPONENT TRANSDUCER
LOAD CELL SENSITIVE AXIS ARRAY

711-61-9
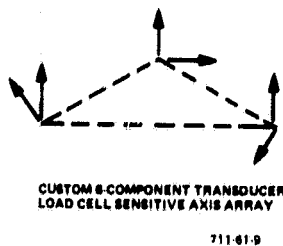
Figure 3-4
Custom Six-Component Transducer Load Cell Sensitive Axis Array

The load-cell outputs will be processed by an electronic sum and difference circuit to extract six orthogonal forces and torques. The schedule and cost estimates included in this report reflect use of the wind-tunnel transducer. The custom transducer requires more design and verification test time than that indicated in this report.

3.3.5 Hoisting Equipment

An overhead crane is necessary to assist in raising and assembling the antenna system before and after testing. A crane that is the equivalent the Yale one-half ton model used on the WATF is recommended. The WATF crane is mounted on a horizontal I-beam attached to the ceiling. The hoisting motor rides on rollers on the I-beam, and is controlled by a manual switch that hangs from the hoist. During use, the ZGTF carriage will be displaced to one side of the tower, thus allowing the hoisting cable to drop down the center of the tower. Antenna system components and tools may then be lifted straight up for assembly. The crane will also be useful during assembly of the ZGTF tower. For this reason, we recommend that the crane be installed in the test building before ZGTF construction.

3.4 ELECTRONICS DESIGN

3.4.1 Motor Drivers

The ZGTF requires a motor-drive electronics unit (MDU) for the X, Y, and Z motors. An input/output block diagram for the MDU is shown in Figure 3-5. Inputs from the control unit electronics provide error signal commands for motor torque to the X, Y, and Z motors and also provide inhibit signals to shut down power to any of the three motors in case of abnormal operating conditions. The outputs are for high and low sides of the windings for the three motors. The MDU will contain one card of logic circuitry, for current crowbar electronics, to sense motor overcurrent conditions. The output of this card is run through OR logic circuitry, with the control unit inhibit signals, which allows either inhibit signal to stop motor power.

The MDU design is similar to the one used on the WATF. Because of the difference in motors and a more restrictive requirement on holding torques, some changes in the servocontroller characteristics will be required, such as higher current capability than that in the present WATF design. Power to the MDU will be from a centrally switched 120-volt, 60-hertz supply.

3.4.2 Control Electronics and Panel

The control electronics unit contains the X, Y, and Z control-loop compensation logic, safety interlock logic, and the manual controls required for operating the ZGTF in an open-loop mode. Block diagrams of the control unit is shown in Figures 3-6 and 3-7.

Figure 3-5
ZGTF Motor Drive Unit Input/Output Diagram

ORIGINAL PAGE IS
OF POOR QUALITY

SYSTEM CLOCK

Z80

ARITH. PROC.

ROM

RAM

A/D

16:1 ANALOG MUX

FORCE ERROR

3 D/A'S AND HOLDS

PARALLEL IN, 16 BIT

PARALLEL OUT, 16 BIT

A B C D E F G H I J K

L
M
N

INHIBIT

X

Y

Z

TO MDU

SIGNAL FROM X-Y LIMIT SWITCHES

(RTC) WATCHDOG TIMER

INHIBIT WATF
— INHBIT MDU
— ENABLE AND ACTUATE CABLE BREAK

LS32

LASER BEAM INTENSITY DETECT (3 EACH)

TO JAC

A — X POSN. POS. MAX.
B — X POSN. NEG. MAX.
C — Y POSN. POS. MAX.
D — Y POSN. NEG. MAX.
E — XLR-L } MANUAL
F — XLR-R }
G — YLR-L }
H — YLR-R
I — ZUD-U
J — ZUD-D
K — MANUAL/AUTO SELECT
L — X INHIBIT } INTERRUPT
M — Y INHIBIT } DEA (OPTION)
N — Z INHIBIT }

FOLDOUT FRAME

Figure 3-6
ZGTF Control Unit

711-61-11

Figure 3-7
Control Unit Auxiliary Circuits

711-61-12

3-13

Inputs are received from the optical position sensor, Z-axis force transducer, Z-axis cable rate sensor, X-Y limit switches, and antenna gimbal commands for processing by a Z80-based logic circuit. Outputs are motor command and inhibit for the X, Y, and Z axes of the MDU. Analog output jacks are provided for recording all input (except limit switches) and output commands as well as the mast base force sensor and gimbal resolver angles. Analog signals are converted to 16-bit digital signals before processing. Fifteen separate inputs are provided for the three optical position sensor detectors. The six sensor X and Y sum inputs supply information on light intensity for each axis. The six X and Y difference inputs indicate percent offset of the light beam in each direction for each sensor. The microprocessor performs a division operation of difference/sum for each sensor and direction (X and Y) to obtain absolute position of the light beam for each optical sensor. The six displacement values are then arithmetically processed to give the X and Y position errors of the X-Y drive carriage. These signals are processed in the X and Y loop-compensation equations to arrive at the motor command signals sent to the MDU. For each of the three optical sensors, the X and Y sum signals are added together and sent through a Schmitt trigger circuit to monitor total light intensity on each sensor. If the light intensity falls below a preset level, signaling loss of the light beam from any sensor, an inhibit signal is sent to the MDU to shut off motor power.

A parallel 16-bit input is used for the optical sensor inhibit signal and for manual control of the ZGTF. The manual inputs command motion of the X-Y carriage and Z cable at a constant rate (in both directions) along each axis. Manual inhibits for each axis and a manual/automatic mode-select switch are also provided at this input port.

The Z-axis load cell output is summed with the Z force reference voltage from a precision potentiometer. The Z-axis force error signal is then digitized, sent through the Z-axis control-loop compensation calculation, and output to the MDU.

A real-time watchdog timer monitors the Z80 microprocessor. In case of Z80 failure or power loss, the timer senses the lack of signals from the microprocessor and sends an inhibit signal to all three motor-drive inputs. Provisions are available to also send an inhibit to the antenna gimbal electronics for this condition.

Another inhibit signal is derived from Z-cable rate. A cable overspeed condition produces an inhibit signal to the Z-motor drive, actuating a fail-safe brake on the Z drive.

Table 3-2 summarizes conditions for safety interlock commands.

TABLE 3-2

ZGTF CONTROL UNIT SAFETY INTERLOCK CONDITIONS

Condition	Drive Inhibited
Motor Overcurrent	X, Y, Z
Manual Inhibit	X, Y, Z
Z80 Failure	X, Y, Z
Loss of Power	X, Y, Z
Optical Sensor Low Light Level/Loss of Light Beam	X, Y
X-Y Position Overtravel	X, Y
Z-Cable Overrate	Z

Failures or power losses in other components of the ZGTF outside the controller can also lead to inhibit signals to the MDU. Examples are Z-force transducer failure, leading to a high cable rate command and triggering the cable overrate inhibit, or the X-Y carriage sticking in place and causing a motor overcurrent command or loss of light beam on the position sensor and leading to X or Y motor inhibit.

The control panel for the ZGTF will be kept simple. Labeled jacks will be provided for each output, along with switches for manual X, Y, Z position command, X, Y, Z inhibit, manual/automatic select, and a master power switch for the entire facility. Schematics for the position command switches (E through J) and the inhibit and mode-select switches (K through N) are shown in Figure 3-6. The master power switch and power distribution schematic are shown in Figure 3-7.

3.4.3 Sensor Electronics

The suggested transducer electronics are, for the most part, off-the-shelf signal conditioning units. Equivalent electronics by other manufacturers than those mentioned will be acceptable. The electronics for the force sensors are Validyne CD-19 carrier-demodulator-amplifier units in an MC-10 power-supply enclosure. Descriptive literature for these units is shown in the appendix. The CD-19s transmit a sine-wave carrier to the force transducer strain-gage bridges. The return signal from the bridges is demodulated and amplified by the CD-19s. The carrier power signal to the bridges provides excellent immunity to electromagnetic interference- (EMI) induced noise from the ZGTF and antenna gimbal motors. Induced noise in the Z-transducer cabling was a problem during initial operation of the WATF. The use of this type of signal conditioner should avoid this problem in the ZGTF. Ten channels of CD-19 plug-in units are required as follows:

- Mast base force sensor   - 6 channels
- Z-axis load cell   - 1 channel
- Mast-mode triax accelerometer - 3 channels

These units may be used with any strain-gage bridge type of transducer, possibly eliminating the need to buy new electronics if future tests require that new parameters be measured.

The optical position sensors require buffer and summing amplifiers at the photodetector output. United Detector Technology Model 301 amplifiers, or equivalent, plus 521 type opamps are connected as shown in Figure 3-8.
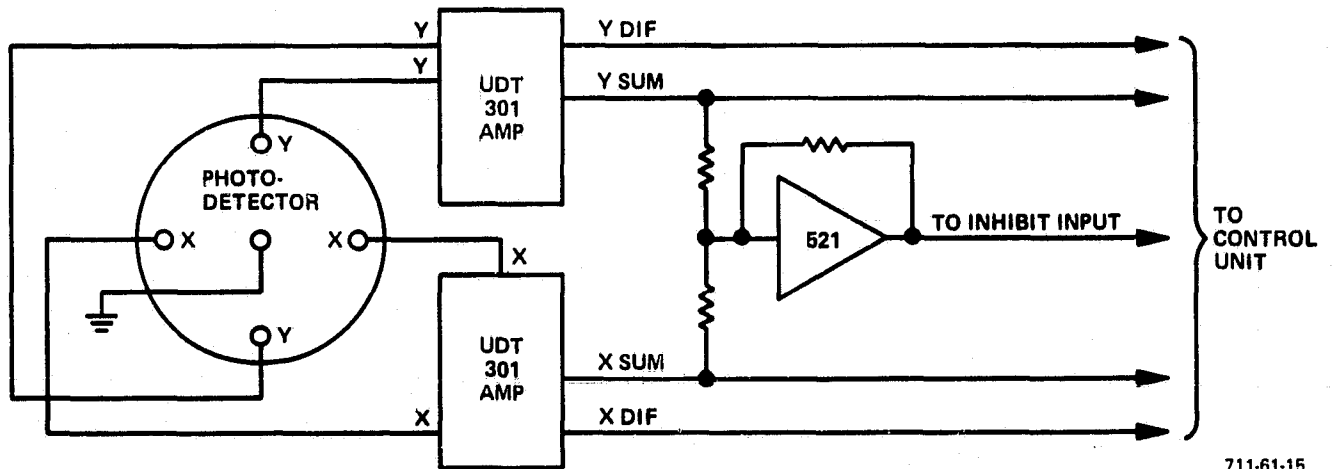
711-61-15

Figure 3-8
Optical Sensor Electronics Schematic

The 301 amplifiers derive the sum and difference signals from the photodetector output. The 521 opamp sums the X and Y sum signals for the loss-of-light-beam inhibit input to the control unit. Six type 301 amplifiers plus three 521 opamps are needed for the three photodetectors in the position sensors.

The final piece of transducer electronics are tri-state logic drivers for the X and Y position-limit switches. The drivers convert the on/off output of the limit switches to high/low logic for the microprocessor. Four logic drivers are necessary for the ZGTF.

3.4.4 X-Y Position Sensor

The position sensor* for the ZGTF X and Y drives must be capable of detecting position error between the X-Y drive carriage and the suspension point for the dummy antenna mass to within a few thousands of an inch. A preliminary design that utilizes laser optics was developed; it appears capable of measuring position error to the required accuracy, unaffected by Z-axis cable dynamics.

The laser light source is mounted on the trolley with the Z-drive mechanism, as shown in Figure 3-9. The light beam is split into three parts and sent straight down to three reflectors mounted on the top of the Z-axis load cell at the base of the Z cable. The three reflected beams travel back up to three optical position detectors mounted on the Z-drive trolley where light spot position is sensed.

711-61-16
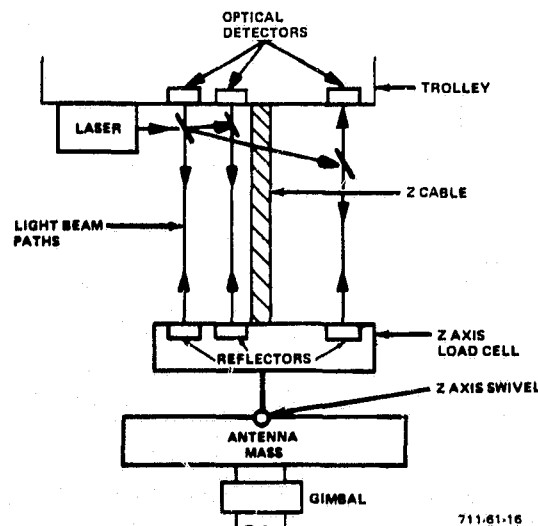
Figure 3-9
X-Y Position Sensor Layout

---

*Optical position sensor refers to the position-sensing system. Optical position detector refers to the photoelectric light spot measuring component.

3-18

The position sensor is designed around the reflective properties of
two types of mirrors - flat and cube corner. The flat mirror reflects light
at an angle equal to the angle of the incident beam of light (Figure 3-10).

FLAT MIRROR

SIDE
(SIMPLIFIED)

INCIDENT BEAM

REFLECTED
BEAM

TOP

CUBE CORNER MIRROR

ZGTF REFLECTORS
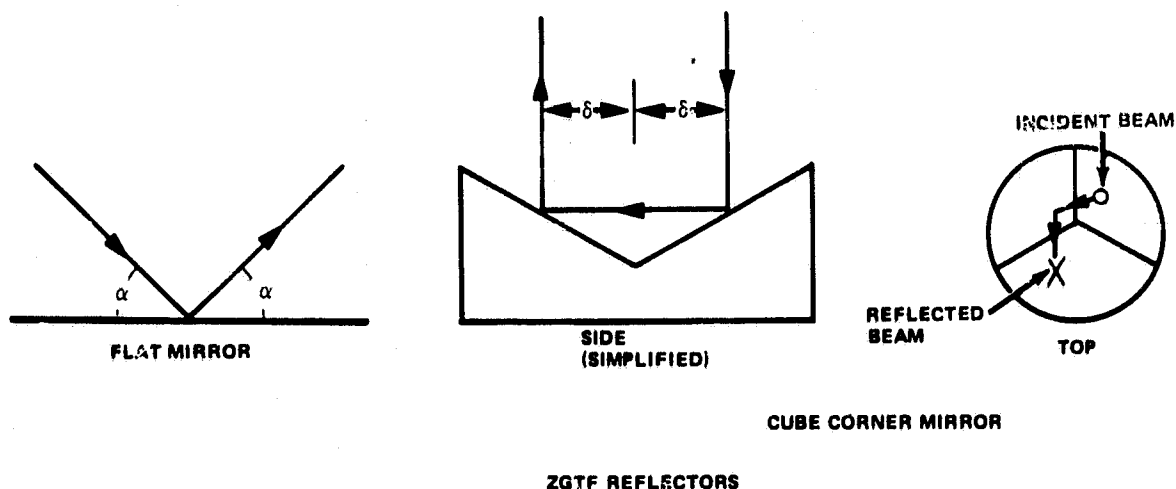
711-61-17

Figure 3-10
ZGTF Reflectors

The cube corner mirror reflects light in the opposite direction from which it
enters the mirror, no matter what the mirror orientiation. The reflected
beam is displaced from the center of the mirror, the same distance as the
incident beam; on the opposite side of the center. This can be demonstrated
by looking in a cube corner mirror. The observer will always see his eye
upside down and centered in the mirror, no matter at what angle the mirror is
held.

The flat mirror, when mounted on the top of the rigid load cell link,
reflects the laser beam back at twice the angle that the link is cocked
(Figure 3-11).
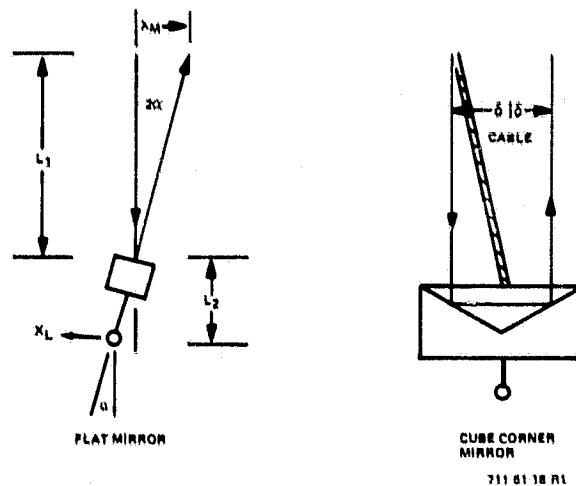
Figure 3-11
Optical Reflector Position Outputs

The displacement of the bottom of the link with respect to the top of the link is:

$$X_L = \frac{-L_2}{2L_1} \; X_M \qquad (1)$$

Therefore, the flat mirror measures the displacement of the link only.

The cube corner mirror reflects its light beam straight back up, displaced twice the distance that the Z-drive trolley is displaced with respect to the top of the load cell link. The cube corner mirror measures Z-cable displacement only. By summing the displacement measurements of the cube corner and the flat mirror beams, the sensor arrives at the displacement of the trolley with respect to the bottom of the load cell link, which is the desired measurement (Figure 3-12).

X OR Y DISPLACEMENT = X_D
FLAT MIRROR DISPLACEMENT = X_F
CUBE CORNER MIRROR DISPL. = X_C

$$X_D = X_F + X_C$$

711-61-19
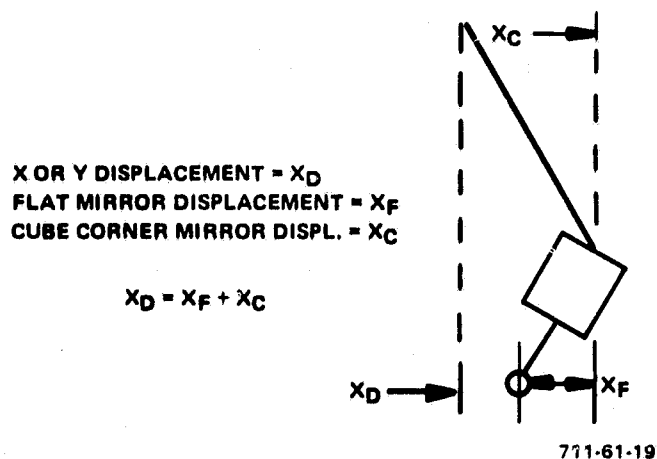
Figure 3-12
X-Y Position Derivation

The calculated displacement is independent of the position of the top of the load cell link because this displacement is cancelled out in the summation process. When cable vibration occurs, the top of the load cell sustains a periodic displacement, even though the trolley and antenna mass may not move. Independence from load-cell displacement makes the position sensor insensitive to cable vibration.

Because of the nature of the cube corner mirror, the position sensor is sensitive to rotation of the load-cell link about the vertical axis. The use of one cube-corner mirror, offset from the link's vertical axis, would result in a displacement signal if the link rotated. For this reason, two cube-corner mirrors on opposite sides of the link axis are used in this design. The outputs of the two are averaged to cancel out rotational effects. Since the flat mirror is insensitive to rotation about the vertical axis, only one is needed; hence three laser beams are needed for this sensor.

The photodetectors used for sensing the reflected light-beam positions each produce X- and Y-position outputs. The detector outputs are appropriately summed and scaled by the sensor and control electronics. The active area of each detector is 1.75 inches in diameter. During ZGTF start-up, the X-Y carriage must be positioned so that the light beams are within this area. Loss of a light beam from any sensor causes the X and Y drives to shut down.

3.5 TEST·EQUIPMENT

3.5.1 Test Structure

It is assumed that the ZGTF may be used at a site other than Sperry Flight Systems. A preliminary test structure is necessary to avoid having to assemble the 24-foot ZGTF tower for preliminary testing of the ZGTF drives at Sperry and then shipping the assembled tower across the country.

The test structure supports the ZGTF X, Y, and Z drives during preliminary checkout tests. The structure is the same as the WATF structure except that the drives are supported only 8 to 10 feet above the ground. At this height the end of the Z-drive cable may be attached to test equipment on the ground. The 8 to 10 feet of Z-cable payout simulates actual operating conditions. The tower uprights will be 8-inch schedule 40 steel pipe with 2-inch pipe diagonal supports. A sketch of the test tower is shown in Figure 3-13. The test structure will be a nondeliverable item.

3.5.2 Motion Simulator

During test facility checkout and verification tests, a motion simulator is necessary to check the facility's slew performance. A conceptual design of such a device is shown in Figure 3-14. The ZGTF Z-drive cable attaches to the moving block through a ball joint. The moving block rides on two linear ball bushings, propelled by a ball screw drive for slew simulation. A constant-speed motor turns the drive screw at predetermined rates. The simulator can be tilted up at angles up to 90 degrees from horizontal for simulating motion in any direction.

For precision static-displacement measurements, a displacement measuring block can be clamped to the simulator. Static displacements are measured with the micrometer head on the block. The motion simulator will be used for periodic recalibration of the ZGTF, and will be a deliverable item.
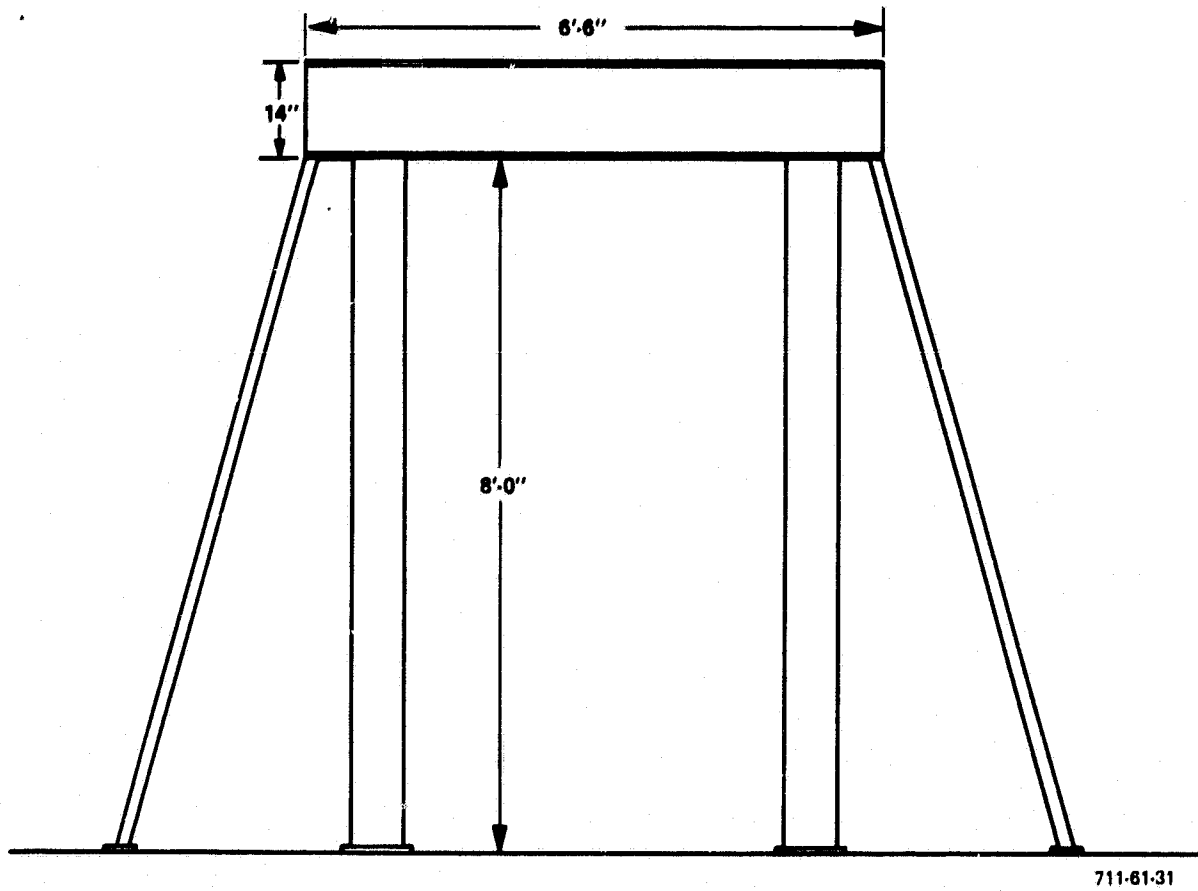
Figure 3-13
ZGTF Test Structure
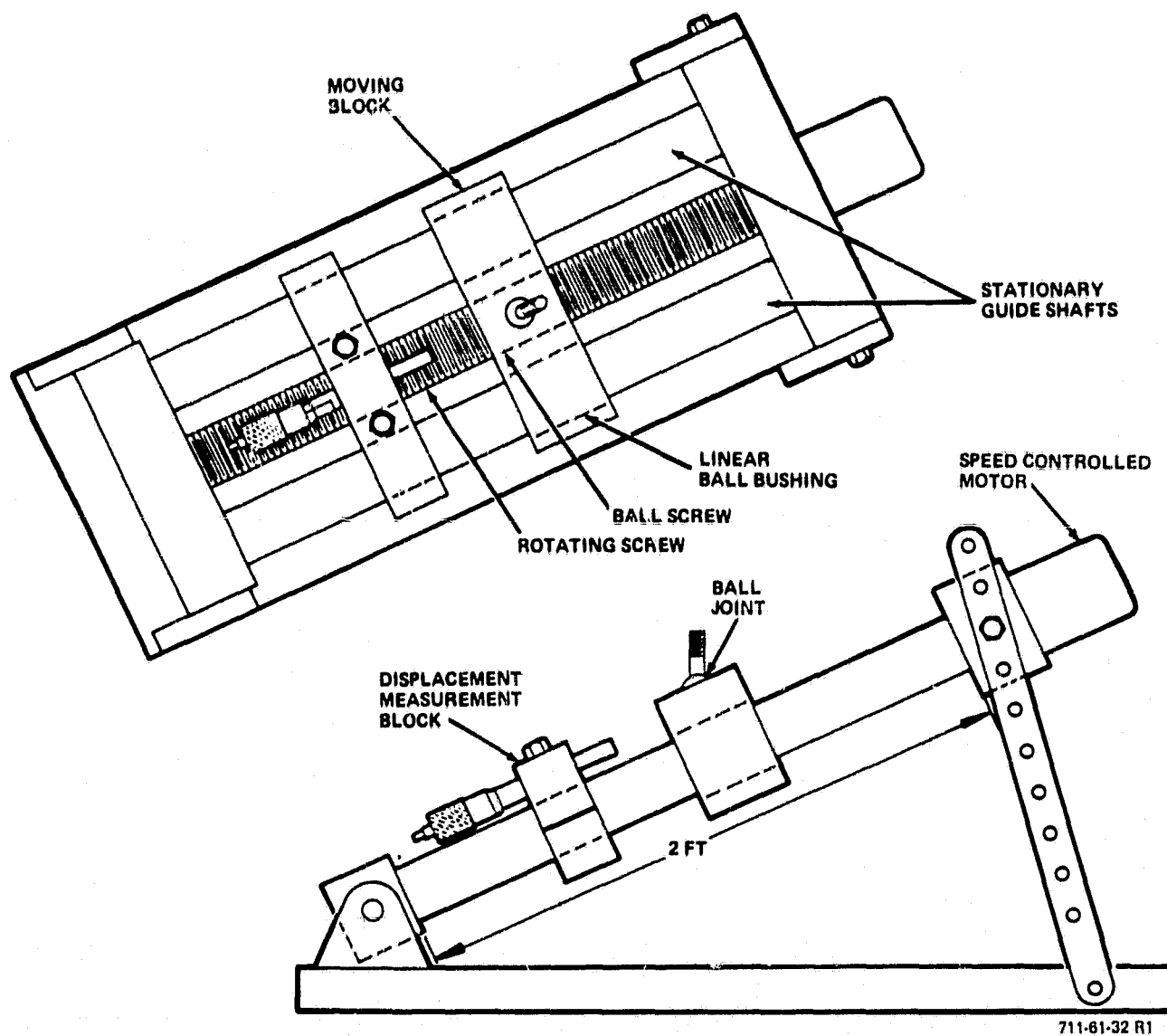
Figure 3-14
Gimbal Slew Simulator-Position Sensor Calibrator

SECTION 4.0

SYSTEM DESIGN

SECTION 4.0

SYSTEM DESIGN

4.1 X-Y POSITION LOOPS

The X and Y position-control loops are designed to keep the X-Y carriage directly above the antenna dummy mass suspension point. The objective is to keep the suspension cable vertical at all times to avoid side forces on the antenna mass. The maximum allowable position error is .020 inch between the carriage and the antenna suspension point. The system block diagram is shown in Figure 4-1 for one axis. The system model for each axis is the same, but there are differences in the mass and stiffness in each direction. The X loop models the bridge and trolley masses and two drive cables. The Y loop contains the trolley and one drive cable. A similar system model without position feedback was used for the WATF X and Y controller. The parameters used for the preliminary design were taken from the WATF system model, except for the carriage mass which was scaled down to reflect the ZGTF mass. The X loop was used for modeling because the higher mass of the bridge and trolley represent the worst-case design problem. The two friction terms shown were neglected in calculating the loop compensation.

The open-loop transfer function is:

$$\frac{K_D K_T N \left(\dfrac{R}{J + MR^2}\right) \left(\dfrac{D_c}{K_c} s + 1\right) G_c(s)}{s^2 \left(\dfrac{JM}{K_c (J + MR^2)} s^2 + \dfrac{D_c}{K_c} s + 1\right) \left(\dfrac{s}{W_D} + 1\right)} \tag{2}$$

where $G_c(s)$ is the compensation transfer function.

The uncompensated open-loop gain is

$$K_D K_T N \frac{R}{J + MR^2} = 1.21 \tag{3}$$

4-1

$X_{PAYLOAD}$

$+$ X_{ERR}

$\dfrac{1}{S}$

CARRIAGE MASS

$\dfrac{1}{MS}$

CARRIAGE FRICTION

FORCE

DRIVE CABLE DAMPING AND SPRING CONST.

$D_C + \dfrac{K_C}{S}$

SPROCKET CABLE VELOCITY

RADIUS

R

R

MOTOR AND DRIVE TRAIN INERTIA

$\dfrac{1}{JS}$

MOTOR FRICTION

TORQUE

MOTOR TORQUE CONST.

GEAR RATIO

$K_T N$

TORQUE

MOTOR DRIVER

$\dfrac{K_D}{\dfrac{S}{W_D} + 1}$

COMPENSATION

$G_C(S)$

POSITION ERROR

X_{REF}

711-61 20 R1
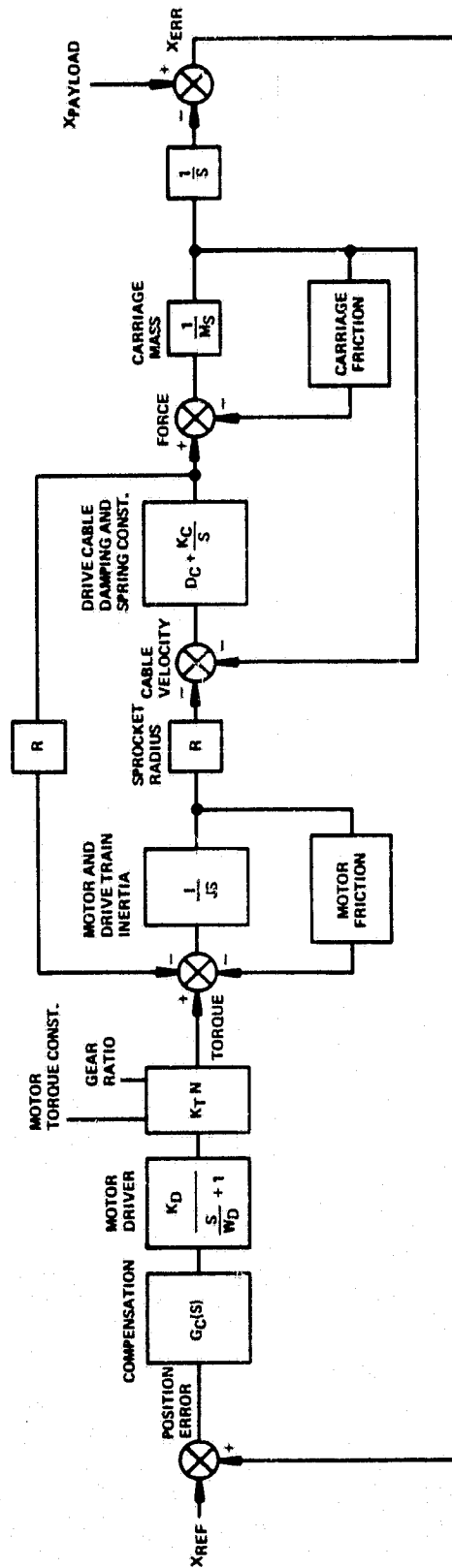
$K_{TN} = 145\ \text{in·lbf}/6.2\ \text{AMP} = 22.6\ \dfrac{\text{in·lb}}{\text{AMP}}$

$J = 26.0\ \text{in·lbf·sec}^2$

$R = 2''\ \text{RADIUS}$

$D_C = 12.5\ \text{lbf·sec/in}$

$K_C = 1400\ \dfrac{\text{lbf}}{\text{ft}} = 116.7\ \dfrac{\text{lbf}}{\text{in}}$

$M = 1050\ \text{lbm} = 2.72\ \dfrac{\text{lbf·sec}^2}{\text{in}}$

$G_C(S) = 345\ \dfrac{\left(\dfrac{S^2}{W_1^2} + \dfrac{1.4S}{W_1} + 1\right)}{\left(\dfrac{S^2}{W_2^2} + \dfrac{1.4S}{W_2}\right)}\ \dfrac{V}{IN}$

$K_D = 1\ \dfrac{\text{AMP}}{W}$

$\omega_D = 6000\ \dfrac{\text{RAD}}{\text{SEC}} \approx 1\ \text{KHz}$

$\omega_1 = 5.5\ \text{RAD/SEC}$

$\omega_2 = 150\ \text{RAD/SEC}$

Figure 4-1
ZGTF X-Y Position-Control Loop Block Diagram

and the uncompensated crossover frequency is about 1.1 radians per second as shown in Figure 4-2. For a 10-Hz loop bandwidth, the compensated zero dB crossover frequency should be about 60 radians per second with a -20-decibel-per-decade slope around the crossover. The compensation picked for this loop was:

$$(4) \qquad G_c(s) = \frac{K\left(\frac{s^2}{\omega_1^2} + \frac{1.4s}{\omega_1} + 1\right)}{\left(\frac{s^2}{\omega_2^2} + \frac{1.4s}{\omega_2} + 1\right)\left(\frac{s}{\omega_3} + 1\right)^2} \qquad \omega_1 < \omega_2 < \omega_3$$

The compensated open-loop Bode plot is shown in Figure 4-2. One peculiarity of this loop is that the cable spring constant K_c is expected to change by a factor of 2:1, depending on the position of the carriage. As the carriage position goes from one side of the tower to the other, the length of cable through which tension is applied changes by 2:1, causing a proportional change in spring constant. This change causes the break frequencies at

$$\omega = \sqrt{\frac{JM}{K_c(J + MR^2)}} = 7.8 \text{ rad/s} \quad \text{and} \quad \omega = \frac{D_c}{K_c} = 14 \text{ rad/s} \qquad (5)$$

to drift down to 5.5 and 7 radians per second, respectively. For this reason the quadratic lead break frequency ω_1 was put at 5.5 radians per second to avoid the possibility of instabilities during saturated operating conditions. The compensation gain was set to K = 345 to obtain the 60 radians per second crossover. The quadratic lag break frequency was set at 150 radians per second. This gives a calculated phase margin of 21.5 degrees at crossover.
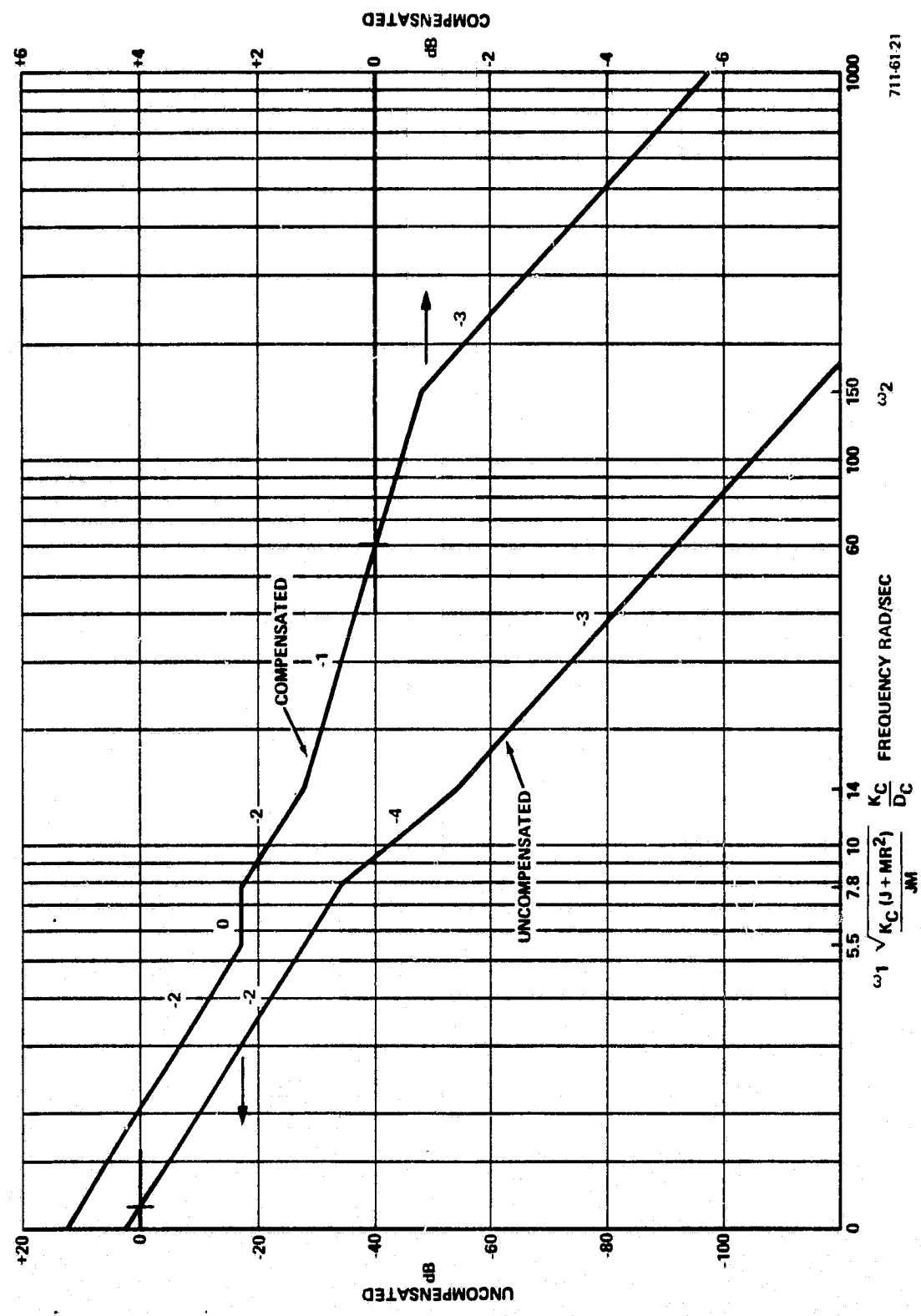
Figure 4-2
ZGTF X Loop Open-Loop Bode Plot

711-61-21

The closed-loop Bode plot is shown in Figure 4-3. The system bandwidth is about 120 rad/s, or twice the goal of 60 rad/s. The X-position loop was dynamically modeled on an Applied Dynamics/4 analog computer. The use of the analog computer allowed immediate examination of modifications to the system and was very useful in tracking down cause-and-effect relations in the loop. The modeled input was a transient ramp change in antenna mass position, at .2 in./s, simulating a 30-degree-per-minute slew of a Sperry HGAS antenna drive. The ramp input voltage was filtered with a 1-hertz lag to simulate the 1-hertz bandwidth of the antenna gimbals. Transient responses that had several of the nonlinearities present in the loop were run to determine the effect of each nonlinearity on the X-loop position error. The transient responses are shown in Figures 4-4 through 4-8. The nonlinearities modeled were as follows:

- ● Saturations (limits)
  - Control electronics voltage - 15 volts
  - Motor torque   - 140 inch-pound
  - Carriage velocity   - .65 inch per second
- ● Dahl friction (no peaking)
  - Motor torque   - 7 inch-pounds
  - Carriage bearings - 14 pounds

Also modeled was tower dynamics, as a linear, second-order negative feedback. Referring to the transient response curves, for saturations only, the peak position error was .0018 inch. The steady-state error diminished to zero. With saturations and the tower dynamics, the transient response showed no change. This was confirmed by an analysis that showed the static gain through the tower dynamics feedback path was 10,000 times less than the position sensor feedback gain because of the high stiffness of the tower.

With saturations and motor friction, the transient response showed a .0025 inch peak pointing error. The steady-state error was about .001 inch. An analysis using the final value theorem predicted a .0009-inch steady-state error, which is in excellent agreement.
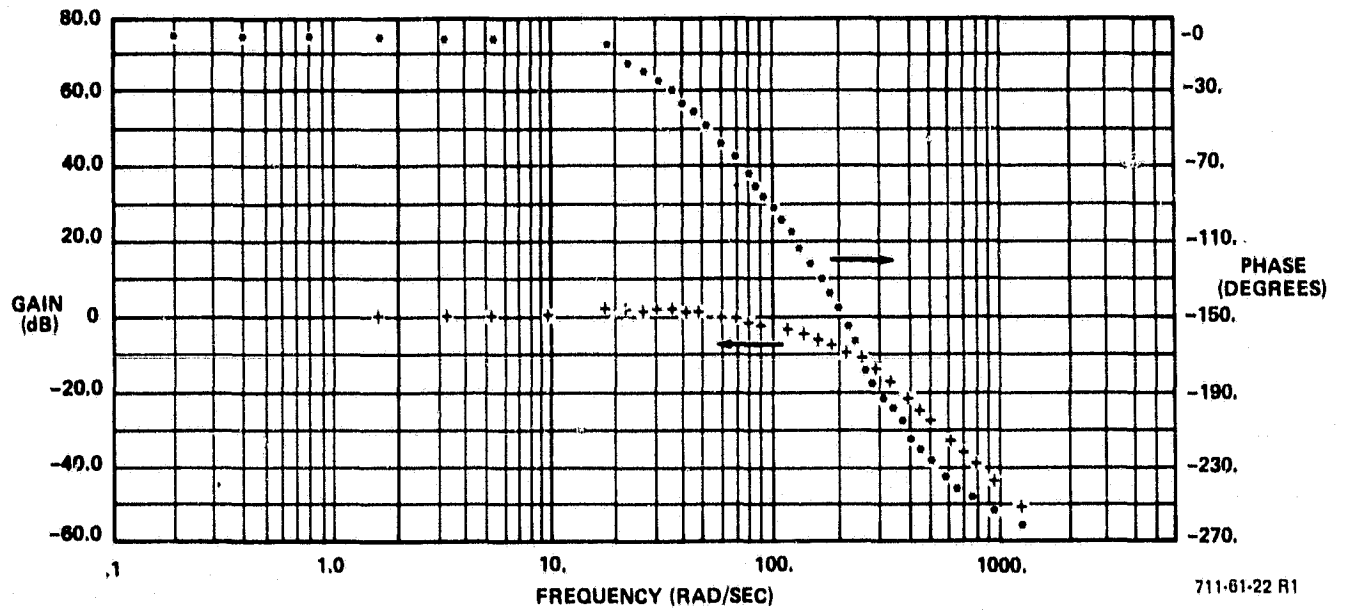
Figure 4-3
X-Y Closed-Loop Response - ZGTF Linear Model
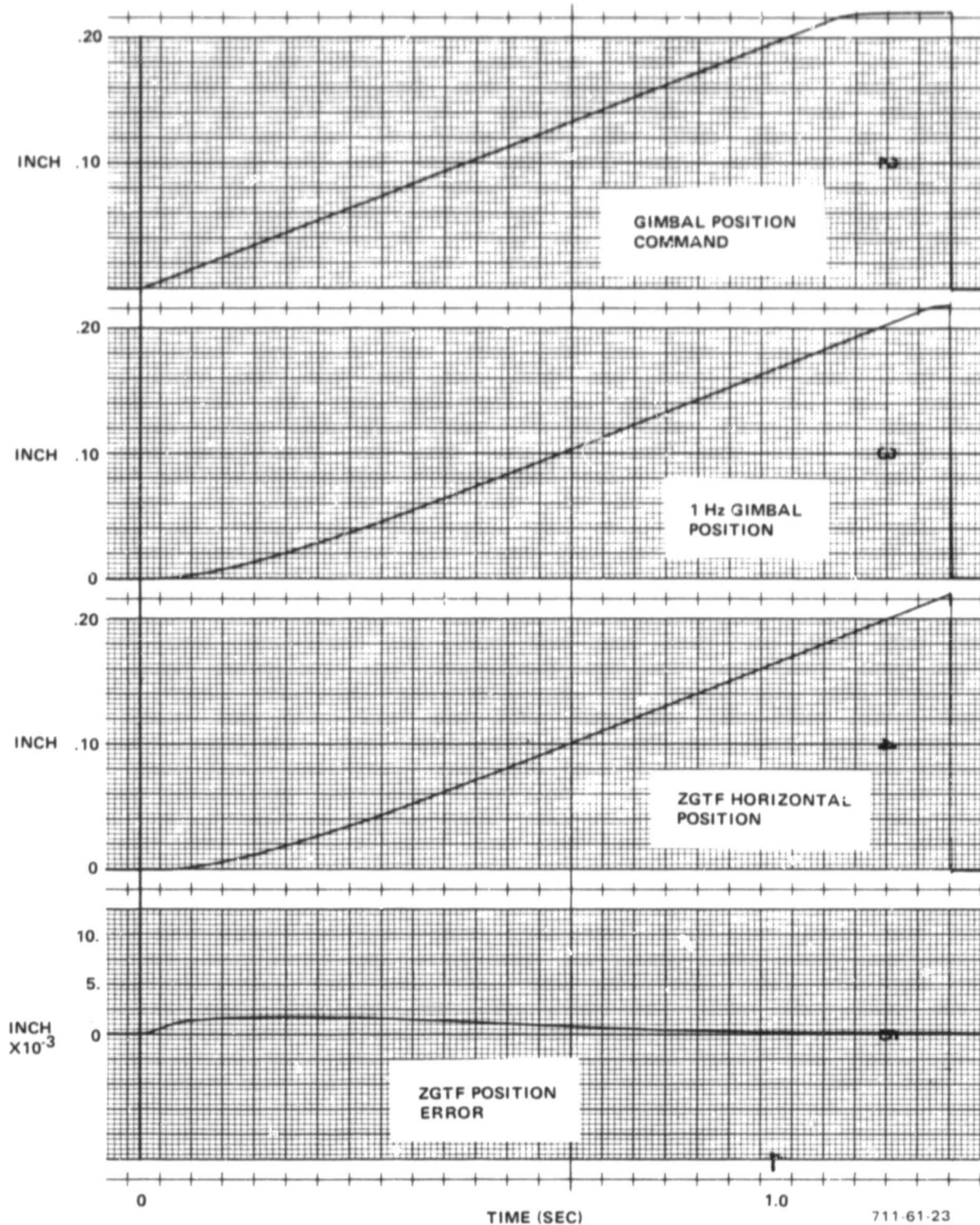
Figure 4-4
ZGTF X-Y Loop Transient Response to Gimbal Slew –
Command Saturations Only
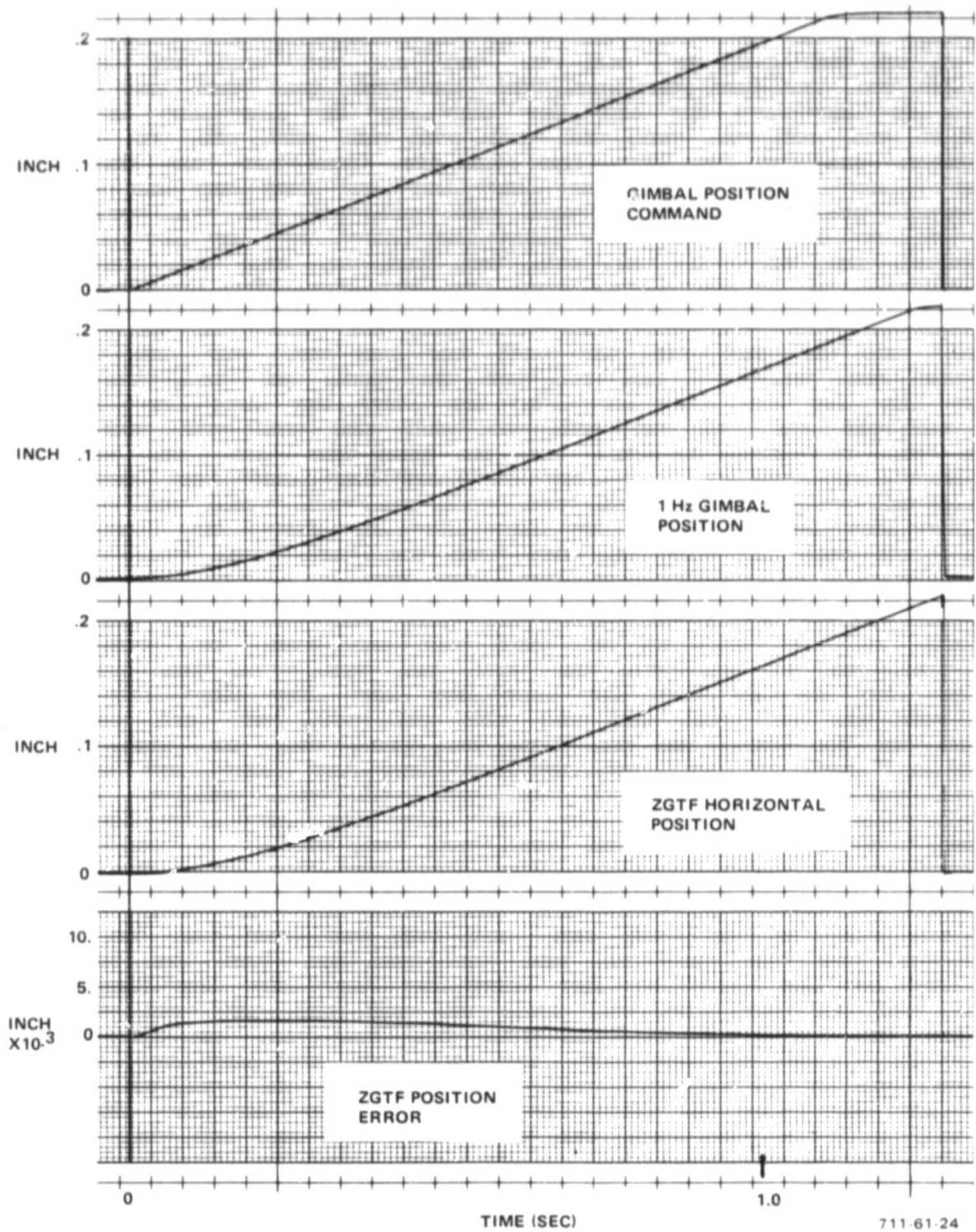
Figure 4-5
ZGTF X-Y Loop Transient Response to Gimbal Slew
Command - Saturation and Tower Dynamics

4-8
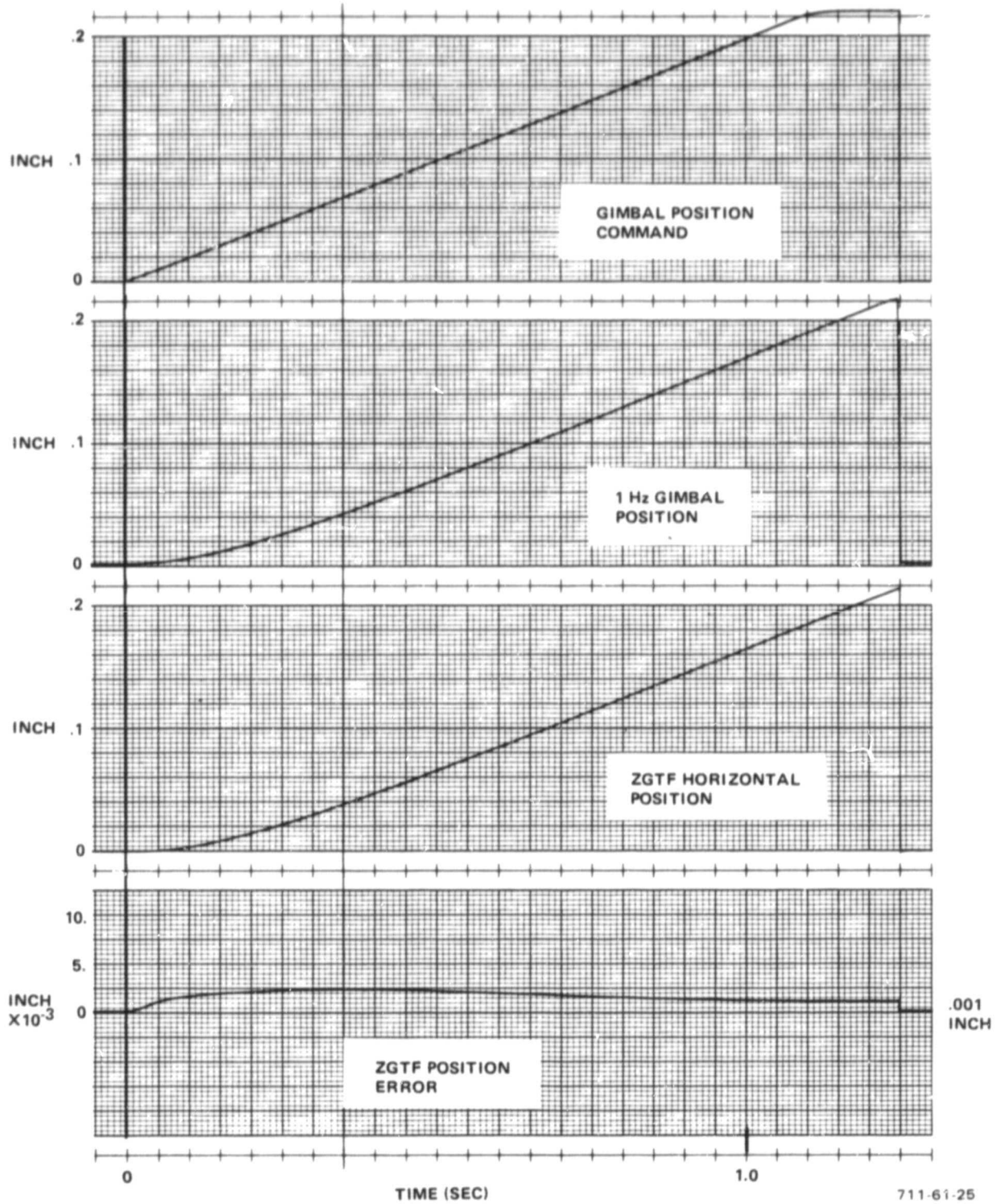
Figure 4-6
ZGTF X-Y Loop Transient Response to Gimbal Slew
Command - Saturation and Motor Friction

4-9
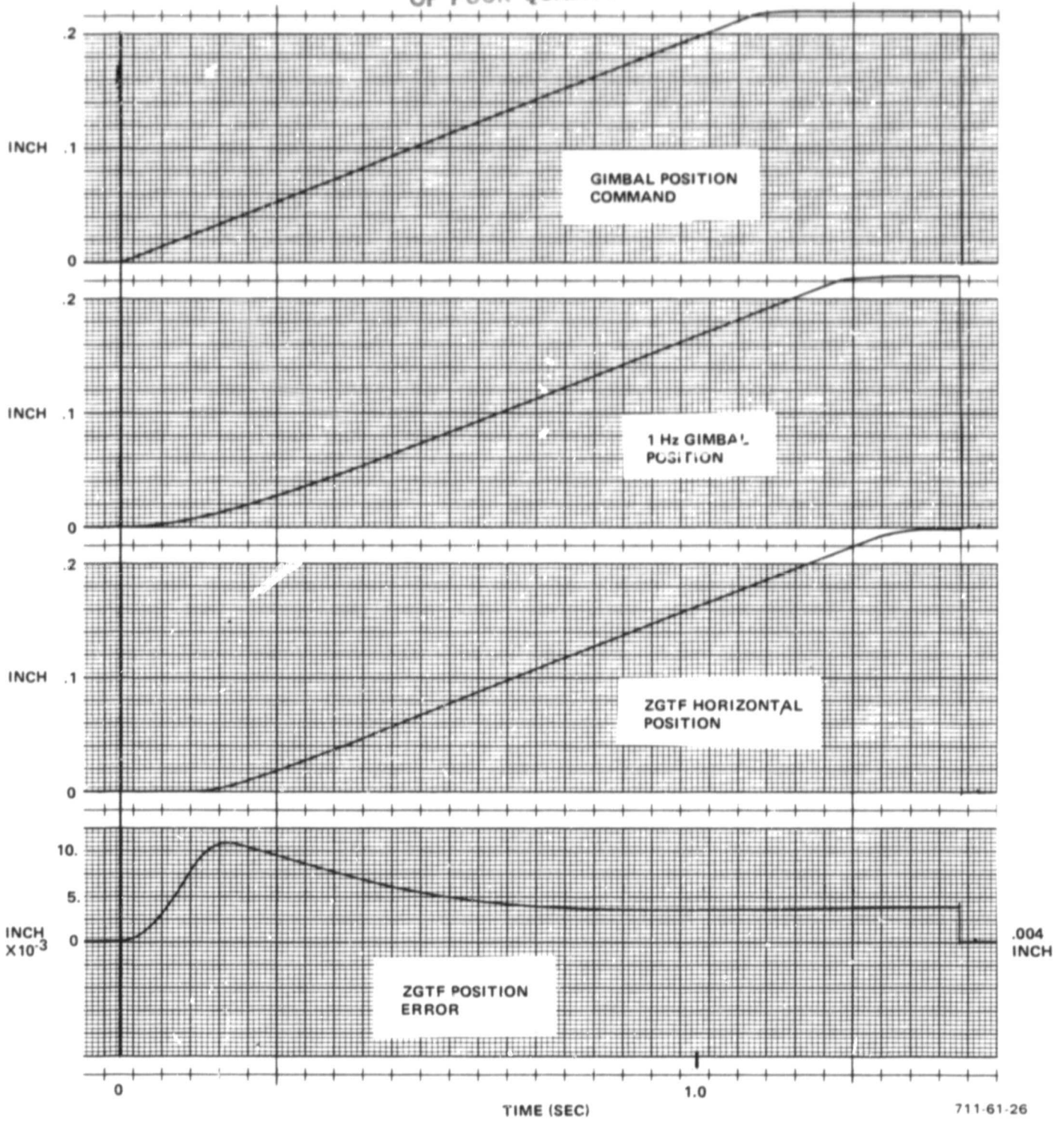
Figure 4-7
ZGTF X-Y Loop Transient Response to Gimbal Slew
Command - Saturation and Carriage Friction

4-10
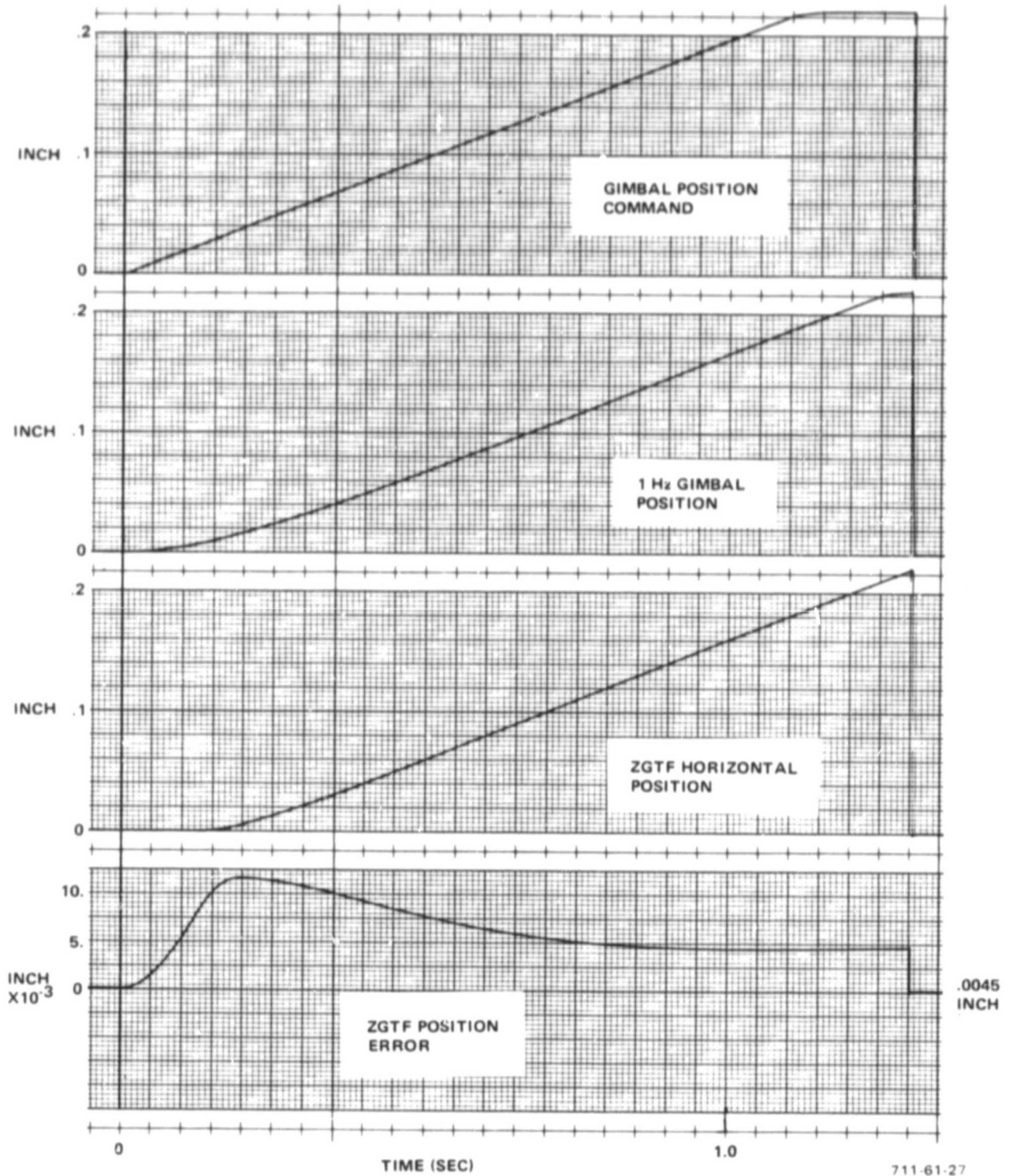
Figure 4-8
ZGTF X-Y Loop Transient Response to Gimbal Slew
Command - All Nonlinearities Included

4-11

With saturations and carriage friction, the peak position error was .011 inch. The steady-state error was about .004 inch. A final value theorem analysis for carriage friction predicted .0036 inch steady-state error, again in excellent agreement.

When all nonlinearities and tower dynamics were included in the model, the peak position error was .0117 inch with .0045 inch steady-state error. These are both within the .020-inch error requirement.

In comparing the sources of position error, all the nonlinearities were insignificant except for the carriage friction. The cause for the large error was traced to the stiffness of the carriage X-drive cable. Figure 4-9 shows the transient response for several points in the X loop ahead of the carriage mass. The large initial difference in velocity at the X-motor output and at the carriage indicates that the X cable is stretching. The stretch continues until the breakaway friction force at the carriage is attained. The motor output and the carriage both settle out to .2 inch/s velocity in a well-behaved manner within .6 second. The motor torque saturates in both directions at 140 in.-lb during the initial transient. The fact that no limit cycling occurs indicates that the control loop is stable. Data runs with the motor torque limit increased to 180 in.-lb also saturated, but showed almost no improvement in the position error response.

If it is necessary to reduce the .020-inch position error requirement, the analysis results indicate that some effort should be made to stiffen the X drive between the motor and the carriage. This can be done by using a heavier cable or redesigning the drive. One solution would be to replace the single motor, two-cable drive with one that uses a pair of stepper motors driving ball screws at each end of the carriage. The stepper motors could be electrically synchronized to avoid cocking the bridge (on the rails at each end) and causing it to jam. A new system analysis would be necessary for this method since the control loop would be significantly different from the one modeled in this study.
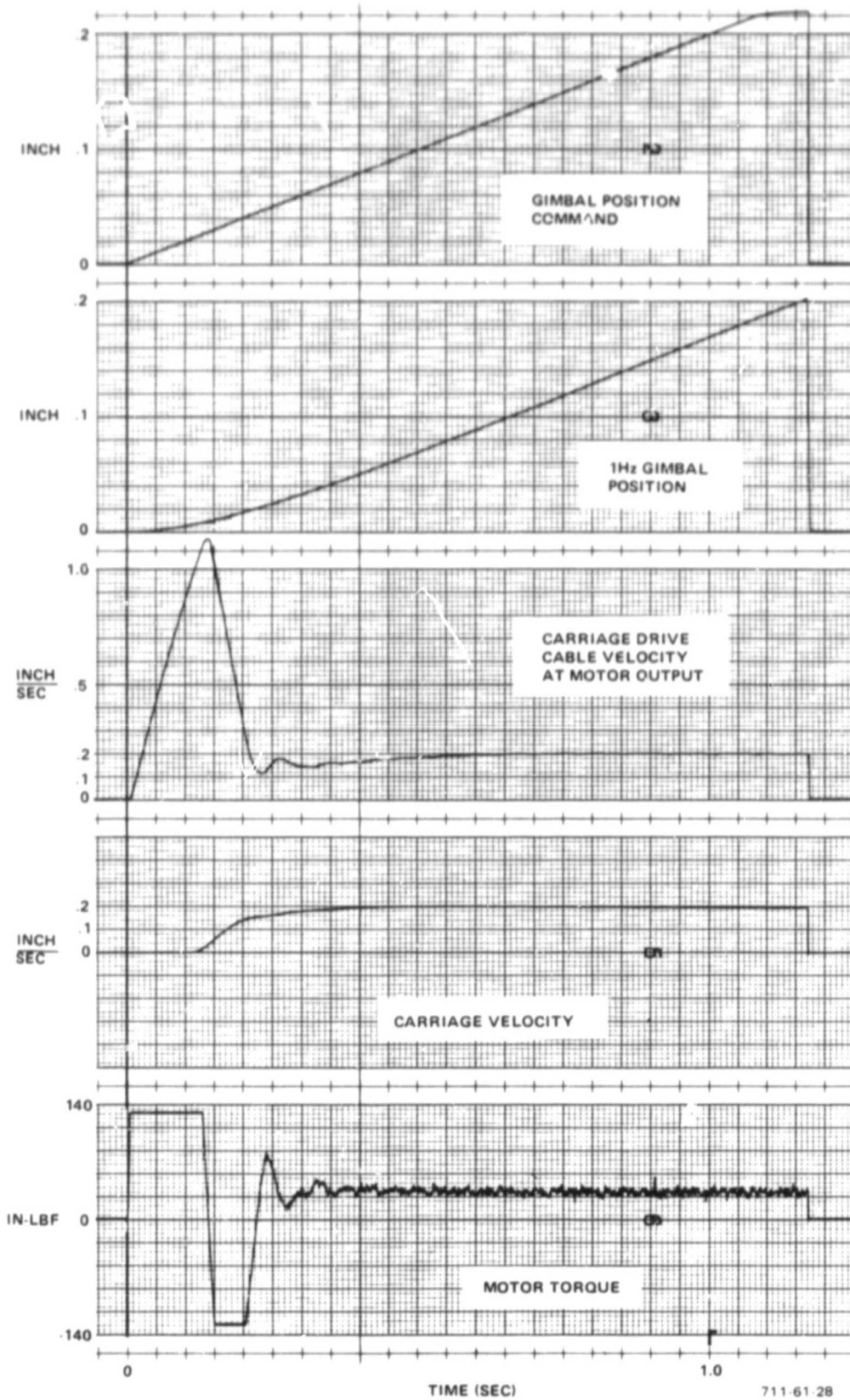
Figure 4-9
ZGTF X-Y Loop Transient Response to Gimbal Slew
Command - All Nonlinearities Included

4-13

4.2   Z-FORCE LOOP

The Z-force loop is designed to apply a constant vertical force on the test item dummy antenna mass to counteract the force of gravity. The Z-loop system model and block diagram shown in Figure 4-10, are the same as those used for the AGS WATF. The changes made in hardware components for the ZGTF loop do not affect the WATF system model. The Z-drive motor will be selected to match the performance of the gimbal torquer used on the WATF. The high-accuracy force transducer for the ZGTF is modeled the same as the one used on the WATF.

A major difference in the WATF and ZGTF loops is the payload mass supported by the cable. The largest mass to be supported by the ZGTF is only one-half the AGS mass. However, this does not affect the loop design because the Z-drive motor acts through a 75:1 gear ratio. The effect of the gear train is to make the motor inertia appear much larger than the load inertia, thus making the loop insensitive to payload mass for the antennas to be tested. This is an advantage for the ZGTF because the loop compensation gain does not have to be changed for each different antenna system.

The compensation for the Z loop is:

$$\frac{K_I}{s} K_A \frac{\dfrac{s^2}{\omega_1{}^2} + \dfrac{1.4s}{\omega_1} + 1}{\dfrac{s^2}{\omega_2{}^2} + \dfrac{1.4s}{\omega_2} + 1} \tag{6}$$

The break frequencies and gain are selected to produce a 100 radians per second open-loop crossover frequency with about 30 degrees phase margin.

The open- and closed-loop Bode gain plots for the Z axis loop are shown in Figure 4-11. The loop has about 10-hertz bandwidth and zero steady-state error for the linear model. An analysis to determine the steady state error with motor friction also results in zero steady state error on force output.

4-14

711-61-29 R1

CABLE FORCE F

CABLE SPRING CONST.

$D_CS + K_C$

DAMPING

Σ Mg

ANTENNA WEIGHT (GRAVITY)

R_D

TORQUE FROM CABLE

Σ X_L $\frac{1}{MS^2}$

X_C

R_D DRUM RADIUS

$^\theta D$

$\frac{1}{J_D S^2}$

MOTOR INERTIA THRU GEARS

Σ

MOTOR TORQUE CONST.

$K_T N_1 N_2$ GEAR RATIOS

MOTOR TORQUE T_D

CONTROLLER GAIN

$G_C(S)$

LOAD CELL

K_{SG}

F_E

Σ

F_C

$$G_C(S) = \frac{K_1}{S} \cdot K_A \frac{\left[\frac{S^2}{W_1^2} + \frac{2\xi}{W_1} S + 1 \right]}{\left[\frac{S^2}{W_2^2} + \frac{2\xi}{W_2} S + 1 \right]}$$

$K_1 = 87.6 \; 1/\text{SEC}$
$K_A = 0.554 \; \text{AMP/VOLT}$
$\xi = 0.5$
$W_1 = 30 \; \text{RAD/SEC}$
$W_2 = 600 \; \text{RAD/SEC}$

UNCOMPENSATED GAIN $K_{OL} = K_A K_{SG} K_T N_1 N_2 \frac{MR_D}{J_D} = .726$ (DIMENSIONLESS)

$K_{SG} = 1.01 \; \text{VOLT/LB}$
$K_T = 0.5 \; \text{FT-LB/AMP}$
$N_1 = 15$
$N_2 = 5$
$J_D = J_m (N_1, N_2)^2 = 2174 \; \text{FT/LB/SEC}^2$
$R_D = 1/6 \; \text{FT.}$
$D_C = 57 \; \text{LB/FT/SEC}$
$K_C = 24,200 \; \text{LB/FT}$
$Mg = 225 \; \frac{\text{LB/SEC}^2}{\text{ft}}$
$M = 225 \; \text{LBm}$

Figure 4-10
ZGTF Z-Axis Tension Control Loop Functional Block Diagram
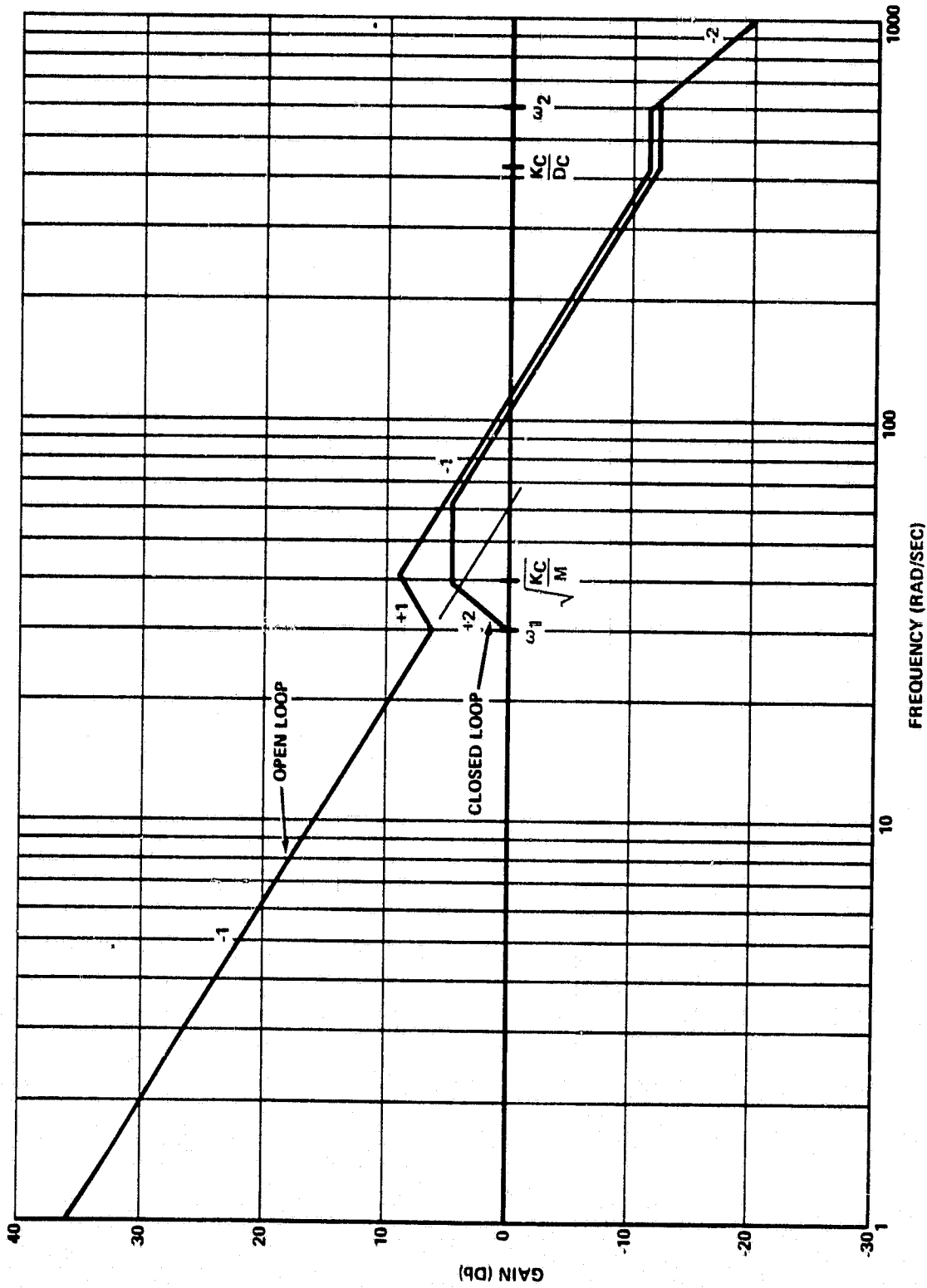
Figure 4-11
WATF Z-Axis Tension Control Loop Bode Gain Plots
(Straight-Line Approximations)

The Z loop like the X and Y loops is affected by changes in cable length. The cable spring constant Kc changes, causing the break frequencies at $\omega = \dfrac{K_c}{M}$ and $\omega = \dfrac{K_c}{D_c}$ to fluctuate. For this reason the compensation break frequencies 1 and 2 were set at the lower limits of the two mechanism frequencies to avoid instability problems.

No computer analysis on the Z loop was done for the ZGTF preliminary design. The stability, gain and phase margins have been demonstrated on the WATF, and at this stage the ZGTF hardware parameters are not defined well enough to make it worthwhile to model the Z loop for fine tuning. Z loop transient modeling should be done at the detailed design stage for the ZGTF.

SECTION 5.0

ANALYSES

SECTION 5.0

ANALYSES

No.

ANALYSIS 5.1

AIR-BEARING TABLE TILT REQUIREMENT

5.1 AIR-BEARING TABLE TILT REQUIREMENT

If the air bearing for the antenna mass rests on an unlevel table, it will tend to slide downhill, assuming no friction is present.
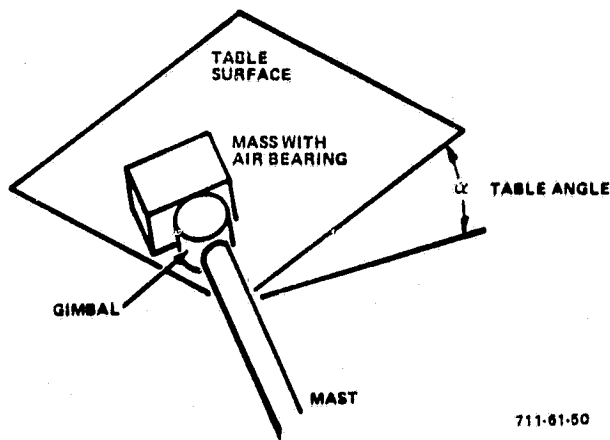
Figure 5-1

Unlevel table will cause a torque error on the gimbal.
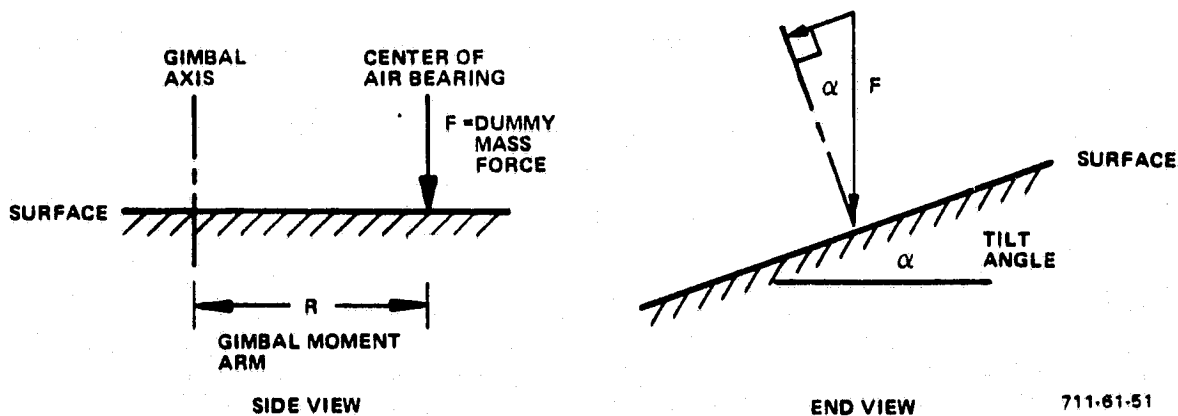
Figure 5-2

The gimbal torque error is

$$Te = FR \tan \alpha = 1 \text{ ounce-inch maximum}$$

for the STAPS antenna system

$$F = 25 \text{ lb} \quad R \approx 16 \text{ inch}$$

$$\tan \alpha = \frac{1 \text{ ounce-inch}}{(25 \text{ lb}) \ 16 \text{ in. } (16 \text{ oz/lb})}$$

$$= \frac{1}{6400}$$

$$\alpha = .00895° = 32 \text{ arcsec} = \frac{1°}{112}$$

ANALYSIS 5.2

ZGTF X-Y TROLLEY POSITION ACCURACY REQUIREMENT

5.2 ZGTF X-Y TROLLEY POSITION ACCURACY REQUIREMENT

5.2.1 ZGTF X-Y Trolley Position Accuracy

Find the maximum position error allowable

THE WORST CASE IS WITH
THE GIMBALS STRAIGHT UP

USE STAPS AS AN EXAMPLE
F = 18.5 LB
16" MOMENT ARM ON GIMBALS
1 OZ-IN. TORQUE LIMIT

(5-1)

711-61-62
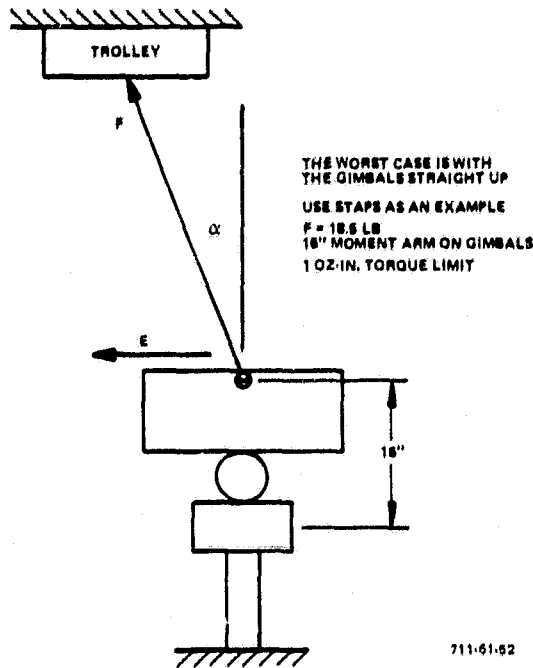
Figure 5-3

$$T_E = E(16") \leq 1 \text{ oz} \cdot \text{in} \quad \text{TORQUE ERROR}$$

$$E_{max} = \frac{1 \cdot \frac{oz \cdot in}{16}}{16 \frac{oz}{lb}} = 3.9 \times 10^{-3} lb \quad \text{FORCE ERROR LIMIT}$$

$$\frac{E}{F} = \frac{F \sin \alpha}{F} = \frac{\text{POSITION ERROR}}{\text{CABLE LENGTH}} = \frac{X_E}{L} = \frac{3.9 \times 10^{-3} lb}{18.5 lb}$$

$$X_E = 2.1 \times 10^{-4} L \quad \text{error proportional to cable length}$$

$$\alpha = \sin^{-1} \frac{E}{F} = .0121°$$

For L = 10 ft X_E = .025" max X-Y position error

5.2.2 ZGTF Z-Axis Force Accuracy

USE STAPS AS AN EXAMPLE
WORST CASE IS WITH GIMBALS
AT 90°
F = 18.5 LB
ERROR TORQUE IS 1 OZ IN.
= T_E

16"

711-61-93
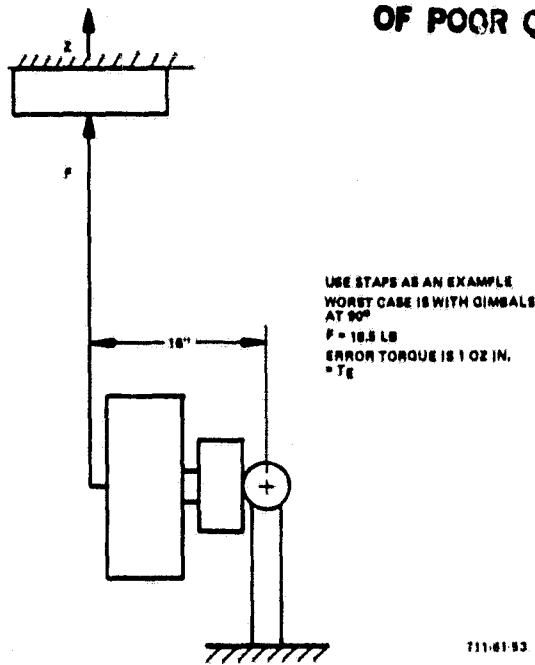
Figure 5-4

$$T_E = (-18.5\,lb + F_{ACTUAL})(16") = 1\,oz\,in = F_E(16") \qquad (5-2)$$

$$F_E = \frac{1\,oz\,in}{16\frac{16\,oz}{lb}} = 3.9 \times 10^{-3}\,lb \quad \text{allowable force error}$$

$$\frac{F_E}{F} = \frac{3.9 \times 10^{-3}\,lb}{18.5\,lb} = 2.1 \times 10^{-4}$$

Force Error = .02 percent

ANALYSIS 5.3

WATF FORCE ERROR ON AGS

5.3 WATF FORCE ERROR ON AGS

Find the position error between the WATF and the AGS
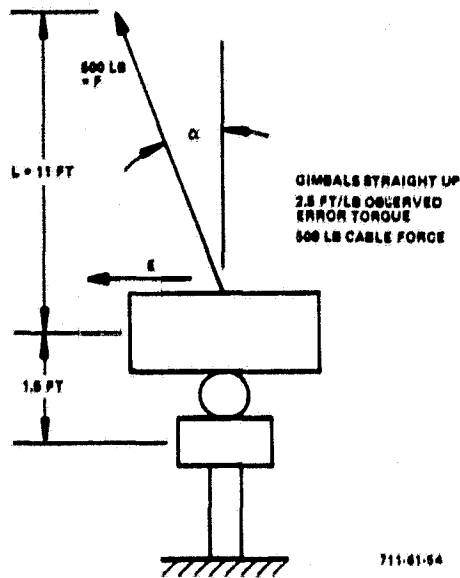
Figure 5-5

$$E = \frac{2.5 \, ft \, lb}{1.5 \, ft} = 1.67 \, lb = 500 \, lb \sin \alpha \tag{5-3}$$

$$\alpha = \sin^{-1} \left(\frac{1.67 \, lb}{500 \, lb} \right) = .19°$$

Trolley X-Y Position Error = X_E

$$\frac{X_E}{L} = \frac{E}{\cdot F} = \frac{1.67}{500} \tag{5-4}$$

$$X_E = 11 \, ft \, \frac{1.67}{500} = .44 \, in.$$

Z-Axis Error
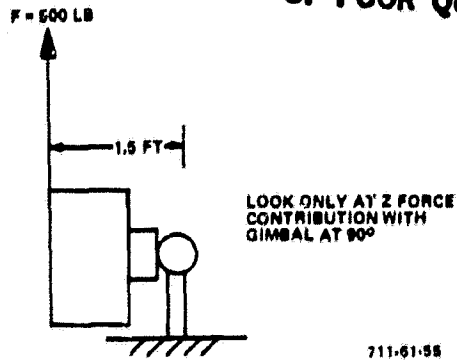
Figure 5-6

$$\frac{2.5 \, ft \, lb}{1.5 \, ft} = 1.67 \, lb \quad \text{FORCE ERROR ON Z-AXIS} \tag{5-5}$$

$$\frac{1.67}{500} = .0033$$

.33 percent error on Z-axis loop

ANALYSIS 5.4

TORQUE ERROR CAUSED BY MASS SUSPENSION LOCATION

5.4   TORQUE ERROR CAUSED BY MASS SUSPENSION LOCATION (Figure 5-7)

The antenna mass is supported from the point at Fc, located ΔZ from the dummy mass center of gravity, W_p.   The variables are defined as:

W_p - dummy mass weight

W_G - gimbal pair weight

Z_{CM} - distance from lateral gimbal axis to antenna center of mass

Z_G - 1/2 distance between gimbal axes

ΔZ - distance from antenna center mass to suspension point

γ - lateral gimbal angle, zero degrees straight up

σ - elevation gimbal angle, zero degrees straight up

F_C - force on suspension cable, straight up

T_{lat} - torque error on lateral gimbal

T_{el} - torque error on elevation gimbal

The force exerted by the cable is the dummy mass weight plus half the weight of the gimbals.
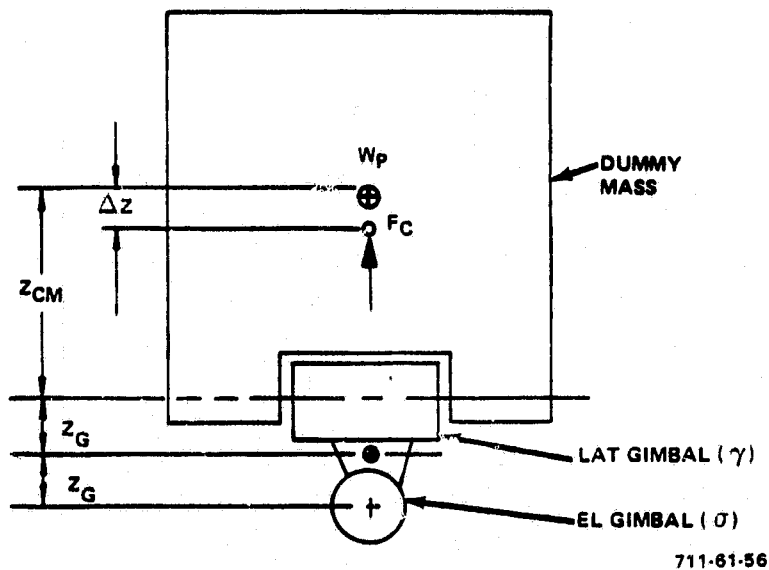
Figure 5-7

$$T_{LAT} = F_c (Z_{cm} - \Delta Z) \sin \gamma \cos \sigma - W_p Z_{cm} \sin \gamma \cos \sigma = \qquad (5\text{-}6a)$$

$$\sin \gamma \cos \sigma [F_c (Z_{cm} - \Delta Z) - W_p Z_{cm}]$$

$$\text{Let} \quad F_c = \left(W_p + \frac{W_c}{2}\right) = \frac{(2W_p + W_c)}{2} \quad \text{and} \quad \Delta Z = \frac{W_c Z_{cm}}{(2W_p + W_c)}$$

$$T_{LAT} = \sin \gamma \cos \sigma \left[\left(\frac{2W_p + W_c}{2}\right)\left(Z_{cm} - \frac{W_c Z_{cm}}{(2W_p + W_c)}\right) - W_p Z_{cm}\right]$$

$$T_{LAT} = \sin \gamma \cos \sigma \left[\frac{(2W_p + W_c)}{2} \cdot \frac{2W_c Z_{cm}}{(2W_p + W_c)} - W_p Z_{cm}\right] \equiv 0$$

$$T_{EL} = F_c \left[(Z_{cm} - \Delta Z)\cos \gamma + 2Z_G\right] \sin \sigma - W_p \left[Z_{cm} \cos \gamma + 2Z_G\right] \sin \sigma \qquad (5\text{-}6b)$$
$$- W_c Z_G \sin \sigma$$

$$T_{EL} = \sin \sigma \left[(F_c - W_p)(Z_{cm} \cos \gamma + 2Z_G) - F_c \Delta Z \cos \gamma - W_c Z_G\right]$$

$$\text{Let} \quad F_c = \left(W_p + \frac{W_c}{2}\right) = \frac{(2W_p + W_c)}{2} \quad \text{and} \quad \Delta Z = \frac{W_c Z_{cm}}{(2W_p + W_c)}$$

$$T_{EL} = \sin \sigma \left[\left(\frac{(2W_p + W_c)}{2} - W_p\right)(Z_{cm} \cos \gamma + 2Z_G) - \frac{2W_p + W_c}{2} \cdot \left(\frac{W_c Z_{cm}}{2W_p + W_c}\right)\cos \gamma - W_c Z_G\right]$$

$$T_{EL} = \sin \sigma \left[\frac{W_c}{2}(Z_{cm} \cos \gamma + 2Z_G) - \frac{W_c Z_{cm}}{2} \cos \gamma - W_c Z_G\right] \equiv 0$$

Torque

error = 0 for all angles with the single-point suspension

ANALYSIS 5.5

ZGTF X-Y CARRIAGE ERROR SENSOR

5.5   ZGTF X-Y CARRIAGE ERROR SENSOR

An optical sensor will be used which senses the position of a beam of laser light reflected off a mirror at the bottom of the Z-drive cable and on top of the Z-axis load cell.
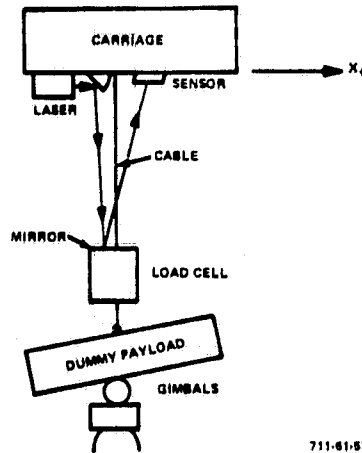
Figure 5-8

5.5.1   Cube Corner Mirror

The light reflects in the opposite direction from which it enters the mirror. The reflected beam is reflected the same distance from the mirror center as the incident beam, on the opposite side of the mirror.
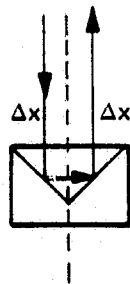
FOR SMALL ANGLE
$$x_{M1} = L_1 2 \sin \alpha$$
$$= L_1 2 \alpha$$
$$= 2(x_{LINK} - x_{CARRIAGE})$$

CUBE CORNER MIRROR

$x_{CARRIAGE} \rightarrow$

$|x_{M1} \rightarrow|$ MEASURED LIGHT DISPLACEMENT

X LINK

L_1

L_2
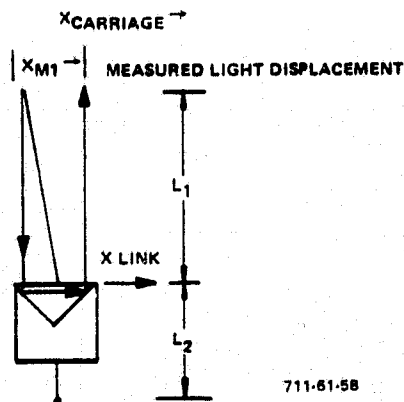
711-61-58

Figure 5-9

A cube corner mirror measures cable angle only.

$$\alpha = \frac{X_{m1}}{2L_1}$$

Flat Mirror

Light reflects at twice the angle of the mirror to the incident beam.

(5-7)

$$-X_{M2} = L_1 \sin 2\theta$$
$$\approx L_1 \, 2\theta$$

$$= 2\frac{L_1}{L_2}(X_{payload} - X_{link})$$

$$X_{payload} - X_{link} = \frac{-X_{m2}}{2}\frac{L_2}{L_1}$$
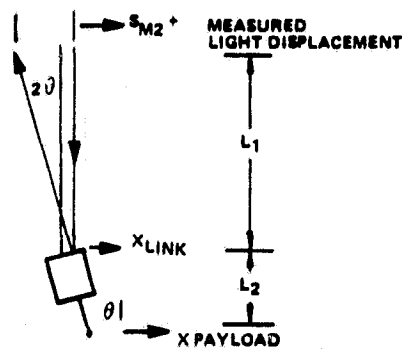
Figure 5-10

The flat mirror measures the link angle only.

The error between the carriage and the payload is

$$Xerr = X_{carriage} - X_{payload}$$

$$= (X_{carriage} - X_{link}) + (X_{link} - X_{payload})$$

$$Xerr = \frac{X_{m1}}{2} - \frac{X_{m2}}{2L_1}L_2$$

Any errors in position measurement due to cable dynamics are eliminated by using both the flat and cube corner mirrors.

5.5.2 Cable Dynamics and Measured Displacements

CABLE TENSION

ANGLES ARE POSITIVE
COUNTERCLOCKWISE

711-61-60
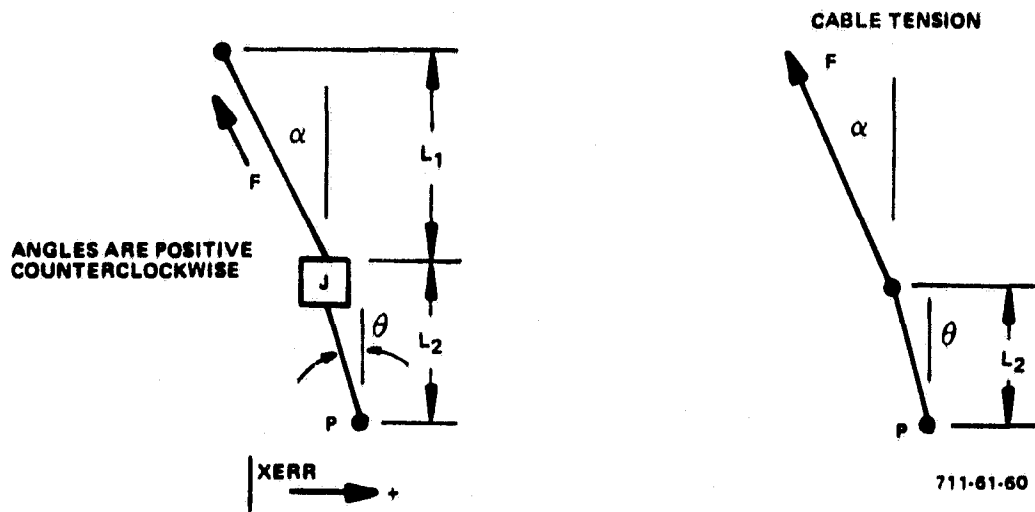
Figure 5-11

The sum of the torques about the payload attachment point is

$$\sum T_P = 0 = F_{L_2}(\sin\alpha\cos\theta - \cos\alpha\sin\theta) + J\ddot\theta \qquad (5\text{-}8)$$

$$\approx F_{L_2}(\alpha - \theta) + J\ddot\theta$$

$$\alpha = \frac{X_{M_1}}{2L_1} \qquad \theta = \frac{-X_{M_2}}{2L_1}$$

X_{err} = displacement between top of cable and suspension point.

The relation between measurements with the two mirrors is

$$0 = J\frac{\ddot X_{M_1}}{2L_1} + \frac{F_{L_2}}{2L_1}(X_{M_1} + X_{M_2}) \qquad (5\text{-}9)$$

$$(JS^2 + F_{L_2})X_{M_2} = -F_{L_2}X_{M_1}$$

$$X_{M_2} = \left(\frac{-F_{L_2}}{JS^2 + F_{L_2}}\right)X_{M_1} = \left(\frac{-1}{\frac{JS^2}{F_{L_2}} + 1}\right)X_{M_1}$$

For the flat mirror above measure Xm2 only

(5-10)

$$X_{an} = \frac{X_{M_1}}{2} - X_{M_2} \frac{L_2}{2L_1}$$

$$= \frac{X_{M_2}}{2} \left[-\left(\frac{JS^2}{FL_2} + 1\right) - \frac{L_2}{L_1} \right]$$

$$X_{an} = \frac{-(L_1 + L_2)}{2L_1} \left(\underbrace{\frac{JL_1 S^2}{FL_2(L_1 + L_2)}} + 1 \right) X_{M_2}$$

cable frequency (undamped)

For the cube corner mirror alone measure Xm1 only

(5-11)

$$X_{an} = \frac{X_{M_1}}{2} - X_{M_2} \frac{L_2}{2L_1}$$

$$= \frac{X_{M_1}}{2} \left[1 - \frac{L_2}{L_1} \left(\frac{-FL_2}{JS^2 + FL_2} \right) \right]$$

cable frequency (undamped)

$$X_{an} = X_{M_2} \frac{(L_1 + L_2)}{L_1} \left(\frac{\overbrace{\frac{JL_1 S^2}{FL_2(L_1 + L_2)}} + 1}{\underbrace{\frac{JS^2}{FL_2}} + 1} \right)$$

link pendulum frequency (undamped) tulum

In either case, the use of only one mirror introduces a pair of undamped poles in the position measurement dynamics.

ANALYSIS 5.6

ZGTF X-Y VERTICAL DEFLECTION AND FREQUENCY

5.6   ZGTF X-Y VERTICAL DEFLECTION AND FREQUENCY

Bridge frequency with trolley and load
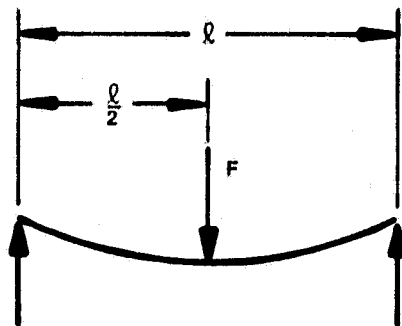
$$Y \text{ MAX} = \frac{F \ell^3}{48EI}$$

$I = 244 \text{ IN.}^4$

$E = 28 \times 10^6 \text{ PSI}$

$F = \frac{200 + 200}{2} \text{ LB} = 200 \text{ LB}$

$\ell = 77''$

711-61-61

Figure 5-12

$$y_{max} = \underline{2.78 \times 10^{-4} \text{ inch}}$$

(5-12)

$$K = \frac{F}{y_{max}} = \frac{48EI}{\ell^3} = 7.18 \times 10^{-5} \frac{lbf}{in}$$

$$\omega_1 = \sqrt{\frac{K}{m}} = \sqrt{\frac{48EI}{m\ell^3}g} = 1177 \frac{rad}{s}$$

$$f_1 = 187 \text{ Hz}$$

With bridge beam weight
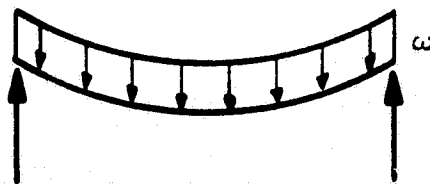
$$Y \text{ MAX} = \frac{5\omega\ell^4}{384EI}$$

$\omega = 28 \text{ LB/FT} = 2.333 \text{ LB/IN.}$

$Y \text{ MAX} = 1.56 \times 10^{-4} \text{ IN}$

711-61-62

Figure 5-13

(5-13)

$$\text{generalized mass} = \int_0^l \phi_i^2(x)\, m(x)\, dx = \int_0^l \frac{M_o}{l} 2\left(\sin^2\left(\frac{n\pi x}{l}\right)\right) dx$$

$$= M_o = 180\ lb$$

$$\text{generalized stiffness}\ K_e = \int_0^l EI\left(\phi_i''(x)\right)^2 dx$$

$$= \frac{EI\, n^4 \pi^4}{l^4} \int_0^l 2 \sin^2 \frac{n\pi x}{l}\, dx$$

$$K_i = \frac{EI\, n^4 \pi^4}{l^3} = \frac{EI\, \pi^4}{l^3}\quad \text{for } n = 1$$

$$K = 1.46 \times 10^6\ \frac{lb}{in}$$

$$\omega_2 \sqrt{\frac{K}{m}} = 291\ Hz$$

$$\frac{1}{f_{bridge}^2} = \frac{1}{f_1^2} + \frac{1}{f_2^2} \qquad\qquad f_{bridge} = 156\ Hz$$

Gantry frequency due to beam weight

$$\ell = 95''$$

711-61-63
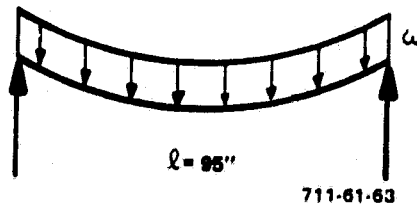
Figure 5-14

W = 28 lbf/ft = 2.33 lbf/in.

(5-14)

$$\omega = \pi^2 \sqrt{\frac{EIg}{W\ell^4}} = 1178\ rad/s \qquad \text{(from "Vibration," Thompson, p. 204)}$$

$$f_3 = 188\ Hz$$

5-15

Gantry frequency due to bridge
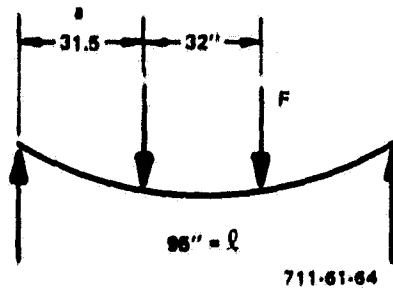
Figure 5-15

$$y_{max} = \frac{Fa}{24EI}(4a^2 - 3\ell^2) \qquad F = \frac{1250}{4} \, lb = 312 \, lb \qquad (5\text{-}15)$$

$$K = \frac{F}{y_{max}} = \frac{24EI}{a(-4a^2 + 3\ell^2)}$$

$$\omega = \sqrt{\frac{k}{m}} = \sqrt{\frac{24EIg}{a(-4a^2 + 3\ell^2)m}}$$

$$f_4 = 528 \, rad/s = 84 \, Hz$$

$$\frac{1}{f^2} = \frac{1}{f_{xx}^2} + \frac{1}{f_3^2} + \frac{1}{f_4^2} = 69 \, Hz$$

Reference: _Formulas for Stress and Strain_, Roark, 5th Edition.

The first mode frequency of the ZGTF tower, in the vertical direction, is at about 69 hertz.

TABLE 5-1

WATF AND ZGTF WEIGHTS AND DEFLECTIONS

	WATF Using 10" I-Beam 25.4 (lb)	WATF Using W 19 x 26 (lb)	WATF (lb)	ZGTF 3/10/81
		WEIGHT		
Trolley	200.	200.	200.	200
Loan	1000.	1000.	1000.00	200
Bridge	615.2	938.16	977.07	847
Gantry	1066.8	1085.2	1112.98	853
TOTAL	2882.0	3223.36	3290.05	2100
		DEFLECTIONS		
Bridge	.006082	.002952	.002998	
Gantry	.01998	.01103	.01194	
TOTAL	.02606	.013982	.02241	

ANALYSIS 5.7

ZGTF TOWER STRUCTURAL MODES

5.7 ZGTF TOWER STRUCTURAL MODES

The ZGTF tower model analysis was done with the aid of the SAP VI computer program developed at the University of California at Berkley. The original design for the tower had vertical legs, as shown in the sketch of the original WATF tower. It had a first mode frequency of about 15 hertz, which was too low.

The revised design looks like an oil derrick - 18 feet wide at the bottom and 6 feet wide at the top. This has a first mode of 23 hertz, which is acceptable.

C-2
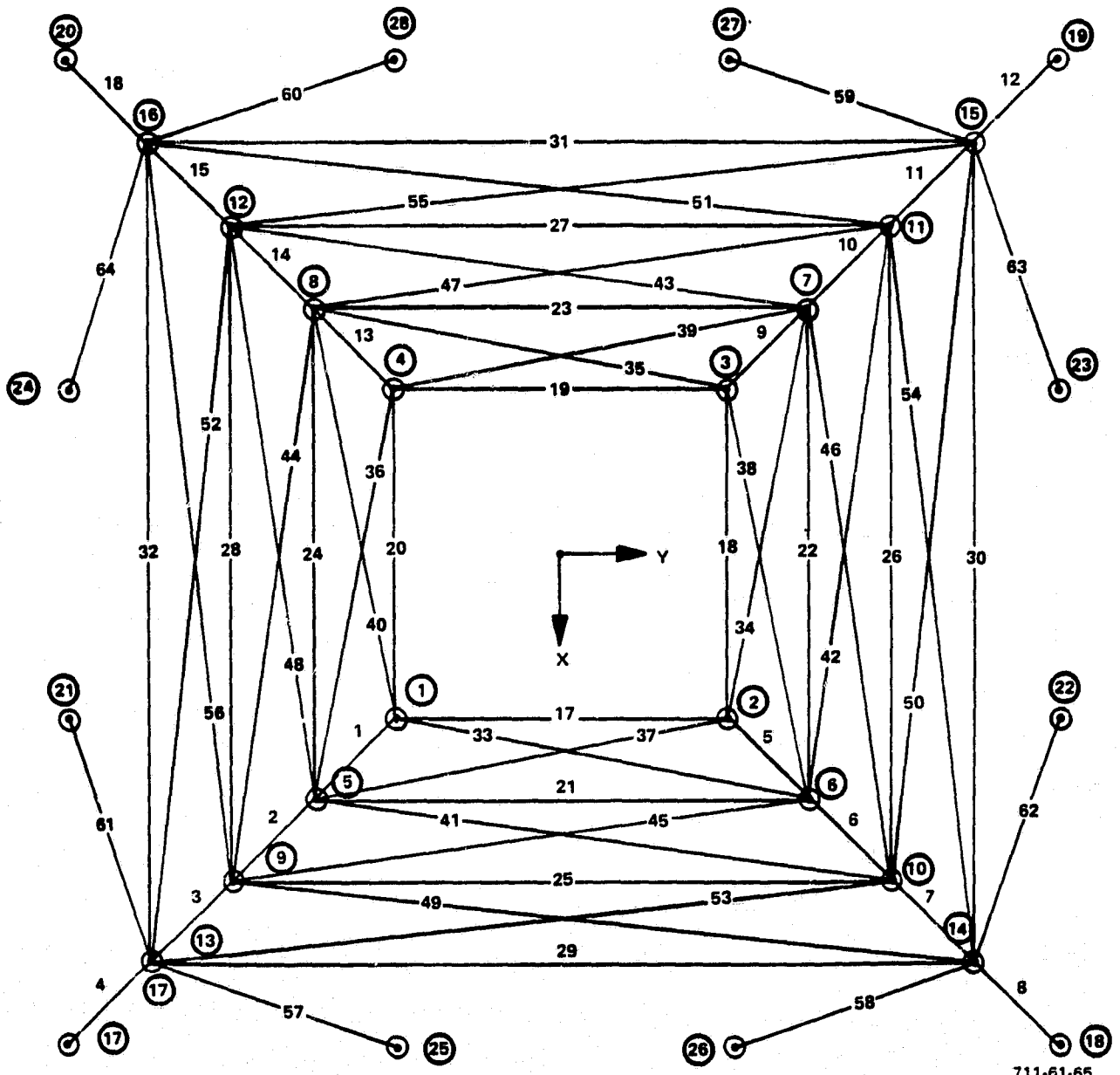
Figure 5-16
Top View of ZGTF Tower Modal Model
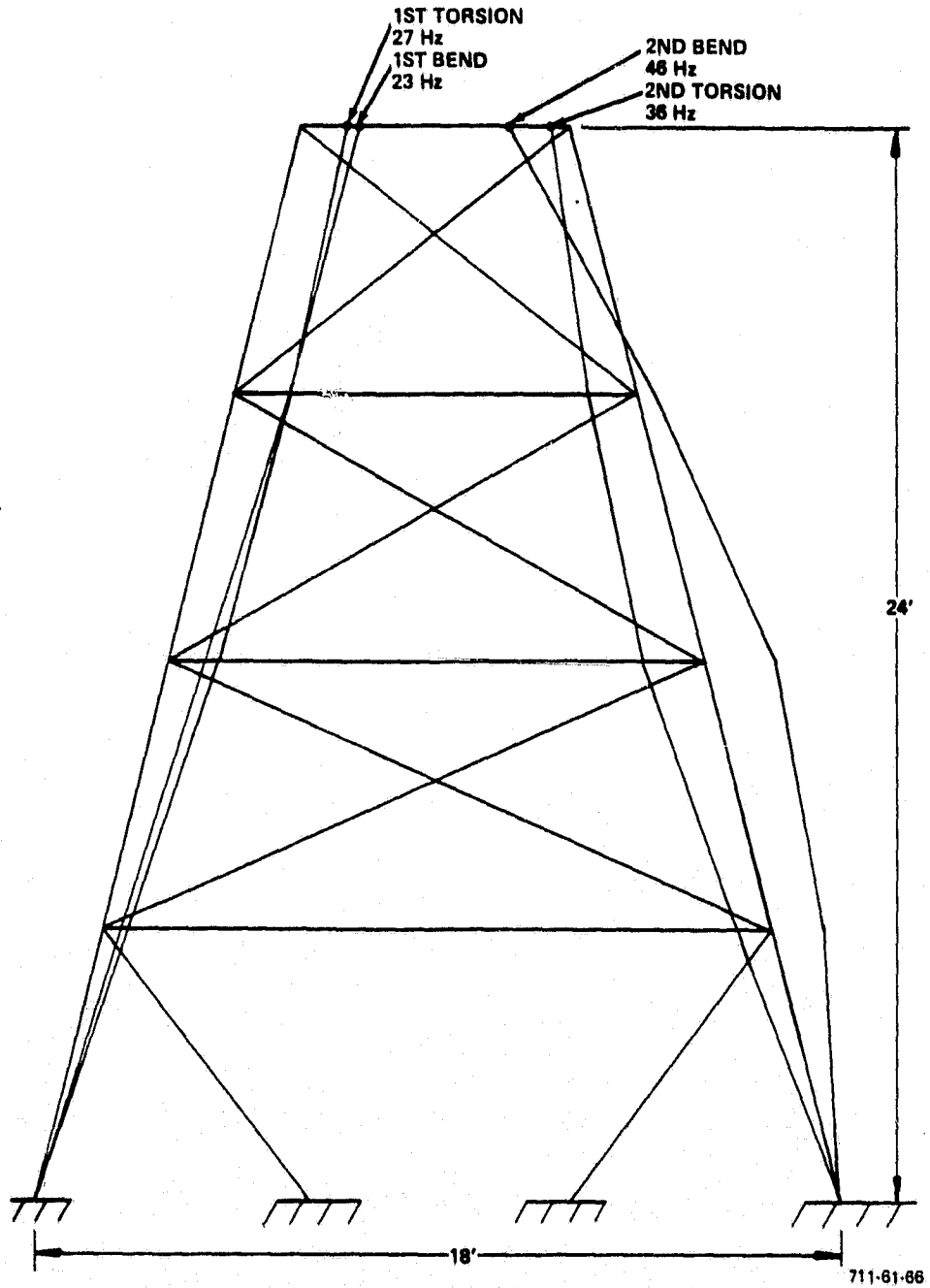
Figure 5-17
Side View of ZGTF Tower Modal Model, Relative Deflections Shown
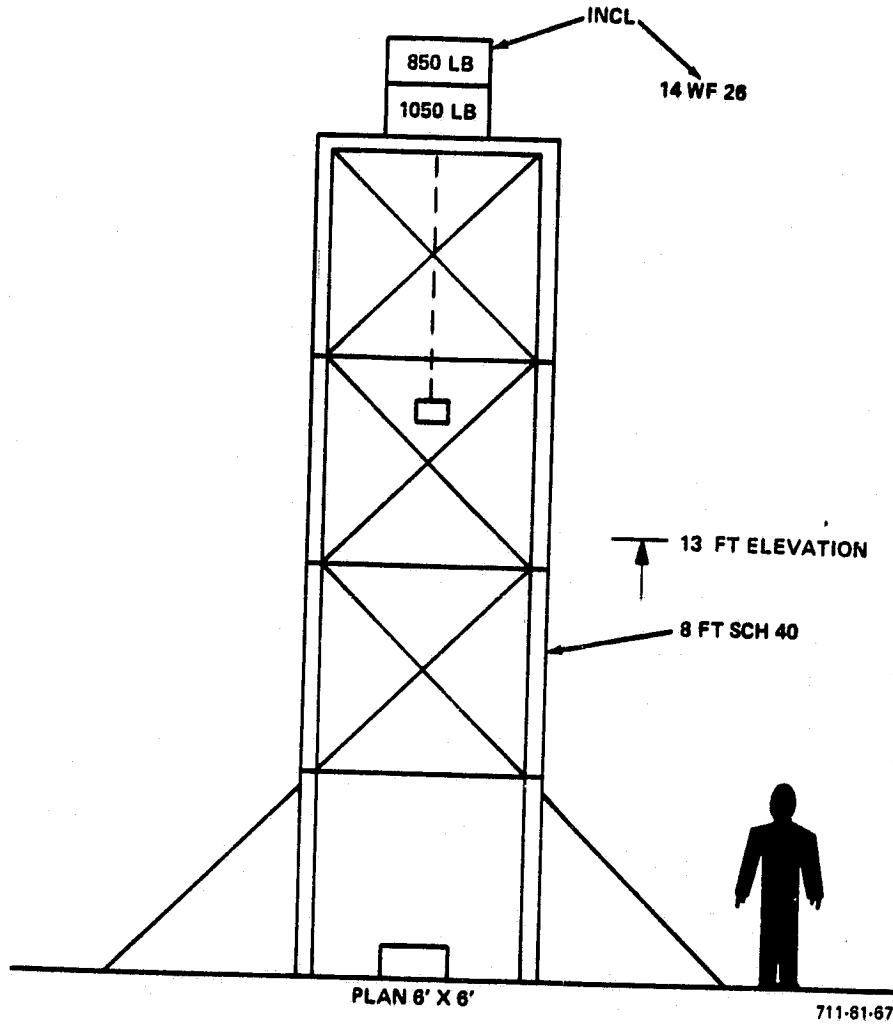
Figure 5-18
Original ZGTF Tower Design

ANALYSIS 5.8

Z-AXIS LOOP ANALYSIS

5.8 Z-AXIS CONTROL LOOP ANALYSIS

The analysis shown is from the updated WATF Z-loop design (9/2/80), Analysis No. 8085.5.1-60. The ZGTF Z-loop design is identical to the WATF design as far as the system analysis is concerned.

The original WATF Z-axis tension-control/loop-design goal was to provide a 10-hertz minimum control-loop bandwidth. This goal was based upon providing a loop bandwidth at least a factor of ten greater than the AGS gimbal control loop nominal bandwidth of 1 hertz to minimize the effect of the WATF upon AGS testing. The original WATF Z-axis tension-control loop bandwidth was approximately 2.5 hertz (Figure 5-19). This was primarily due to designing the loop based upon an incorrect value of the Z-axis drive inertia. However, the WATF frame/yoke had a bending mode at approximately 6 hertz, which also influenced the maximum achievable bandwidth. A discussion of present WATF Z-axis tension-control loop design follows.

5.8.1 WATF Z-Axis Tension-Control Loop Design Synthesis

The present WATF Z-axis tension-control loop block diagram is shown in Figure 5-20. It can be simplified to the forms shown in Figure 5-21. The simplification which assumes $J_D \gg MR_D^2$ is valid since

$$J_D = J_m (N_1 N_2)^2 = (0.012)(75)^2 = 67.5 \text{ slug-ft}^2$$

$$MR_D^2 = (14)(1/6)^2 = 0.389 \text{ slug-ft}^2$$

The lower block diagram in Figure 5-21 shows that the control loop open-loop transfer function is

(5-16)

$$\frac{F}{F_c} = \frac{K_{16} K_1 K_A K_T N_1 N_2 M R_o \left[\frac{S^2}{\omega_1^2} + \frac{2\rho_1}{\omega_1} S + 1\right] \left(\frac{D_c}{K_c} S + 1\right)}{J_o S \left[\frac{M}{K_c} S^2 + \frac{D_t}{K_c} S + 1\right] \left[\frac{S^2}{\omega_2^2} + \frac{2\rho_2}{\omega_2} S + 1\right]}$$

Substituting the parameter values shown in Figure 5-20 into the expression for the open loop transfer function yields

(5-17)

$$G_{oL}(S) = \frac{F}{F_c} = \frac{63.54}{S} \times \frac{\left[\frac{S^2}{(30)^2} + \frac{(2)(.5)}{(30)} S + 1\right] \left(\frac{S}{425} + 1\right)}{\left[\frac{S^2}{(41.6)^2} + \frac{(2 \times .049)}{(41.6)} S + 1\right] \left[\frac{S^2}{(600)^2} + \frac{(2)(.5)}{(600)} S + 1\right]}$$

The closed-loop transfer function is

(5-18)

$$\frac{F}{F_c} = \frac{G_{oL}(S)}{1 + G_{oL}(S)} = \frac{\left[\frac{S^2}{(30)^2} + \frac{(2)(.5)}{(30)} S + 1\right] \left(\frac{S}{425} + 1\right)}{\left[\frac{S^2}{(39.44)^2} + \frac{(2)(.675)}{(39.44)} S + 1\right] \left(\frac{S}{62.6} + 1\right) \left[\frac{S^2}{(637)^2} + \frac{(2)(.353)}{(637)} S + 1\right]}$$

The straight-line approximations to the Bode gain plots for both the open- and closed-loop transfer functions are presented in Figure 5-22.

5-23

Figure 5-22 also indicates that the closed-loop, -3 decibel bandwidth is approximately 150 radians per second (23.9 hertz). Note that the bandwidth is greater than the resonant frequency of the cable/dummy payload which is at 41.6 radians per second (6.62 hertz). The second-order lag at 41.6 radians per second due to this resonance is approximately canceled by the double lead at 30 radians per second in the loop compensation. The resonant frequency of the cable/dummy payload will vary with cable length because the cable spring constant (Kc) is a function of cable length.

The cable spring constant used in the original Z-axis tension-control loop design was 68,500 16/ft (Reference A1). This value of cable spring constant came from a test on a 2-inch long specimen of cable which indicated the cable spring constant was

$$\kappa_c(\text{lb/ft}) = \frac{750,000 \text{ lb}}{\text{Cable Length (ft)}}$$

and assumed an 11-foot cable length. However, the resonant frequency observed on the hardware with a known payload weight did not agree with the frequency predicted when using this value of cable spring constant. Consequently, another cable test was performed on a 10.5-inch specimen of cable which determined that the cable spring constant is,

$$K_c(\text{lb/ft}) = \frac{290,280 \text{ lb}}{\text{Cable Length (ft)}}$$

assuming a 12-foot cable length gives Kc = 24,200 lb/ft, which is the value used in this analysis. The original cable test (11 May 1979) is documented in Reference B3, and the later cable test (12 December 1979) is documented in Reference B4.

The apparent inertia at the output shaft of the worm gear is approximately

$$J_D = J_m (N_1 N_2)^2 = (0.012)(15 \times 5)^2 = 67.5 \text{ slug-ft}^2$$

Figure 5-19
ZGTF Z-Axis Tension-Control Loop Functional Block Diagram

$$G_C(S) = \frac{K_1}{S} \cdot K_A \frac{\left[\frac{S^2}{\omega_1^2} + \frac{2\zeta_1}{\omega_1} S + 1 \right]}{\left[\frac{S^2}{\omega_2^2} + \frac{2\zeta_2}{\omega_2} S + 1 \right]}$$

$K_1 = 87.6/SEC$

$K_A = 0.554$ AMP/VOLT

$\zeta_1 = 0.5$

$\omega_1 = 30$ RAD/SEC

$\zeta_2 = 0.5$

$\omega_2 = 600$ RAD/SEC

UNCOMPENSATED GAIN $K_{OL} = K_A K_{SG} K_T N_1 N_2 \dfrac{MRD}{J_D} = .726$ DIMENSIONLESS

$K_{SG} = 1.01$ VOLT/LB

$K_T = 0.5$ FT-LB/AMP

$N_1 = 15$

$N_2 = 5$
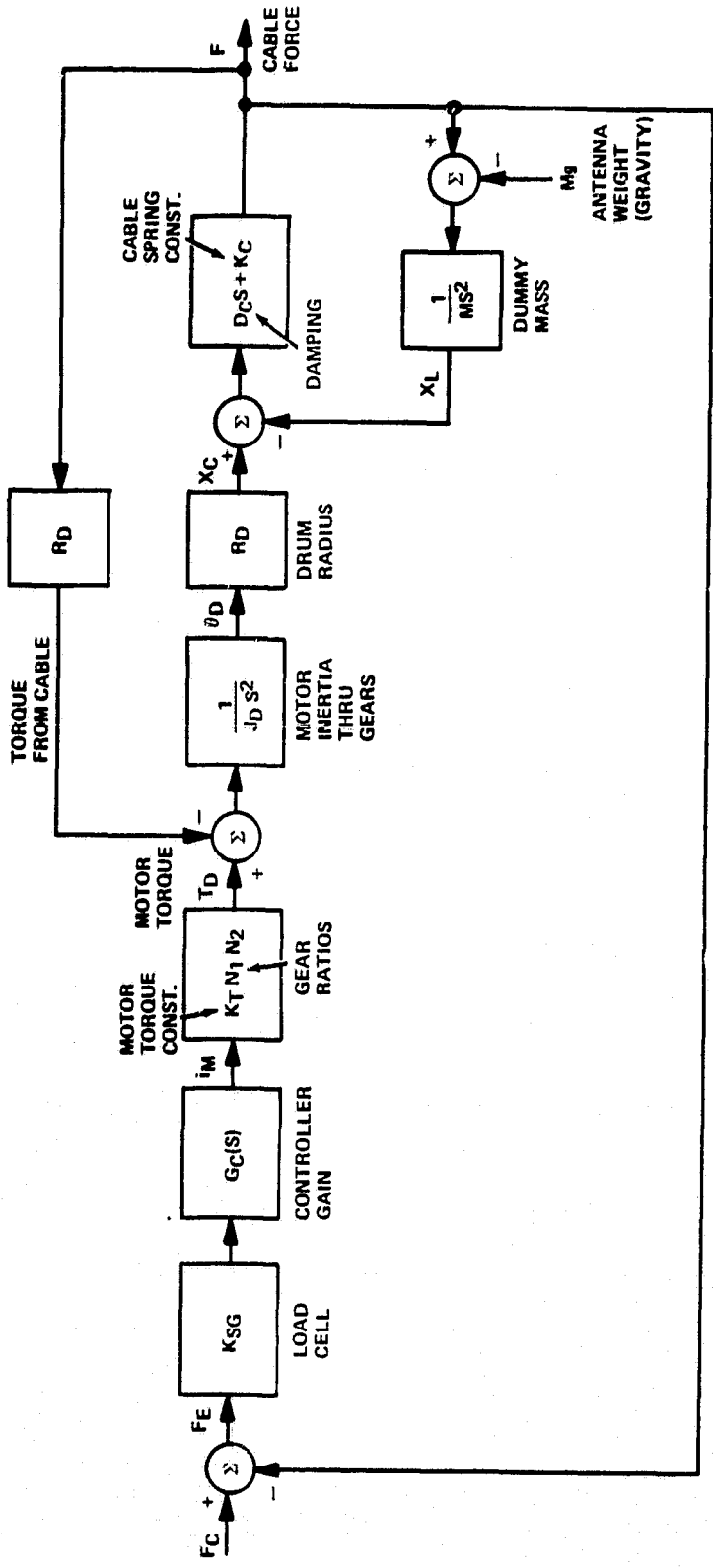
$J_D \simeq J_M (N_1 N_2)^2 = 2174$ FT-LBF-SEC^2

$R_D = 1/6$ FT

$D_C \simeq 57$ LB/FT/SEC

$K_C = 24,200$ LB/FT

$Mg = 225 \dfrac{\text{LBF SEC}^2}{\text{FT}}$

$M = 225$ LBM

711-61-68
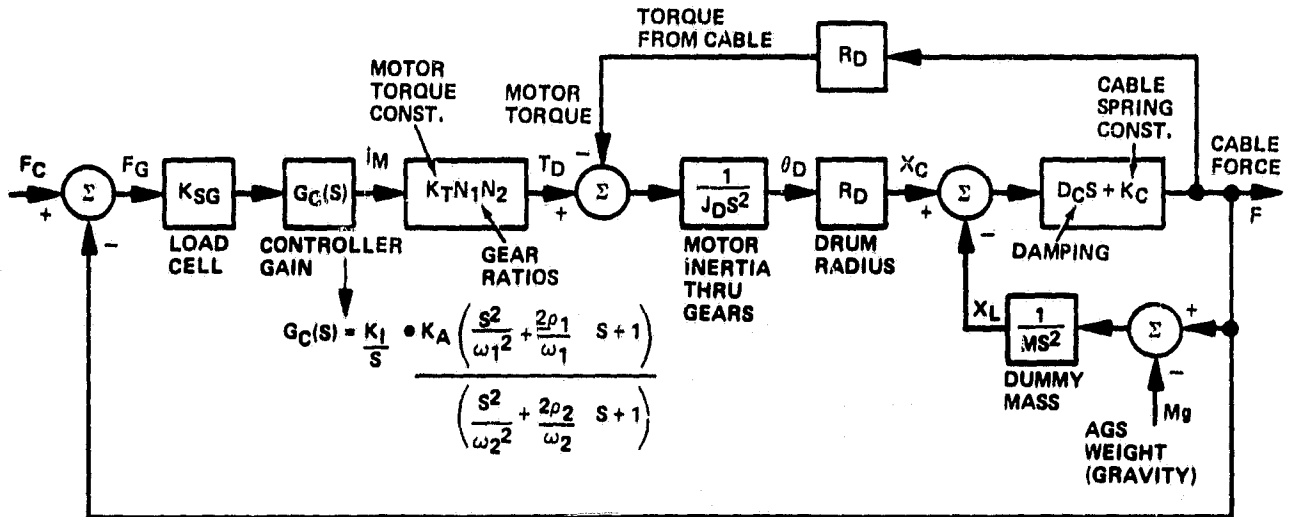
K_{SG} = 1.01 VOLT/LB
K_T = 0.5 FT·LB/AMP
N_1 = 15
N_2 = 5
$J_D \simeq J_m (N_1 N_2)^2 = (0.012)(75)^2$ = 67.5 SLUG·FT^2
R_D = 1/6 FT
$D_C \simeq$ 57 LB/FT/SEC
K_C = 24,200 LB/FT
M = 14 SLUGS $\left(\dfrac{LB/SEC^2}{FT} \right)$
Mg = 450.5 LBM

K_I = 87.6 1/SEC
K_A = 0.554 AMP/VOLT
ρ_1 = 0.5
ω_1 = 30 RAD/SEC
ρ_2 = 0.5
ω_2 = 600 RAD/SEC
UNCOMPENSATED $K_{OL} = K_A K_{SG} K_T N_1 N_2 \dfrac{M R_D}{J_D}$ = .726 DIMSIONLESS

711·61·69

Figure 5-20
Present WATF Z-Axis Tension-control Loop Functional Block Diagram
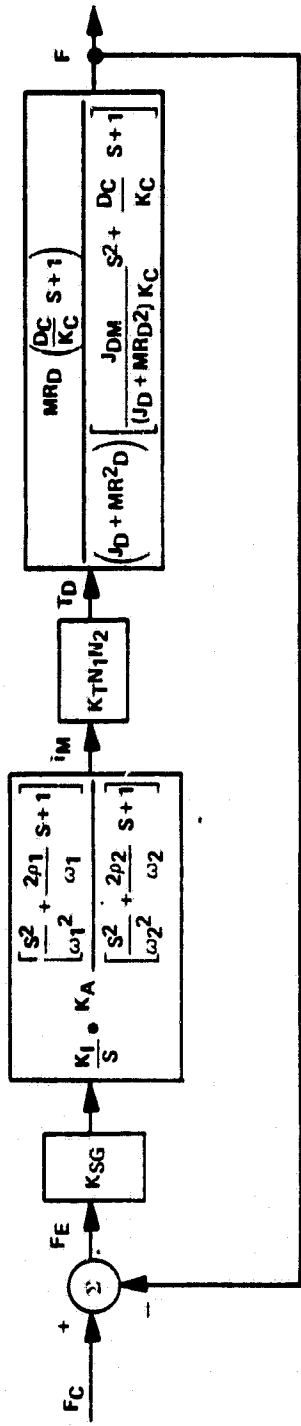
5-26
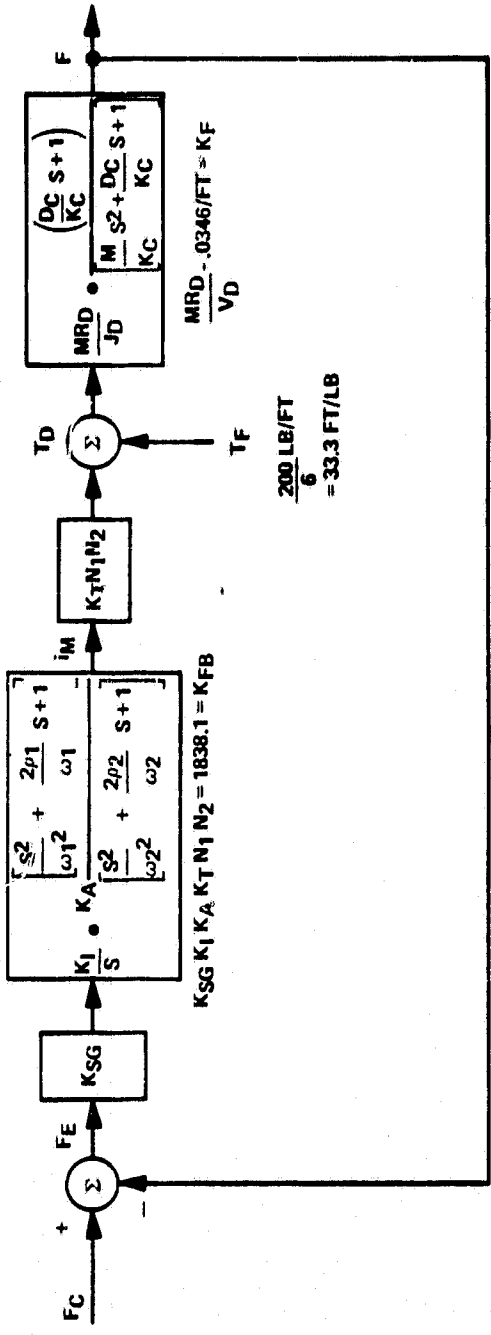
Figure 5-21
WATF Z-Axis Tension-control Loop Simplified Functional Block Diagrams
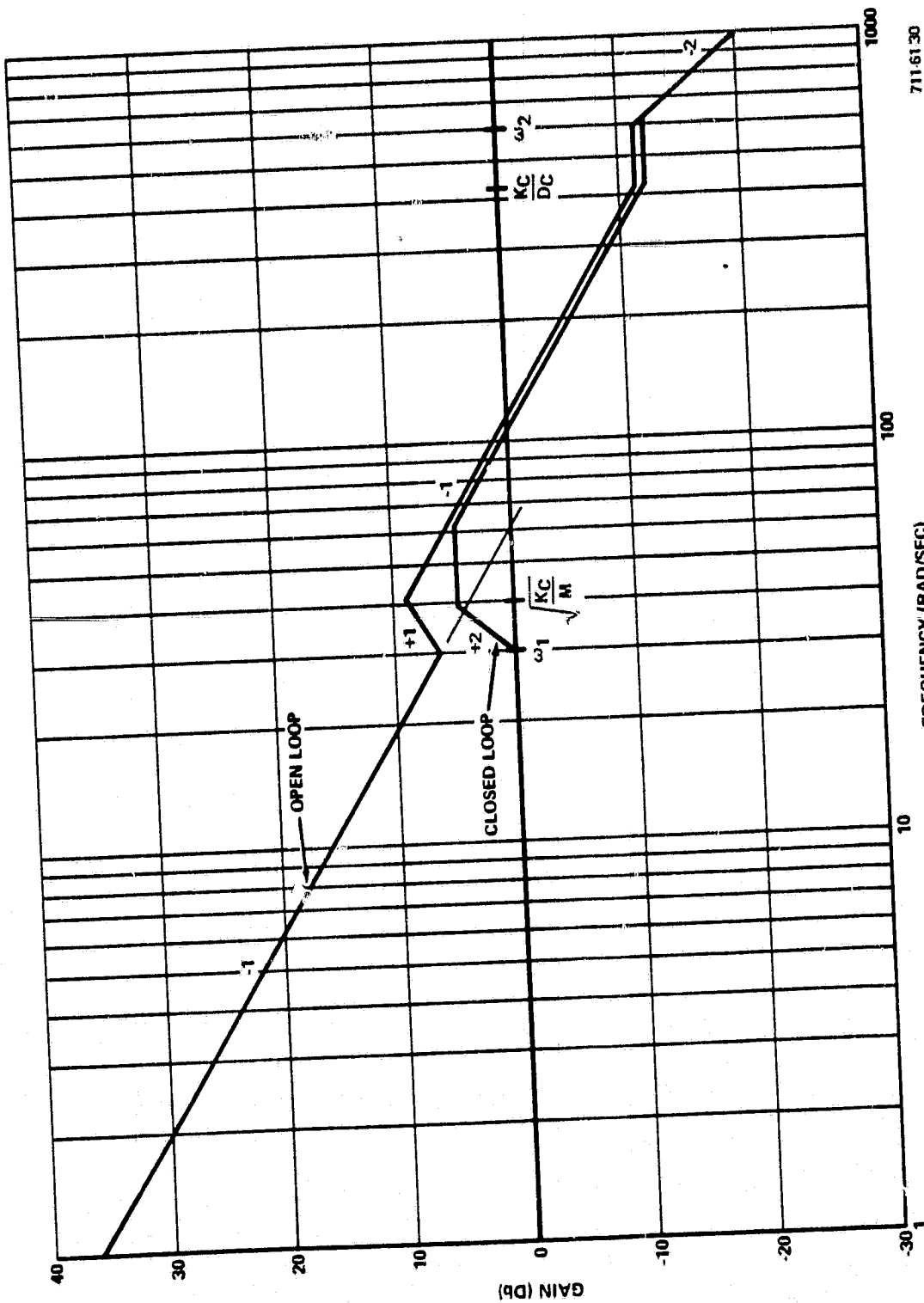
Figure 5-22
WATF Z-Axis Tension-Control Loop Bode Gain Plots
(Straight-Line Approximations)

ANALYSIS 5.9

Z-AXIS ERROR CAUSED BY FRICTION IN THE GEAR TRAIN

5.9 Z-AXIS ERROR CAUSED BY FRICTION IN THE GEAR TRAIN

Use the block diagram from analysis 8085.5.1-60 (Figure 5-21) with $J_D \gg MR_D^2$

711-61-72
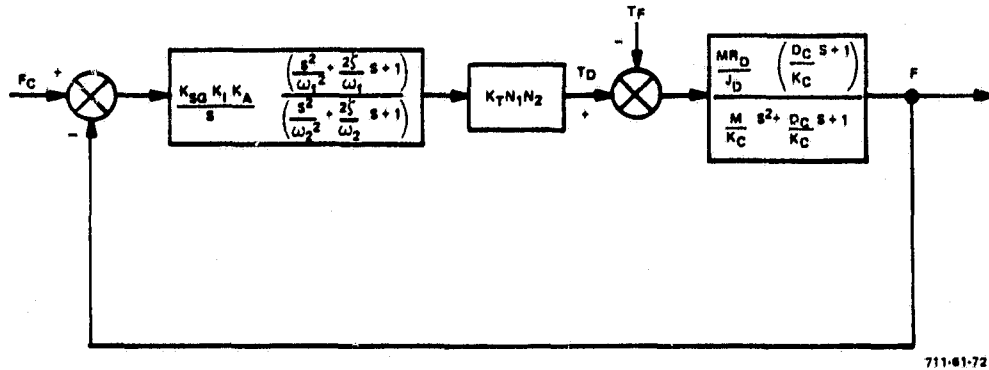
Figure 5-23

T_F is the friction torque disturbance to the gear train

let $K_{FB} = K_{SG}\, K_I\, K_A\, K_T\, N_1\, N_2$

$$K_F = \frac{MR_D}{J_D}$$

the loop can be redrawn as shown.

711-61-73
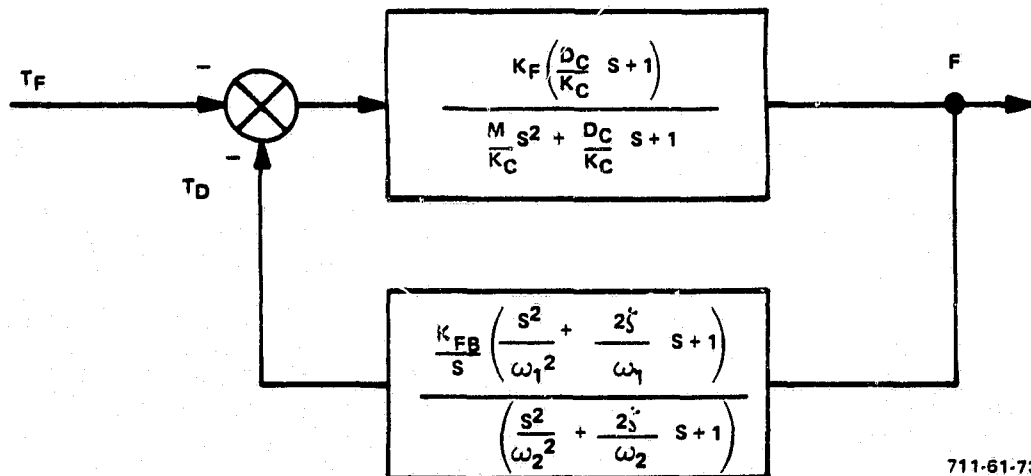
The closed-loop transfer function is

(5-19)

$$\frac{\bar{F}}{TF} = \frac{F^s \left(\frac{D_a}{K_e}S+1\right)\left(\frac{S^2}{\omega_1^2}+\frac{2f}{\omega_1}S+1\right)}{S\left(\frac{M}{K_e}S^2+\frac{D_a}{K_e}S+1\right)\left(\frac{S^2}{\omega_1^2}+\frac{2f}{\omega_1}S+1\right)+K_fK_e\left(\frac{D_a}{K_e}S+1\right)\left(\frac{S^2}{\omega_1^2}+\frac{2f}{\omega_1}S+1\right)}$$

Use the final value theorem to find the steady-state error

$$\lim_{t \to \infty} f(t) = \lim_{s \to 0} s\, F(s)\, I\,(s)$$

with a step input of friction to simulate Dahl friction, $I(s) = 1/s$

$$\lim_{t \to \infty} f(t) = \lim_{s \to 0} s/s\, F(s)$$

$$= 0 \text{ because of the s term in the numerator of}$$

$$\frac{\bar{F}}{TF}$$

there is zero steady-state tension error due to motor friction.

ANALYSIS 5.10

X-Y LOOP ANALYSIS

5.10 X-Y LOOP ANALYSIS

Derive the open-loop transfer function from the loop block diagram.

Design a compensation $G_C(s)$ that produces an open-loop crossover frequency of 60 radians per second, with an adequate phase margin for stability.

711-61-74

COMPENSATION

POSITION
ERROR

$G_C(S)$

MOTOR
DRIVER

$\dfrac{K_D}{\dfrac{S}{W_D} + 1}$

MOTOR
TORQUE CONST.

GEAR RATIO

$K_T N$

TORQUE

MOTOR AND
DRIVE TRAIN
INERTIA

$\dfrac{1}{JS}$

MOTOR FRICTION

SPROCKET
RADIUS

R

CABLE
VELOCITY

SPROCKET RADIUS

R

DRIVE CABLE
DAMPING AND
SPRING CONST.

$D_C + \dfrac{K_C}{S}$

FORCE

CARRIAGE
MASS

$\dfrac{1}{MS}$

CARRIAGE
FRICTION

$\dfrac{1}{S}$

X_{ERR}

$X_{PAYLOAD}$

$G_C(S) = 345 \left(\dfrac{\dfrac{S^2}{\omega_1^2} + \dfrac{1.4S}{\omega_1} + 1}{\dfrac{S^2}{\omega_2^2} + \dfrac{1.4S}{\omega_2} + 1} \right) \dfrac{V}{IN}$
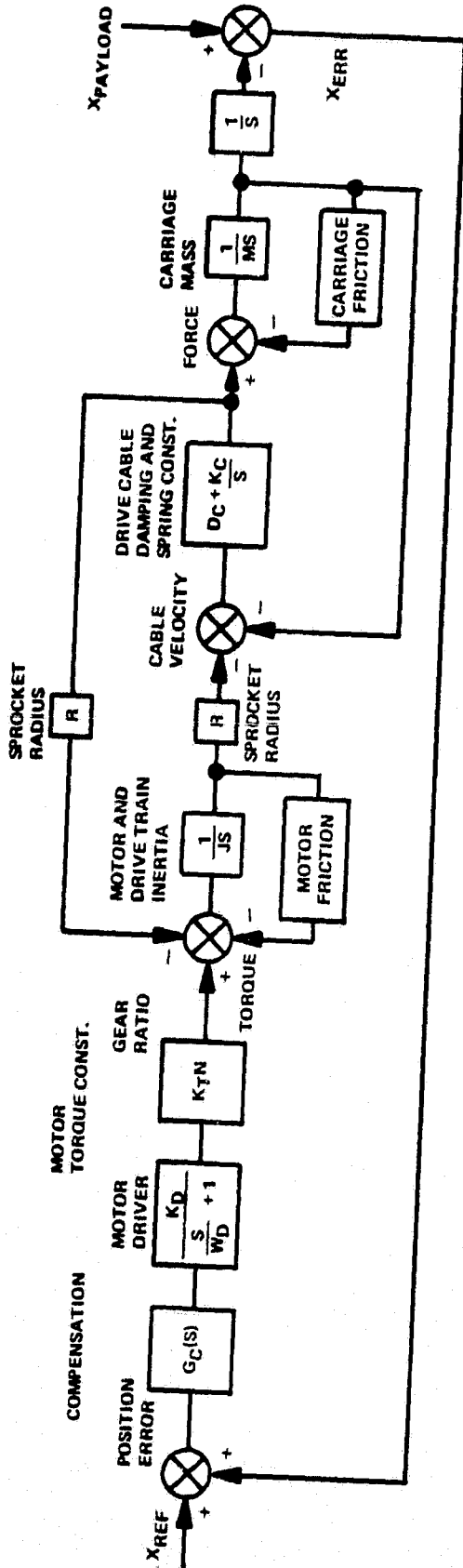
$K_D = 1 \ \dfrac{AMP}{V}$

$\omega_D = 6000 \ RAD/SEC \approx 1 \ KHz$

$\omega_N = 150 \ (RATIO)$

$K_T N = 140 \ IN \ LBF/6.2 \ AMP = 22.6 \ \dfrac{IN \ LB}{AMP}$

$J = 26.4 \ IN \ LBF \ SEC^2$

$R = 2'' \ RADIUS$

$D_C = 12.5 \ LBF \ SEC/IN.$

$K_C = 1400 \ \dfrac{LBF}{FT} = 116.7 \ \dfrac{LBF}{IN}$

$M = 1050 \ LBM = 2.72 \ \dfrac{LBF \ SEC^2}{IN}$

LET $A = G_C(S) \ K_D \ K_T \ N$

$\dfrac{S}{W_D} + 1$

Figure 5-25
ZGTF X-Y Position Control-Loop Block Diagram

Figure 5-26

$$(5-20)$$
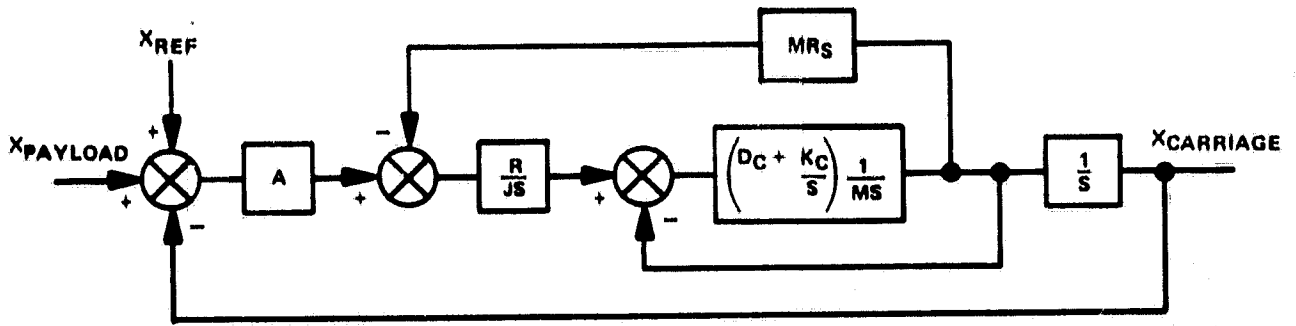
$$\frac{D_c + \frac{F_c}{S}}{MS + D_c + \frac{K_c}{S}} = \frac{(D_c S + K_c)}{MS^2 + D_c S + K_c} = \frac{\left(\frac{D_c}{K_c} S + 1\right)}{\frac{MS^2}{K_c} + \frac{D_c}{K_c} S + 1}$$
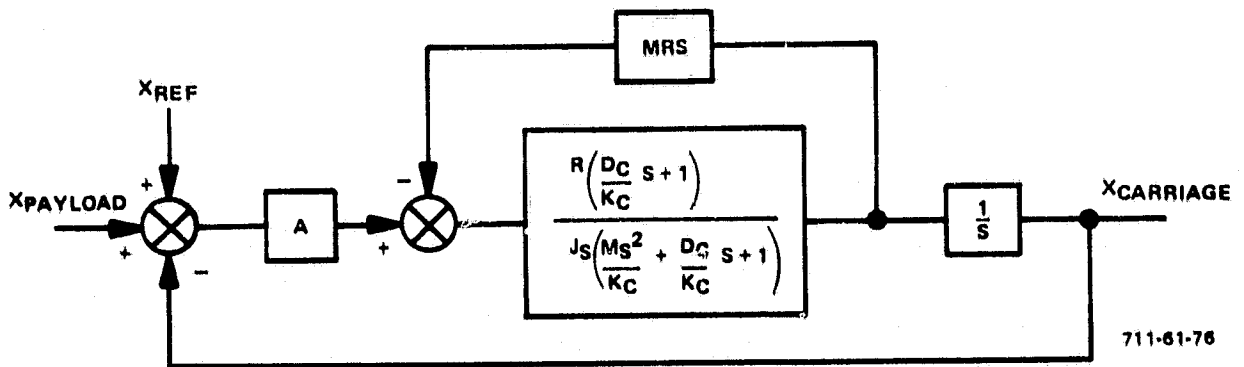
Figure 5-27

$$(5-21)$$

$$\frac{R\left(\frac{D_c}{K_c} S + 1\right)}{JS\left(\frac{MS^2}{K_c} + \frac{D_c}{K_c} S + 1\right) + MR^2 S\left(\frac{D_c}{K_c} S + 1\right)}$$

$$\frac{R\left(\frac{D_c}{K_c} S + 1\right)}{S\left[\frac{MJS^2}{K_c} + \frac{D_c}{K_c}\left(J + MR^2\right)S + \left(J + MR^2\right)\right]}$$

$$\frac{\frac{R}{J + MR^2}\left(\frac{D_c}{K_c} S + 1\right)}{S\left(\frac{JMS^2}{K_c\left(J + MR^2\right)} + \frac{D_c}{K_c} S + 1\right)} = B$$

5-33

711-61-77
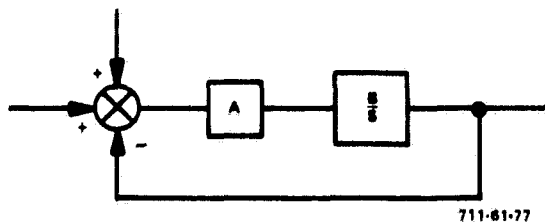
Figure 5-28

Open-loop transfer function

(5-22)

$$\frac{\frac{R}{J+MR^T}\left(\frac{D_c}{K_c}S+1\right) K_D K_T N \; G_c(S)}{S\left(\frac{JMS^2}{K_c(J+MR^2)}+\frac{D_c}{K_c}S+1\right)\left(\frac{S}{\omega_0}+1\right)}$$

Substituting in values gives

(5-23)

$$\frac{R}{J+MR^T}=\frac{.05365}{14\,d^2} \qquad K_D K_T N = 22.58 \; \frac{in\,lbf}{V}$$

$$\frac{JM}{K_c(J+MR^2)}\,S^2=\frac{S^2}{60.57}=\left(\frac{S}{7.783}\right)^2 \rightarrow \omega = 7.783 \; rad/s$$

$$\frac{D_c}{K_c}S=\frac{S}{14}=\frac{2\zeta}{\omega}S \rightarrow \zeta = .278$$

Uncompensated gain $= \dfrac{R}{J+MR^2}$ $K_D K_T N = 1.21 \; \dfrac{in}{sV^2}$

The cable spring constant K_c can change by a factor of two from 1400 to 700 lbf/ft so the uncompensated break frequencies are

(5-24)

$$5.5 \; \frac{rad}{s} < \sqrt{\frac{K_c(J+MR^2)}{JM}} < 7.78 \; \frac{rad}{s}$$

$$7 \; \frac{rad}{s} < \frac{K_c}{D_c} < 14 \; \frac{rad}{s}$$

The open-loop Bode plot approximation is shown in Figure 5-29 for the loop with and without compensation.

5-34
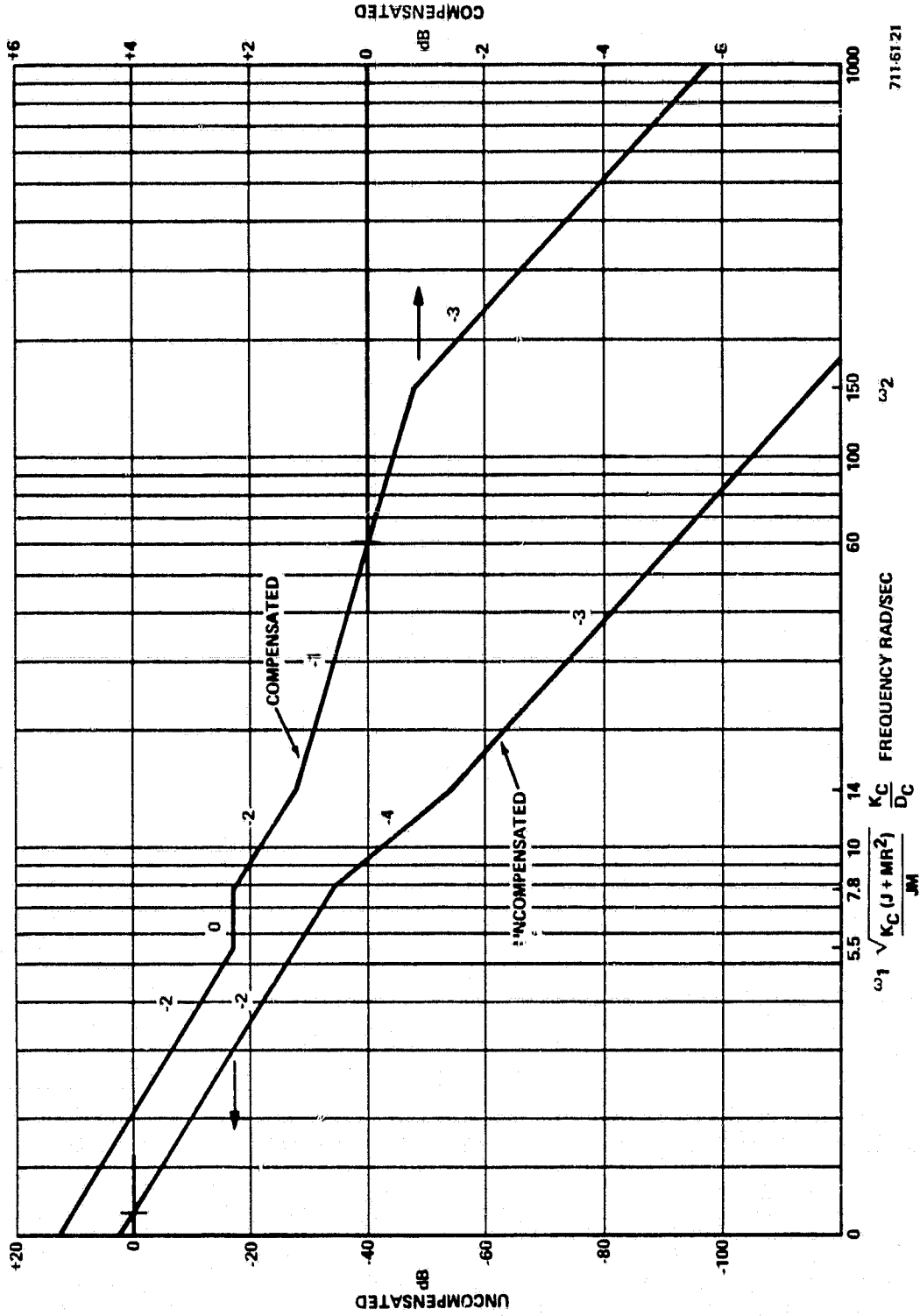
Figure 5-29
ZGTF X-Y Open-Loop Bode Plots Before and After Compensation

$$\text{pick } G_c(s) = \frac{K\left(\frac{s^2}{\omega_1^2} + \frac{1.43}{\omega_1} + 1\right)}{\left(\frac{s^2}{\omega_2^2} + \frac{14s}{\omega_2} + 1\right)\left(\frac{s}{\omega_3} + 1\right)^2}$$

critical damping
$\zeta = .7$

$\omega_1 \approx 5.5 \ \frac{rad}{s}$

$\omega_2 \approx 150 \ \frac{rad}{s}$

$$\text{pick } \omega_1 < \sqrt{\frac{K_c(J + MR^2)}{JM}} \text{ for all } K_c$$

$\omega_3 = 600 \ \frac{rad}{s}$

$\omega_1 = 5.5$ rad/s avoids a -3 slope below the crossover frequency when Kc changes, guaranteeing stability of the loop during saturation conditions.

ω_3 is used to attenuate noise at high frequencies in the control electronics, but is not necessary for loop compensation.

5.10.1 Compensated Phase Margin

Use the break frequencies shown on the graph.

(5-26)

$$\text{quadratic} \quad \phi = \pm \tan^{-1} \frac{2\zeta \frac{\omega}{\omega_c}}{1 - \left(\frac{\omega}{\omega_c}\right)^2}$$

$$\text{1st order} \quad \phi = \pm \tan^{-1} \frac{\omega}{\omega_c}$$

$$\phi_m = 180° - 180° + \tan^{-1}\left(\frac{1.4\left(\frac{60}{5.5}\right)}{1 - \left(\frac{60}{5.5}\right)^2}\right) - \tan^{-1}\left(\frac{.556\left(\frac{60}{7.8}\right)}{1 - \left(\frac{60}{7.8}\right)^2}\right) + \tan^{-1}\left(\frac{60}{14}\right) - \tan^{-1}\left(\frac{1.4\left(\frac{60}{150}\right)}{1 - \left(\frac{60}{150}\right)^2}\right) - 2\tan^{-1}\left(\frac{60}{600}\right)$$

$$= 180° - 180° + 165.49° - 175.80° + 76.87° - 33.69° - 11.42°$$

$= 21.45°$ phase margin

$(32.9°)$ without ω_3 in the loop

5-36

ANALYSIS 5.11

X-Y STEADY-STATE ERROR CAUSED BY CARRIAGE FRICTION
IN THE X-Y LOOP

5.11 X-Y STEADY-STATE ERROR CAUSED BY CARRIAGE FRICTION IN THE X-Y LOOP

With carriage friction as the input
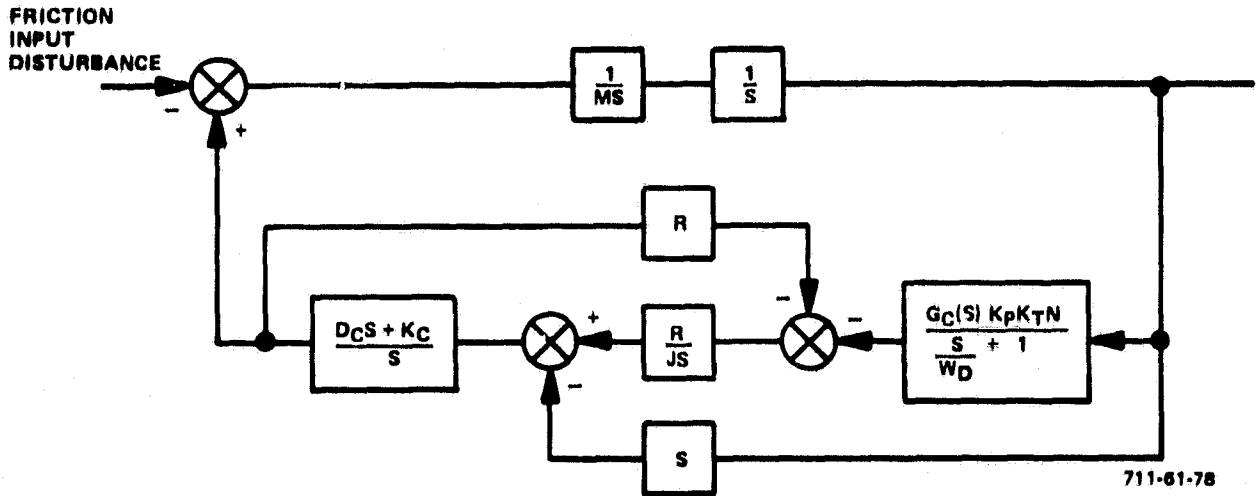
Figure 5-30

Reduce the feedback section

Figure 5-31

$$\boxed{G_c \frac{(S) K_D K_T N}{\frac{S}{\omega_D}+1} + \frac{JS^2}{R}} \quad \otimes \quad \boxed{\frac{R(D_c S + K_c)}{JS^2}}$$

$$\boxed{R}$$

$$\frac{R(D_c S + K)}{JS^2 + R^2(D_c S + K_c)}$$

$$\boxed{-\left(\frac{G_c(S) K_D K_T N}{\frac{S}{\omega_D}+1} + \frac{JS^2}{R}\right) \frac{R(D_c S + K_c)}{JS^2 + R^2(D_c S + K_c)}}$$
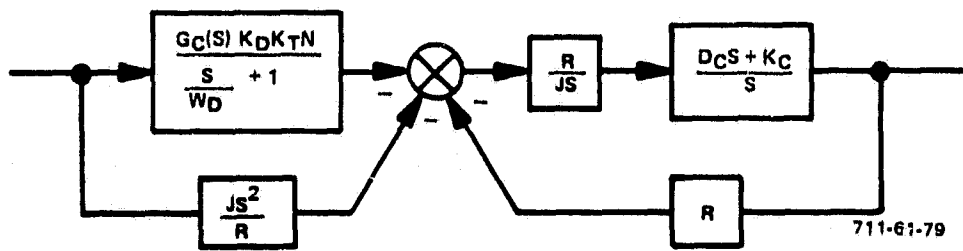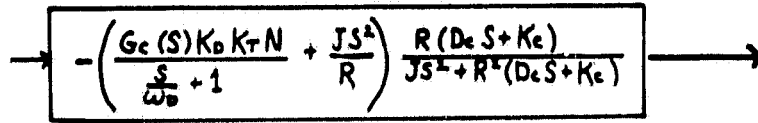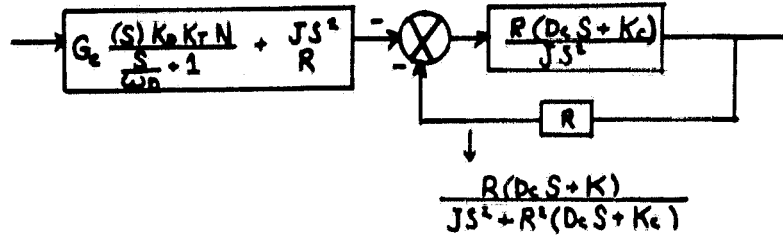
$$\frac{R\left[G K_D K_T N R + \left(\frac{S}{\omega_D}+1\right) JS^2\right] (D_c S + K_c)}{\left(\frac{S}{\omega_D}+1\right) R \left[JS^2 + R^2 (D_c S + K_c)\right]}$$

$$-\frac{\left[JS^2\left(\frac{S}{\omega_D}+1\right) + G K_D K_T N R\right](D_c S + K_c)}{\left[JS^2 + R^2(D_c S + K_c)\right]\left(\frac{S}{\omega_D}+1\right)} = \textit{feedback gain}$$

For a negative input loop
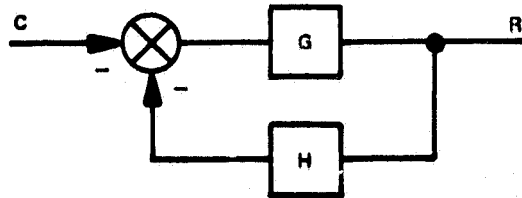
$$R = -CG - GHR$$
$$R(1 + GH) = -GC$$
$$\frac{R}{C} = \frac{-G}{1 + GH}$$

711-61-80

Figure 5-32

(5-28)

$$\frac{X_c}{F} = \frac{\frac{1}{MS^2}}{1 - \frac{1}{MS^2}\left(\frac{\left[JS^2\left(\frac{S}{\omega_0}+1\right)+GK_0K_TNR\right]\left(D_cS+K_c\right)}{\left[JS^2+R^2\left(D_cS+K_c\right)\right]\left(\frac{S}{\omega_0}+1\right)}\right)}$$

$$\frac{\left[JS^2+R\left(D_cS+K_c\right)\right]\left(\frac{S}{\omega_0}+1\right)}{MS^2\left[JS^2+R^2\left(D_cS+K_c\right)\right]\left(\frac{S}{\omega_0}+1\right)-\left[JS^2\left(\frac{S}{\omega_0}+1\right)+GK_0K_TNR\right]\left(D_cS+K_c\right)}$$

$$\Big\downarrow \qquad\qquad \Big\downarrow \qquad\qquad \Big\downarrow \qquad\qquad \Big\downarrow \qquad\qquad \Big\downarrow$$

$$MS^2\left[JS^2+\left(R^2+\frac{I}{m}\right)\left(D_cS+K_c\right)\left(\frac{S}{\omega_0}+1\right)\right]-\left(D_cS+K_c\right)GK_0K_TNR$$

Use final value theorem with a step input to simulate Dahl friction

$$\lim_{t \to \infty} f(t) = \lim_{s \to 0} S\,F(S)$$

with a step input for friction

(5-29)

$$\lim_{s \to 0} \frac{S}{S} F(S) = \frac{R^2 K_c C}{GK_0K_TNRK_c}$$

$$= \frac{RC}{GK_0K_TN}$$

$$= \frac{2C}{345(22.6}\ \frac{in.}{lbf}$$

$$= 2.57 \times 10^{-4} C\ in/lbf$$

for 14 lbf = C $\rightarrow$ <u>3.6 x 10-3</u> in. steady-state error

ANALYSIS 5.12

X-Y LOOP STEADY-STATE ERROR CAUSED BY MOTOR TORQUE FRICTION

5.12 X-Y LOOP STEADY-STATE ERROR CAUSED BY MOTOR TORQUE FRICTION
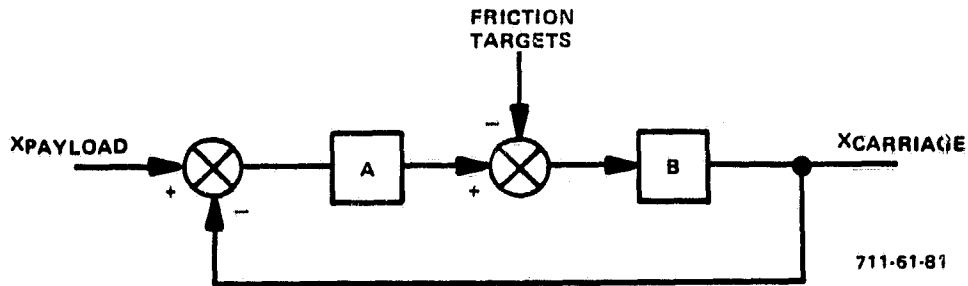
Figure 5-33

Refer to the carriage friction analysis for derivation of A and B.

$$(5\text{-}30)$$

$$A = G_c(S) \frac{K_B}{\frac{S}{\omega_0}+1} K_T N$$

$$B = \frac{\frac{R}{J+MR^2}\left(\frac{D_c}{K_c}S+1\right)}{S^2\left(\frac{JMS^2}{K_c\ J+MR^2}+\frac{D_c}{K_c}S+1\right)}$$
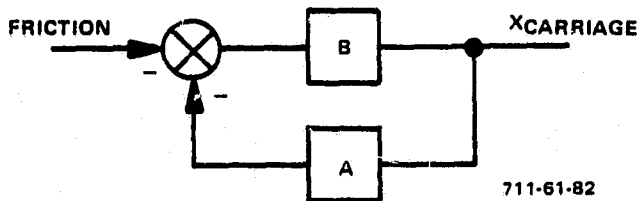
Figure 5-34

$$(5\text{-}31)$$

$$\frac{X_{carriage}}{friction} = \frac{B}{1+AB}$$

$$\frac{X_{carriage}}{friction} = \frac{\frac{R}{J+MR^2}\left(\frac{D_c}{K_c}S+1\right)\left(\frac{S}{\omega_0}+1\right)}{S^2\left(\frac{JMS^2}{K_c(J+MR^2)}+\frac{D_c}{K_c}S+1\right)\left(\frac{S}{\omega_0}+1\right)+\frac{RG(S)K_BK_TN\left(\frac{D_c}{K_c}S+1\right)}{J+MR^2}}$$

Use a step input of friction and the final value theorem

$$\lim_{t \to \infty} f(t) = \lim_{s \to 0} s/s\ F(s)$$

(5-32)

$$\lim_{t \to \infty} f(t) = \lim_{s \to 0} \frac{s}{s} F(s)$$

$$= \frac{\dfrac{R}{J + MR^2}\ C}{\dfrac{R\ G(s)\ K_D\ K_T\ N}{J + MR^2}}$$

$$= \frac{1\ C}{G_e\ K_D\ K_T\ N} \frac{in}{in\ lbf} = \frac{1C}{345\,(22.6)} = 1.28 \times 10^{-4}$$

for 5 percent of 140 in lbf friction torque → 7 inch-pound = C

steady-state error = 9 x 10^{-4} inch error

ANALYSIS 5.13

X-Y LOOP DIGITAL SIMULATIONS (FREQUENCY RESPONSE)

5.13 X-Y LOOP DIGITAL SIMULATIONS (FREQUENCY RESPONSE)

The X-Y control loop was modeled on the General Systems Analysis (GSA) computer program to plot the gain and phase transfer functions for the loop. The closed-loop frequency response for the linearized loop with a reference force as the input and carriage position as the output is shown in the first figure. The frequency is scaled down by 100 so the bandwidth is about 120 radians per second (20 hertz).

The second figure shows the loop frequency response with motor friction or torque ripple as the input and carriage position as the output. The dc gain is about -78 decibels, which agrees with the steady-state ripple torque analysis result of 1.28×10^{-4} for gain. The gain starts to rolloff at 4 radians per second, showing very good attenuation for ripple torque.
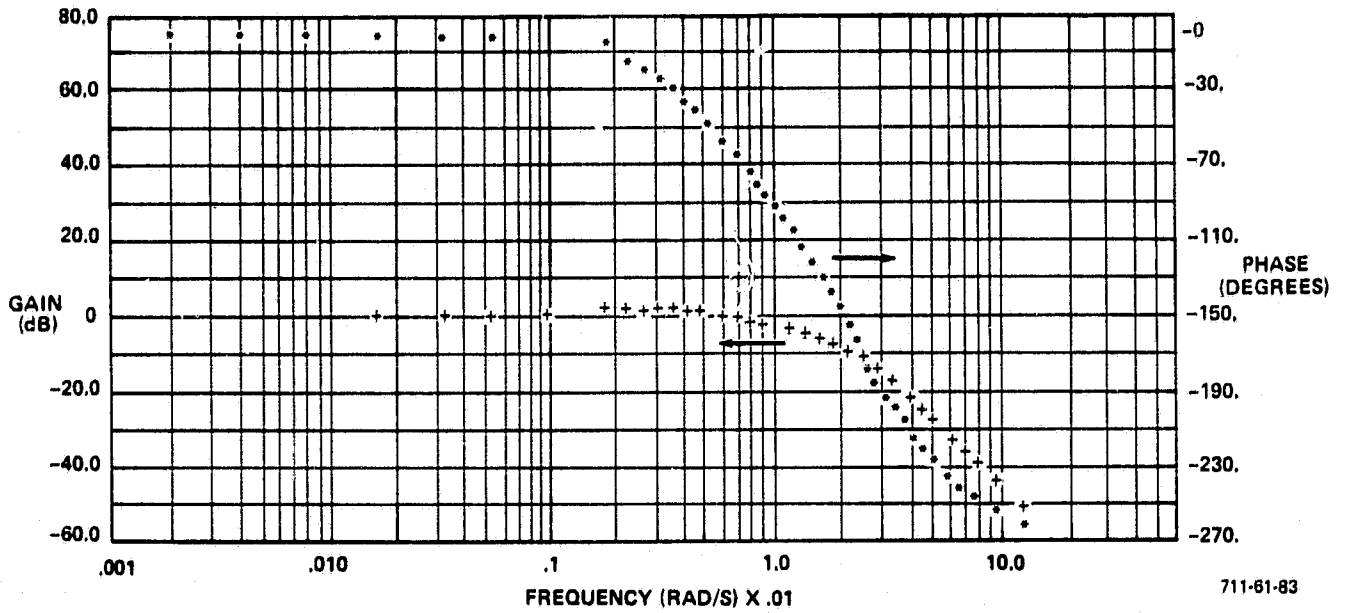
Figure 5-35
X-Y Closed-loop Response ZGTF Linear Model
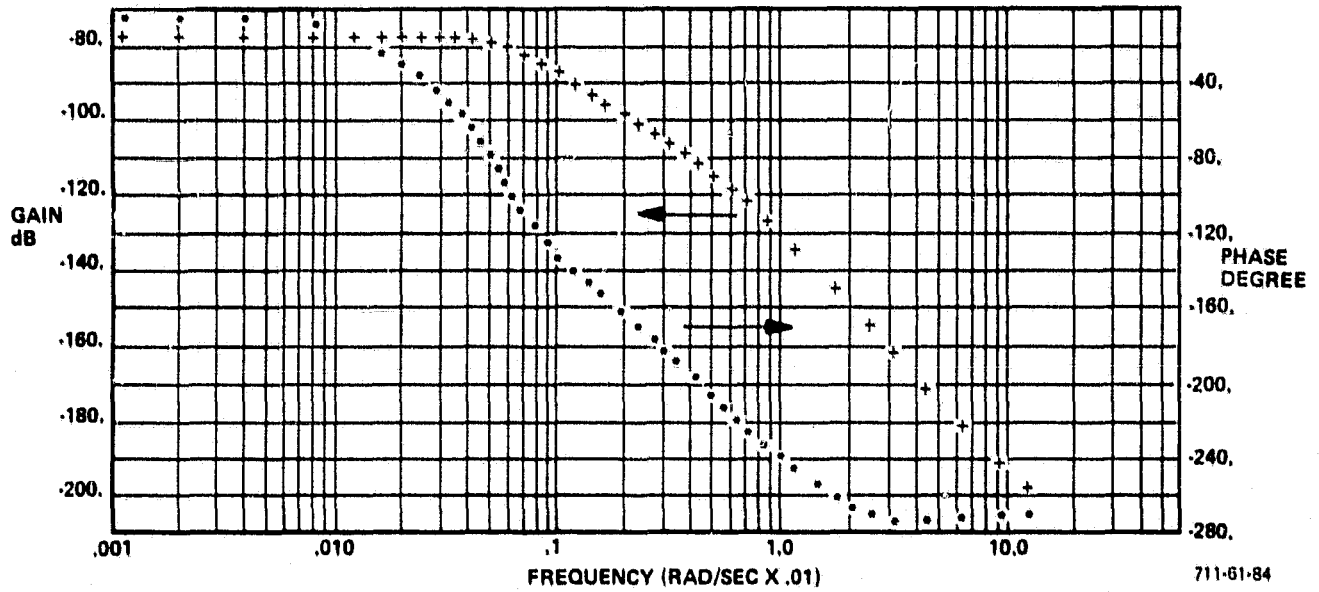
Figure 5-36
ZGTF Closed-loop Transfer Function
for Motor Ripple Torque and Friction as Input

5-44

ANALYSIS 5.14

X-Y LOOP ANALOG SIMULATIONS (TRANSMIT RESPONSE)

5.14 X-Y LOOP ANALOG SIMULATIONS (TRANSMIT RESPONSE)

The X-Y position loop was simulated on the Advanced Dynamics-4 analog computer. The computer schematic is shown in Figure 5-37. Auxiliary circuits are also described. The auxiliary circuits used were: ramp generator, 1-hertz gimbal loop filter, tower dynamics, motor and carriage friction, and motor ripple torque. The ripple torque could not be implemented with the frequency scaling used on the X-Y loop because of saturation problems in the resolver section of the ripple generator. The X-Y loop frequency was scaled down by 100. Amplitude scaling is shown in tabular form for the circuit variables and constant gains. Transient responses were run for simulated gimbal slew of 30 degrees per minute (.2 inch per second suspension point travel). The transient responses for the loop with each nonlinearity are shown on the strip-chart recordings. The error sensitivities are as follows:

Nonlinearity	Peak Error $\times 10^{-3}$ in.	SS Error $\times 10^{-3}$ in.
Saturation	1.7	0
SAT plus Tower Dynamics	1.7	0
SAT plus Motor Friction	2.3	1.0
SAT plus Carriage Friction	10.9	4.0
All Nonlinearities Combined	11.7	4.5

The peak error is 11.7×10^{-3} inches, which is within the .020-inch error requirement with 8 feet of cable. The final strip-chart recording shows velocity at each end of the X-drive cable. The difference in speed for each end at the initial transient shows that the cable is stretching until the 14-pound carriage breakaway friction is reached. The velocity at both ends of the cable then goes nicely to .2 inch per second. The motor torque during the initial transient saturates in both directions. No limit cycle occurs, demonstrating the stability of the loop. Increasing the motor torque limit to 180 in-lb-ft did not significantly improve the transient behavior of the loop.

The steady-state error level with all the nonlinearities is acceptable, but may be eliminated with an integral term in the compensation. However, this would lead to limit cycle problems during saturation. The loop could be arranged so that the integral gain of the controller would be deactivated during saturation to avoid instability, then activated at low error conditions to get rid of the steady-state error.

Figure 5-37

711-61-93

Figure 5-38

Figure 5-39

$X_T \times 10^4$

.5506
207   X,1   200   +
                    −

357   $X \cdot 10^{-2}$
      .0104

216
.254

.207   SJ   .225   SJ   X,1   X1   .6
202   SJ   201 + 204   SJ 210 + FX10 211 + FX10 220 + 217   SJ 271 + 234
             X,1   −   X,1   −   −   220   .010   274   −
                  .10   .010

LIM

207   203
      .207

214   215
 +   −
.45   .45

20F
.21

206
.225

X.05

MOTOR
RIPPLE

FRICTION

.2511   SJ   .0227
      SJ   FX10 + 237   SJ 240 + 244   SJ FX10 241 +
          231   SJ   −
           −   X,01

236
.5

LIM

212   213
 +   −
.467 .467

$X_C \times 500$

Figure 5-40
ZGTF X-Y Loop Analog Computer
Simulation AD-4 Computer

711·61·85
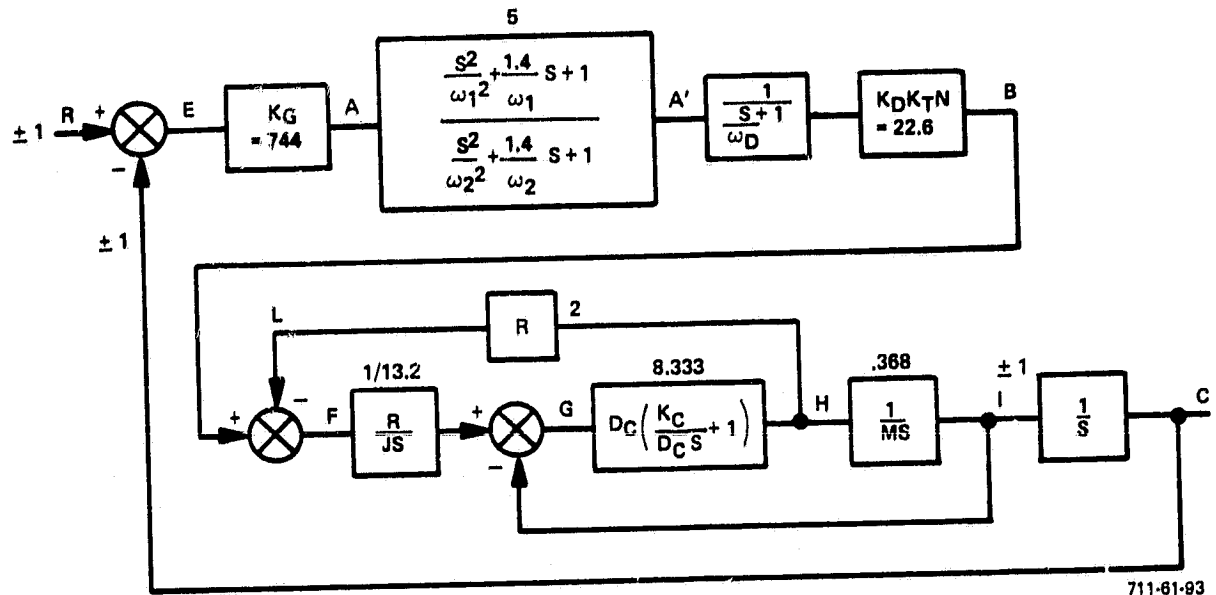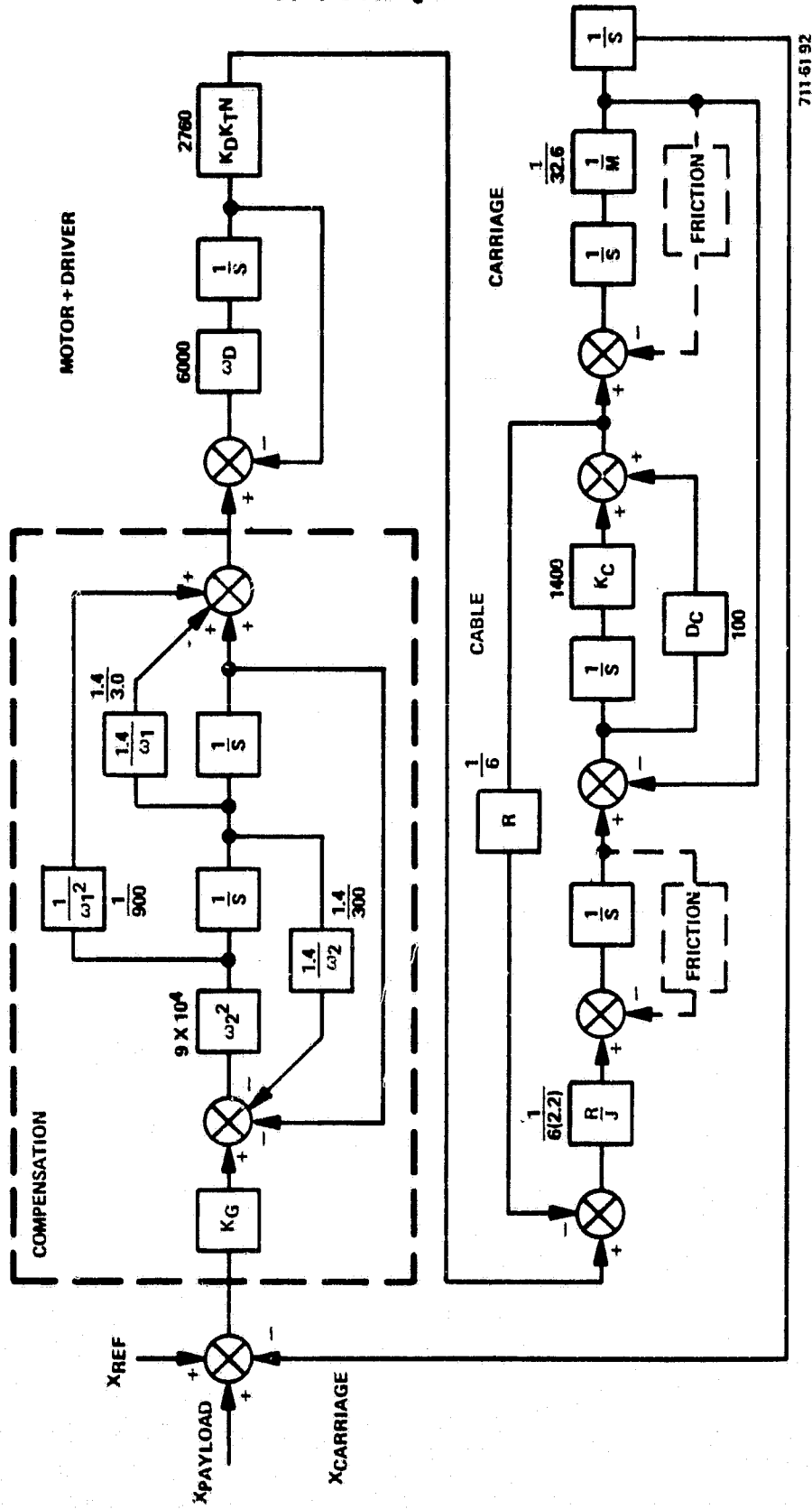
5.14.1 Tower Dynamics

Second-order system W_n = 22.63 Hz

= 142.2 rad/s

(5-33)

$$F = (mS^2 + CS + K)X$$

$$\frac{X}{F} = \frac{\frac{1}{K}}{\frac{S^2}{\omega_n^2} + \frac{2\zeta}{\omega_n}S + 1}$$

assume $\zeta = .07$ then $\frac{1}{K} = 3.526 \times 10^{-6}$

scale ω by $\frac{1}{100}$ so $\left(\frac{100}{\omega_m}\right)^2 = 2.022$ and $\frac{200\zeta}{\omega_m} = .09845$

5.14.2 Motor Torque Ripple

Five percent of command torque at 25 x motor frequency.

Use chain-drive speed for motor speed

$$2'' \dot{\theta}_m = Q \qquad\qquad \dot{\theta}_m = \frac{Q}{2}$$

$$\dot{\theta}_R = 25 \dot{\theta}_m = 12.5 Q$$

5.14.3 Auxiliary Circuits
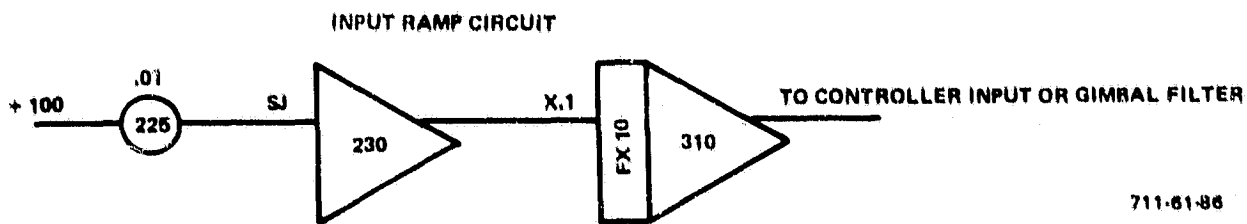
Figure 5-41

5.14.4 Gimbal Filter
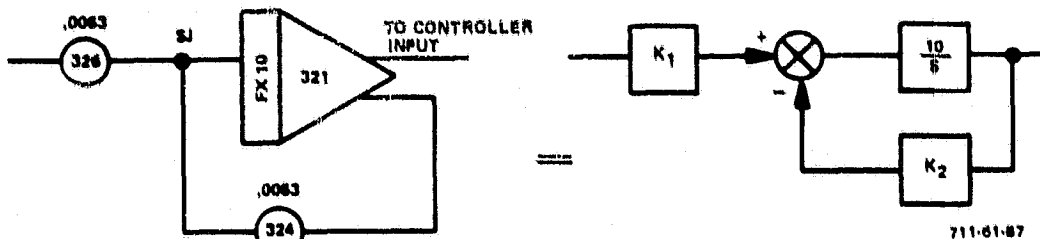
Figure 5-42

$$(5-34)$$

$$\omega = 10K_2 = .063$$

$$K_1 \left(\frac{\frac{10}{S}}{1 + \frac{10K_2}{S}} \right) = \frac{K_1}{K_2} \left(\frac{1}{\frac{S}{10K_1} + 1} \right)$$

5.14.5 Tower Dynamics

Figure 5-43

5-52
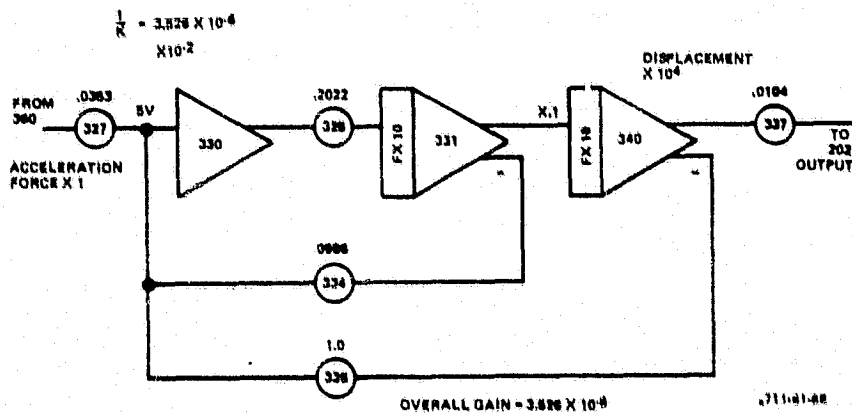
5.14.6 Motor Torque Ripple

- Five percent of torque output at a frequency proportional to motor speed.
- 82 to 181 times motor speed
- 21 rpm maximum speed = 2.2 rad/s
  gear ratio 150/1

$T = J\alpha$
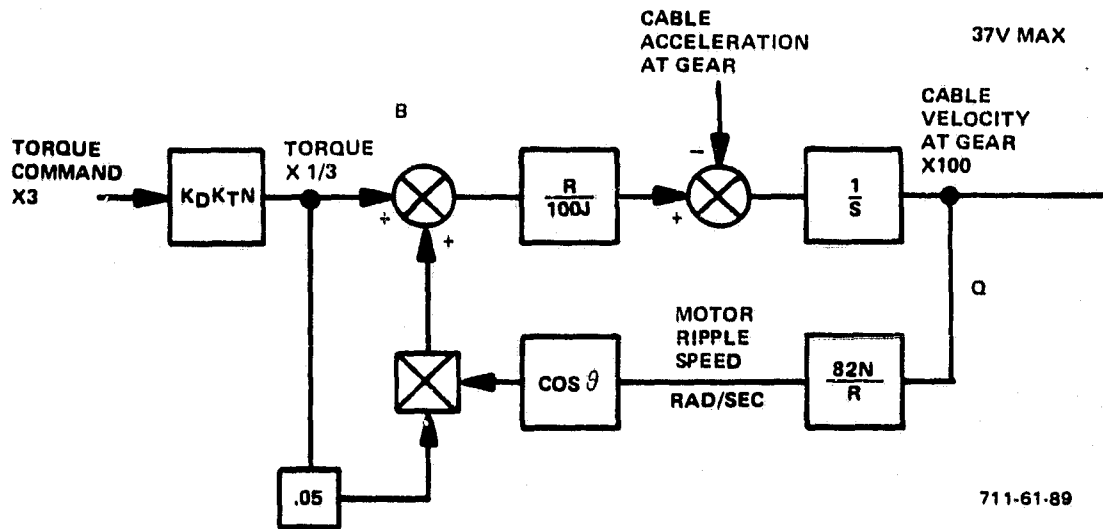
Figure 5-44

5.14.7 Friction
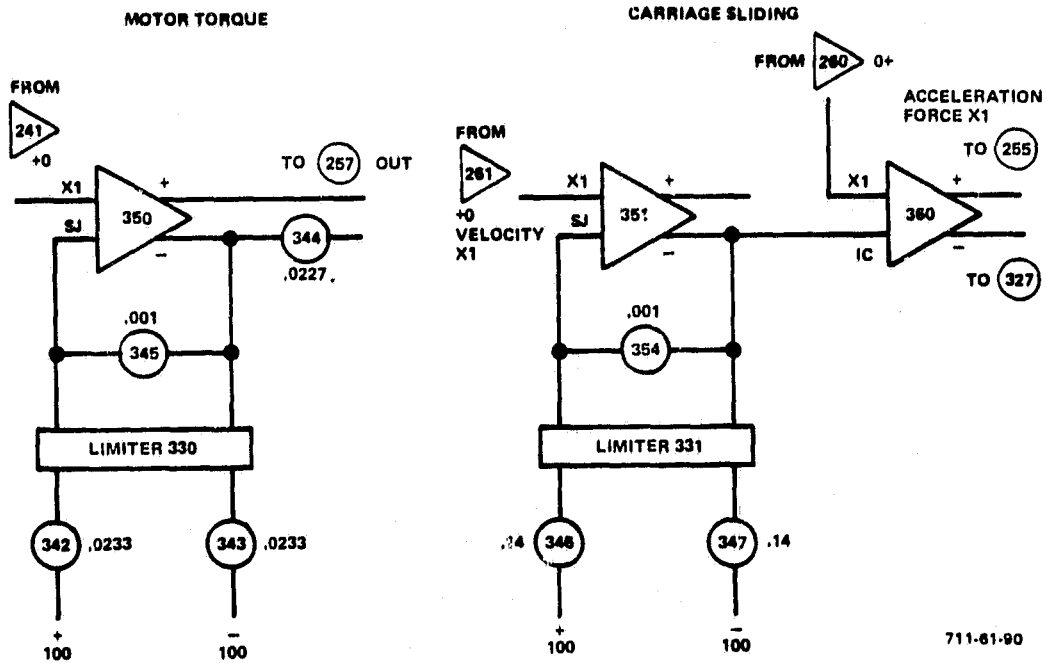
Figure 5-45

for motor torque friction use five percent of Tmax

$$140 \text{ in-lb } (.05) = 7 \text{ in lbf}$$

with scaling $\frac{7}{3} = 2.333$

5.14.8 Ripple Torque

Figure 5-46

5-54
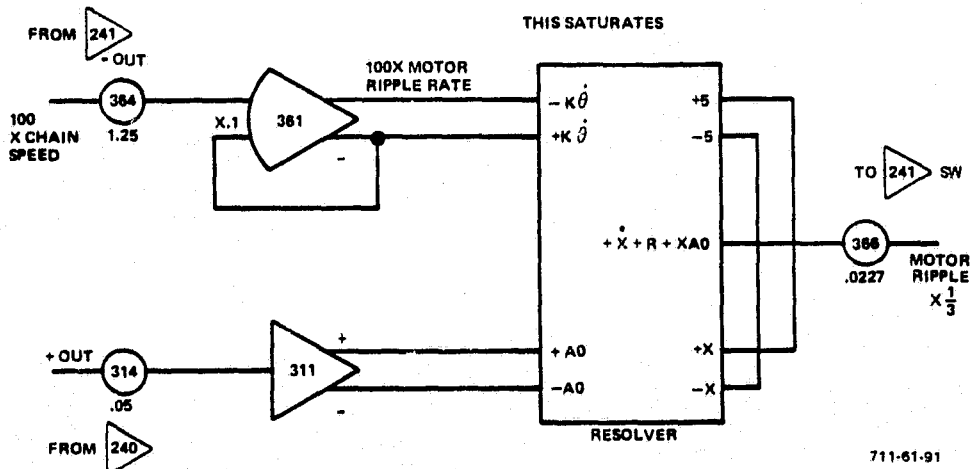
TABLE 5-2

AMPLITUDE SCALING

Variable	Scaled Variable
$X_p = \pm 10V \; (\pm .1 \text{ in})$	$5X_p(v) \; (500 \; X_p \text{ in.})$
$X_c = \pm 10V \; (\pm .1 \text{ in})$	$5X_c$
$E = \pm 20V$	$2E$
$A = \pm 15V$	$\dfrac{50}{15} A = 3.33 \; A \text{ use } 3A$
$A' = 75V$	$\dfrac{50}{75} A' = .667A' \text{ use } A'$
$B = 140 \text{ in-lb-ft}$	$\dfrac{50}{120} B = .357B \text{ use } \dfrac{B}{3}$
$I = \pm .65 \text{ in/s}$	$\dfrac{50}{.65} I = 76.9I \text{ use } 100I$
$H = 70 \text{ lbf}$	H
$L = 140 \text{ lbf}$	$\dfrac{50}{140} L \text{ use } \dfrac{L}{3}$
$G = 1.3 \text{ in/s}$	$\dfrac{50}{1.3} = 38.46 \text{ use } 100G$
$P = \dfrac{280}{1320} = .212\dfrac{\text{in}}{\text{s}}$	$\dfrac{50}{.212} P \text{ use } 200P$
$Q = .65 \text{ in/s}$	use $10 \; Q$

TABLE 5-3

LIMITER GAIN SCALING

Equation	Gain	Limiter
$3\,A = \dfrac{3}{500}\,K_c\,(500\,(X_p - X_c))$	$\dfrac{3}{500}\,K_c = 2.07$	45
$3\,A = \dfrac{3}{10^4}\,K_c\,10^4\,X_T$	$\dfrac{3}{10^4}\,345 = .1035$	
$3\,A' = 3A$		
$\dfrac{B}{3} = \dfrac{K_D K_T N\,3A'}{3(3)}$	$\dfrac{K_D K_T N}{3} = 7.533$	46.7
$100\,I = \left(100\,\dfrac{1}{M(100)}\right) H$	$.368$	65
$100\,P = H\,100\,\dfrac{R^2}{1000}$	$.1515$	
$100\,P = \dfrac{B}{3}\,100(3)\,\dfrac{R}{100V}$	$.2273$	65
$H = \dfrac{D_c}{100}\,100G$	$D_c = .08333$	
$H = \dfrac{K_c}{100}\,\dfrac{100G}{100}$	$K_c = .011667$	
$500\,X_c = (100I)\dfrac{C}{1005}$	$100\dfrac{C}{} = .05$	
$X_c = \dfrac{I}{S}$		

TABLE 5-4

POTENTIOMETER LIST

Potentiometer Number	Setting	Potentiometer Number	Setting
202	.207	254	.1196
203	.207	255	.0368
204	.225	257	.0152
205	.21	262	.650
206	.225	263	.650
207	.3636	264	.650
212	.467	265	.650
213	.467	266	.005
214	.45	274	.010
215	.45	276	.50
216	.2545	277	.50
217	.0100	314	.050
225	.01	324	.0063
		325	.2022
		326	.0063
		327	.0353
		334	.0986
		335	1.0
234	.5	337	.0104
236	.5	342	.0233
237	.2511	343	.0233
244	.0227	344	.0227
245	.0833 (.0856)	346	.14
247	.0100	347	.14
354	.001	354	.001
364	1.25	364	1.25
366	.0227	366	.0227

SECTION 6.0

ZGTF PERFORMANCE VERIFICATION PLAN

SECTION 6.0

ZGTF PERFORMANCE VERIFICATION PLAN

Verification of ZGTF performance will be done in the following areas.

- X-Y position loop
- Z-force loop
- Tower dynamics and stiffness
- Force sensor at the mast base and in Z loop
- X-Y loop optical position sensor
- Force sensor electronics
- Safety devices

These tests will demonstrate that the ZGTF will perform as designed, and will introduce errors into the test article below the allowable limits. The tests to be run will measure the following parameters:

- Controller electronics frequency response and calibration (analog-to-digital converters)

- Force sensor electronics calibration

- Structural frequencies and stiffnesses (tower, bridge, Z cable)

- X-Y-Z drive friction

- Optical position sensor accuracy and isolation from cable dynamics

- Force sensor calibration check (Z loop and mast base)

- Safety device trip points and operation

- Z-force error during slew and static conditions

- X-Y position error during slew and static conditions

The tests are listed in the order of system complexity, starting at the component level for the control electronics test, to the subsystem level for the sensor tests, to full-up system level for the X, Y, and Z loop error tests. All tests will be performed at Sperry except for the structural frequency and stiffness tests on the tower, which will be performed at the test facility site. The electronics and sensor calibrations should be performed periodically as a regular calibration routine for the ZGTF. Other tests, such as the structural frequency test, need not be redone unless major structural changes are made to the facility.

6.1 TEST EQUIPMENT

Several items of test equipment are necessary for the verification tests. Most of the commercial equipment will also be necessary for antenna pointing system testing or recalibration of the ZGTF, making it advantageous for NASA to purchase or have available the items listed below.

- H-P 5423 structural dynamics analyzer (or equivalent)

- X-Y plotter (H-P 9872B, or equivalent)

- 2 or 3 triaxial strain-gage type accelerometers (Entran EGAX3-10D, or equivalent)

- Accelerometer signal conditioners (Validyne CD-19, or equivalent)

- Instrumented hammer (PCB Piezotronics)

- Wheatstone bridge calibrator (BLH 624/625, or equivalent)

- 4 to 6 channel strip chart recorder

- Calibrated weights and hangers

- Precision voltage supply

- High-precision digital voltmeter

Also necessary is a slew motion simulator-position sensor calibrator, which will be designed and fabricated as one of the subtasks for the ZGTF program. A conceptual drawing of a simulator is shown in Figure 3-14.

6.2   VERIFICATION TESTS

This section describes the test objective, performance criteria and test setup for each test. A list of the necessary equipment is also given.

6.2.1   Control Electronics Calibration (Figure 6-1)

Objective: To calibrate the A/D and D/A converters in the control electronics

Performance Criteria: The converters must be linear to within TBD percent with less than TBD volts offset.

Equipment: Precision power supply
High-precision DVM (16-bit resolution)
H-P 5423 Analyzer
X-Y Plotter
Microprocessor development system
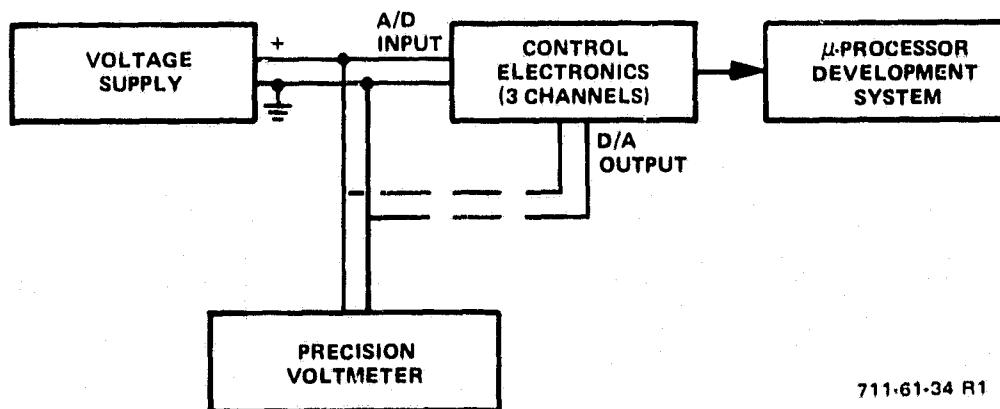
711·61·34 R1

Figure 6-1
Test Setup: Control Electronics Calibration

Test: A known constant voltage is applied to each channel of the control electronics analog-to-digital (A/D) converters. The digital output of the converters is read out on the microprocessor development system. The A/D outputs are routed through the digital-to-analog (D/A) converters, and their output is read on the DVM. The A/D output is compared to the expected digitized value for the input voltage to verify that the converter is working properly. The D/A output voltage is compared to the A/D input voltage to verify that the gain through both converters is one. If not, the gain and offset can be adjusted on the D/A converter to produce the proper output. This test should be done as part of the normal calibration procedure.

6.2.2 Control Electronics Frequency Response (Figure 6-2)

Objective: Demonstrate that the electronic controller has the proper transfer function programmed into it.

Performance Criteria: The transfer function gain and break frequencies will be within TBD percent of the proper values.
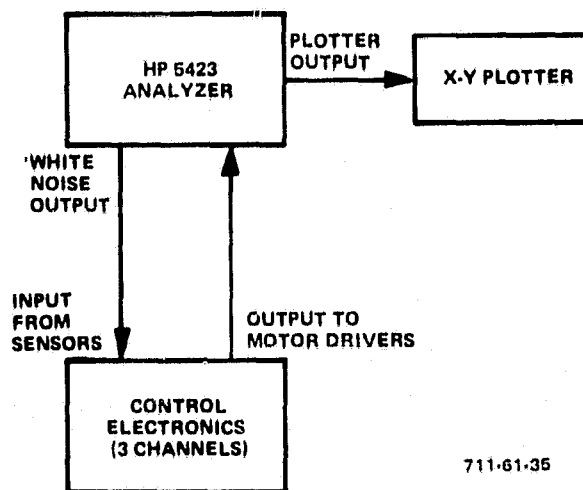
Figure 6-2
Test Setup: Control Electronics Frequency Response

Test: The white noise output of the H-P 5423 is applied in sequence to the X, Y, and Z channels of the control electronics. The controller outputs are fed back into the H-P analyzer for frequency analysis. The analyzer outputs the controller gain and phase frequency response to the plotter. Since this test is simple to set up and run, it can be done as a routine test during calibration. However, the electronics transfer function should not change once it is programmed into the controller, making this test noncritical.

6.2.3 Force Sensor Electronics Calibration (Figure 6-3)

Objective: Verify the signal conditioning electronics are noise free and set to the proper gain.

Performance Critera: The electronics gain shall be linear within TBD percent with less than TBD volts offset.

Equipment: Wheatstone Bridge Calibration (BLH 624/625)
DVM and Oscilloscope or H-P 5423 Analyzer

WHEATSTONE BRIDGE CALIBRATOR → STRAIN GAGE ELECTRONICS (I0 CHANNELS) → OSCILLOSCOPE OR HP 5423 OR DVM

711-61-37 R1

Figure 6-3
Test Setup: Force sensor Electronics Calibration

Test: The Wheatstone bridge calibrator simulates a resistance bridge transducer, such as a load cell, and produces calibrated bridge unbalances that can be interrogated by the strain-gage electronics. The strain-gage electronics are connected to the calibrator and the electronics outputs are displayed on the H-P analyzer, DVM, or oscilloscope. The static gain and linearity of the electronics are checked with the H-P analyzer or the DVM (for high precision). A series of bridge unbalances is produced with the calibrator, and the strain-gage electronics output voltage is compared with a predicted output voltage, which is proportional to the calibrator setting. The result is plotted as the calibration curve for the strain-gage amplifier. The oscilloscope or analyzer is connected to the electronics output to look for ripple from the electronics carrier frequency or noise in the transducer system. The ripple can be balanced out with adjustments to the strain-gage electronics.

This test should be performed as a routine calibration on the signal-conditioning electronics. It is also useful for troubleshooting the sensor electronics in case of problems with them.

6.2.4 <u>Structural Frequencies Testing</u> (Figure 6-4)

Objective: To do a modal analysis of the ZGTF and to verify the accuracy of the structural dynamics simulations for the tower and drive carriage

Performance Criteria: All tower modes must be above 20 hertz

Equipment: HP 5423 Analyzer
Instrumented Hammer
Large ladder or Cherry Picker
Triaxial Accelerometer (plus spare)
Strain-Gage Signal Conditioners
X-Y Plotter
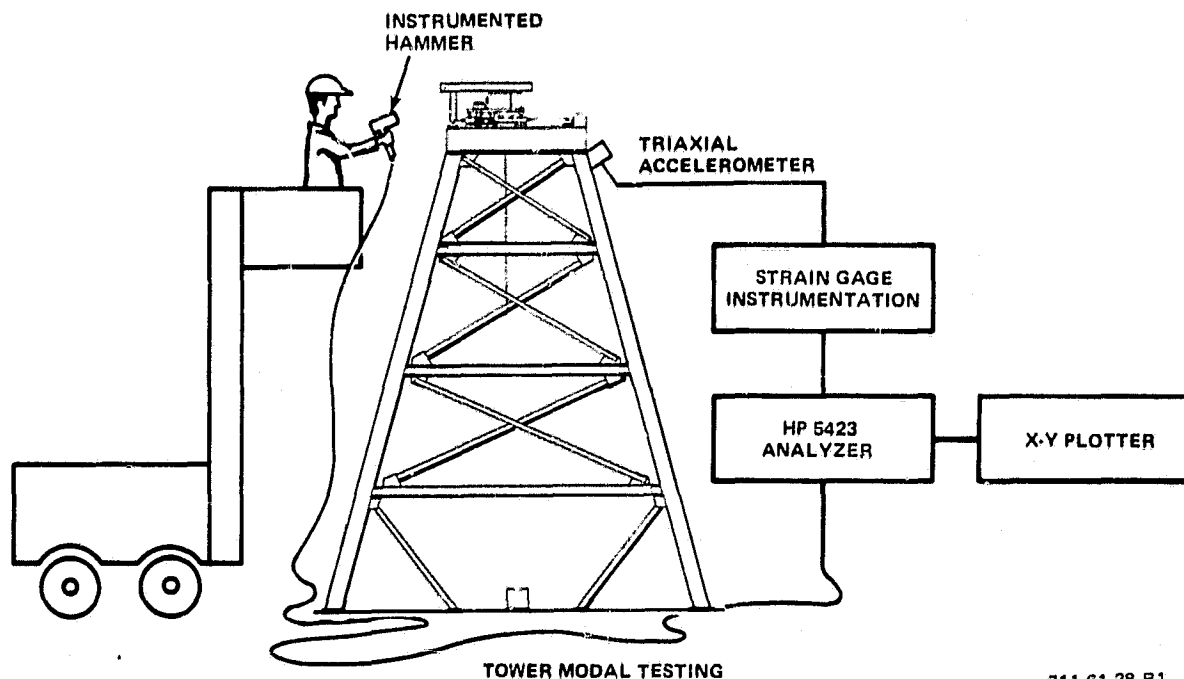
Figure 6-4
Test Setup: Tower Modal Testing

Test: The test method is to measure and process the acceleration response to impulses app''ed to various points on the ZGTF structure.

The structure is excited with a hammer, that is instrumented with an accelerometer, at points defined as nodes by a structural model programmed into the H-P analyzer. The tower vibration response to the impulses is measured with a triaxial accelerometer, attached to a point on the structure which can be modeled as a node, and which has a measurable response to disturbances at all points on the structure. The output of the accelerometer is fed into the HP analyzer for data processing. Since the object of this test is to define disturbances to the suspension for the test article, the best point to mount the accelerometer is at the top of the tower where the disturbances are fed into the Z-axis cable. It is advisable that the person hitting the tower not be standing on the tower while the disturbance is

applied since this will introduce additional damping and mass to the tower. Additional unmeasured forces would also be applied to the tower because of the reaction of swinging the hammer. To avoid these problems, the operator should stand on a ladder or cherry picker while hitting the tower.

The modes of interest on the structure are vertical bending of the cross beams at the top of the tower (computed at ~70 hertz), a cantilever beam mode of the tower in the horizontal direction (computed at ~23 hertz) and torsion of the tower about the vertical axis (computed at ~27 hertz). This test will verify frequencies and mode shapes for the ZGTF structure, and only has to be done once following assembly of the ZGTF. Major structural rework of the tower will require that the test be rerun.

6.2.4.1 Cable Vibration Frequency (Figure 6-5)

Objective: Determine the vibration frequencies for the Z-axis cable
     for the range of tensions and lengths used during actual
     testing.

Performance Criteria: TBD (dependent on cable length and tension)

Equipment: Rigid attachment for bottom of Z-axis cable
      H-P analyser or Strip-Chart Recorder
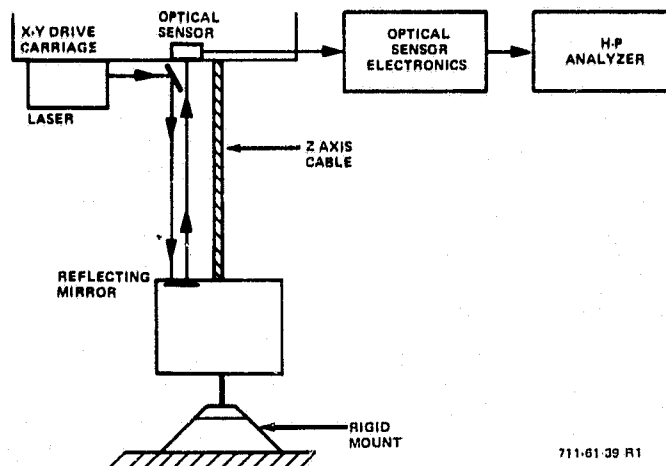
Figure 6-5
Test Setup: Cable Vibration Frequency

Test: The X-Y position sensor consists of an array of reflecting mirrors and optical position detectors which measure position and angular error of the top of the load cell link at the base of the Z-axis cable. The combined output of the sensor is proportional to X-Y position error and independent of cable motion. However, the output of any one detector is very dependent on cable motion, and can be used to measure its vibrational frequency.

For this test, the bottom of the cable is attached to a rigid mount and positioned so that the output of one of the sensors is zero. The cable force is commanded to some typical test level and the cable is twanged lightly. The output of the optical detector, proportional to the amplitude of the cable vibration, is fed into the analyzer or strip-chart recorder where the cable frequency and damping ratio can be measured. The test should be repeated for several typical cable force levels and payout lengths since the frequency is predicted to be proportional to the square root of cable tension and is dependent on cable length. The range of calculated cable frequencies can therefore be verified and mapped for each particular test.

This test should be done before each series of antenna tests, using the force and cable lengths expected, for reference information. It will also be done following construction of the ZGTF, using the extreme design values of cable force and lengths to bracket the frequencies of cable vibration to be expected.

6.2.5 <u>X-Y-Z Drive Friction</u> (Figure 6-6)

Objective: Verify the friction character and level assumed in the
X-Y and Z control loop analyses

Performance Criteria: TBD

Equipment: Z-Axis Load Cell
Strain Gage Signal Conditioner
Oscilloscope or H-P Analyser
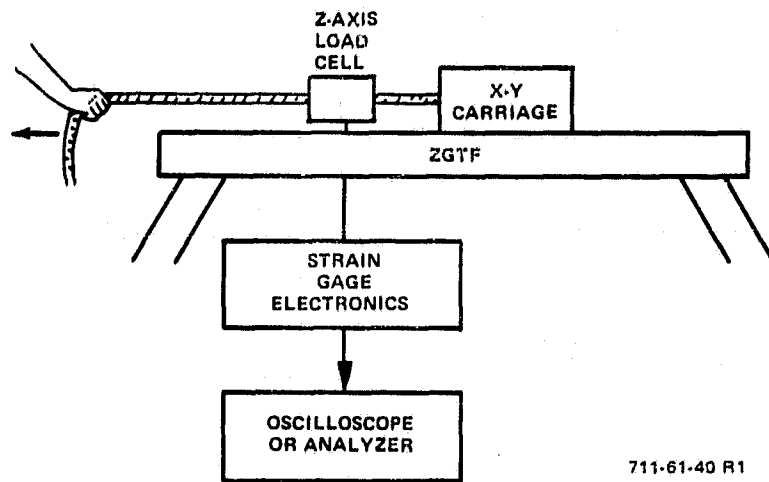
Figure 6-6
Test Setup: X-Y-Z Drive Friction

Test: The load cell for the Z-axis loop is attached to the X or Y drive
carriage with a rope attached to the opposite end of the load cell for
manually pulling the carriage. The force on the carriage is gradually
increased until carriage motion occurs, at which point the force level is
read on the strip-chart recorder. The test should be repeated with the
carriage in various positions to check for variations in friction with
position.

The Z-axis force is measured in a similar manner with the load cell attached to the bottom of the Z cable. Force is applied to the load cell until the cable drum starts to rotate, at which point the force is read on the strip-chart recorder. The force levels obtained will be compared to the friction force levels assumed in the systems analyses to verify the accuracy of the analyses. This test will be run once after fabrication of the ZGTF since the friction is a function of the facility's mechanical design and cannot be adjusted.

6.2.6 Optical Position Sensor Test (Figure 6-7)

Objective: Verify the calibration of the optical position sensor. Check its sensitivity to cable vibration.

Performance Criteria: The sensor gain will be linear within TBD percent with less than TBD bias. Cable vibration amplitude will be less than TBD percent of the cable angle displacement amplitude (cube corner mirror displacement)

Equipment: Gimbal Slew Simulator-Calibrator
Oscilloscope or H-P Analyser
DVM
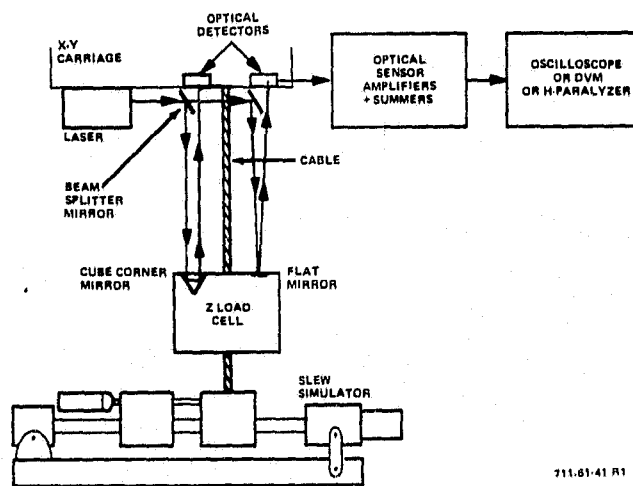
Figure 6-7
Test Setup: Optical Position Sensor Test

6-11

6.2.6.1 Position Sensor Calibration Verification

The optical sensors used in this system produce a voltage that is proportional to the position of the light dot on the face of the sensor. The cube corner mirror reflects the beam that measures cable angle, and the flat mirror reflects the beam that measures angle of the rigid link at the bottom of the cable. Summation and scaling of the two signals are done in the sensor amplifier which is calibrated separately. The slew simulator-calibrator is bolted down with the ball screw drive horizontal in the X or Y direction, with the displacement measurement block attached. The Z-drive cable is attached to the moving block of the slew simulator with some tension in the cable. The position of the calibrator is adjusted until the position sensor output reads zero, then the micrometer is zeroed. The moving block of the simulator is displaced and the distance measured with the micrometer. The micrometer reading is then compared to the position sensor output, read on the DVM or analyzer, allowing a calibration curve to be drawn for the sensor. Errors in calibration must be adjusted by changing the gains of the optical sensor amplifiers, since no adjustments can be made to the optical sensors or mirrors, other than zero adjustment. This test should be done every time the gain of the link angle sensor (for the flat mirror) is changed to compensate for cable length changes. It should also be done periodically to check the position-sensor calibration.

6.2.6.2 Sensitivity to Cable Vibration

The position sensor is designed to be insensitive to cable vibrations. In this test the cable is aligned veritically (position sensor output equal to zero) with the bottom link attached to a rigid mount. The sensor amplifier output is viewed on a strip chart while the cable is lightly twanged. Since the X-Y carriage and the bottom of the cable are constrained to be motionless, the position sensor output should be zero. Oscillating outputs indicate improper gains in the optical sensor amplifiers that should be readjusted. This test should also be done every time the link angle sensor gain is changed, and periodically during regular calibration.

6.2.7 Force Sensor Calibration Check (Figure 6-8)

Objective: Verify the calibration of the Z-axis force sensor and
and the 6-component mast base transducer.

Performance Criteria: The transfer ratio of the transducers will be
linear within TBD percent with less than TBD
bias.

Equipment: Calibrated weights plus hangers
DVM or H-P Analyzer
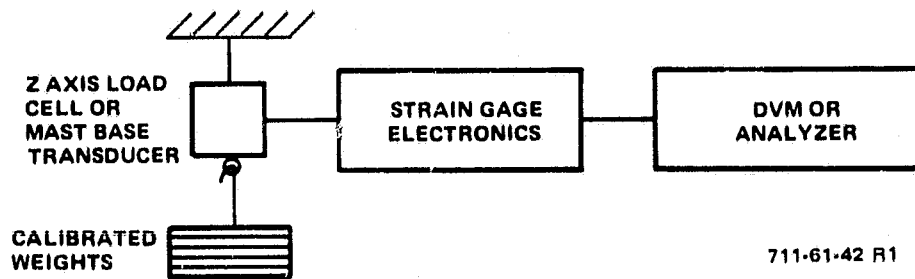
Figure 6-8
Test Setup: Force-Sensor Calibration Check

Test: Calibrated weights are hung on the Z-axis load cell and the six-axis
mast base transducer to verify the transducer calibration. The six-component
transducer is supplied with a calibration body on which the weights are hung,
thus allowing both forces and torques to be applied to the transducer. This
test is a standard calibration procedure, and should be done regularly.

6.2.8 Safety Device Verification

Objective: Verify the operation of the fail-safe brake on the
              Z-axis loop, and the X-Y position limiters.

Performance Criteria: Safety device function will be verified before
                         operation of the ZGTF. Devices to be tested
                         are the fail-safe brake on the Z-axis and the
                         X- and Y-axes travel limiters. The fail-safe
                         brake should engage any time there is a failure
                         in the Z-axis control loop; for example, power
                         failure to the electronics or disconnection of
                         the force sensor or torque motor from the
                         electronics.

Test: Function of the brake will be tested by disconnecting the force
transducer, the motor, and the electrical power from the Z-axis control
electronics. For this test, the bottom of the Z-axis cable will be attached
to an unmovable object (such as the floor), with a constant force command to
the cable.

The X- and Y-axes travel limiters should interrupt power to the X- or
Y-axes motors whenever the limiters are tripped. These can be tested by
manually driving the ZGTF carriage in the X and Y directions until the
limiters are tripped and monitoring the motor power in the appropriate axis.
Motor power should go to zero when the limit of travel is reached. Both of
these tests should be done regularly during calibraton and before beginning a
series of tests to ensure that the test article or test facility will not be
inadvertently damaged by an electronics failure.

6.2.9 Z-Axis Force Error Test (Figure 6-9)

Objective: Measure the force error produced at the bottom of the Z-cable under simulated operating conditions.

Performance Criteria: The force output of the Z-loop will vary by less than .02 percent during operation.

Equipment: Slew Simulator Calibrator
Full-Up ZGTF
Strip-Chart Recorder
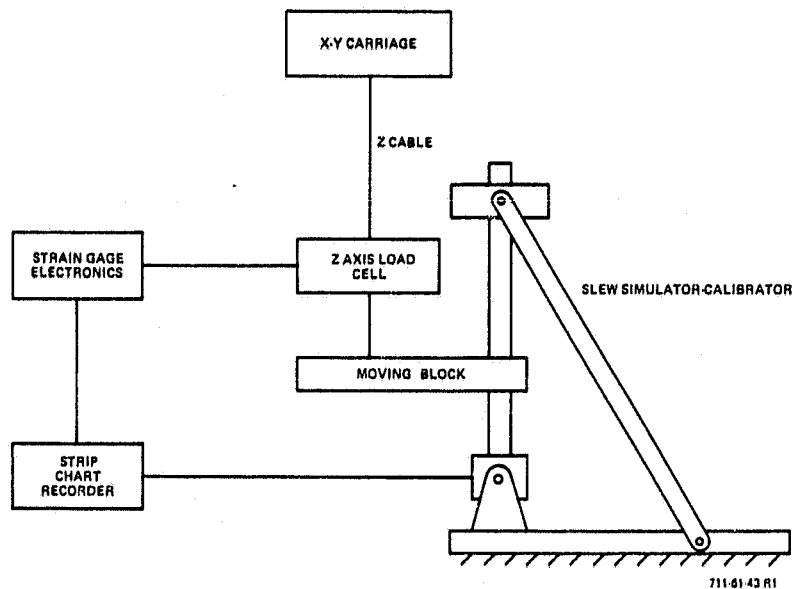
Figure 6-9
Test Setup: Z-Axis Force Error Test

Test: The Z-axis loop is designed to apply a constant vertical force to the item under test. The slew simulator checks the level of error present in the Z loop during dynamic testing. The simulator is set up in the vertical position with the Z-axis cable attached to the moving block. The X-Y carriage is positioned so that the X-Y position sensor reads zero (Z cable vertical). The cable force is commanded to some typical test value and the force sensor reading is output to the strip-chart recorder. The slew simulator position and Z-loop error are also recorded. A constant speed command equal to the maximum test article rate is applied to the simulator, producing a ramp position change for the Z cable. After the desired amount of travel is reached, the simulator is stopped. The recorded data will show the Z-loop error response to a ramp input and the loop steady-state error for the time after the simulator is stopped. From this data the expected torque error applied by the Z loop to the test articles can be calculated. This test will be done once following the facility start-up to verify the accuracy of the system analyses and should be repeated if changes are made to the control-loop compensations.

6.2.10 X-Y Loop Position Error Test (Figure 6-10)

Objective: Measure position error between the X-Y carriage and the suspension point at the bottom of the Z-cable during simulated operation. Transient and steady-state errors will be measured.

Performance Criteria: The position error in either X or Y directions will be less than .020 inch under operating conditions.

Equipment: Slew Simulator-Calibrator
Full-Up ZGTF
Strip-Chart Recorder

6-16

711-61-44 R1
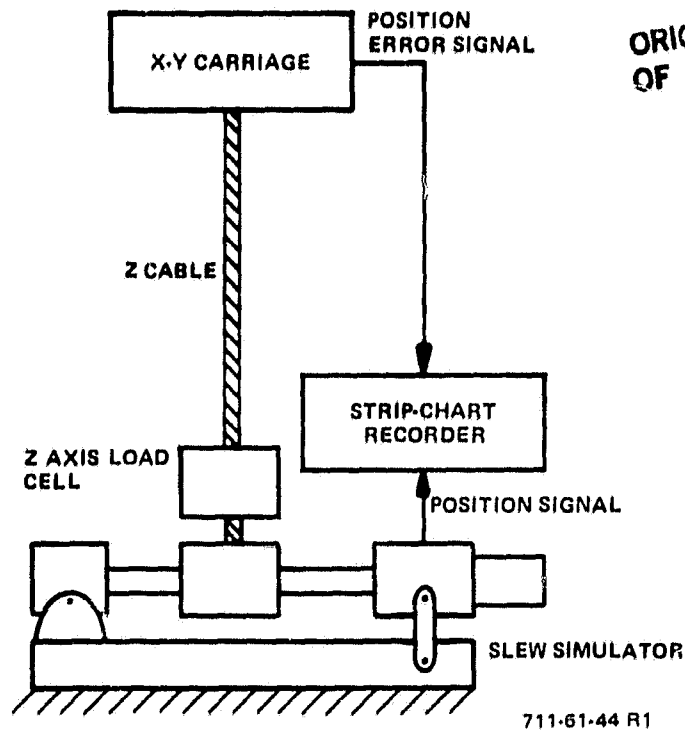
Figure 6-10
Test Setup: X-Y Loop Position Error Test

Test: The X and Y position loops are designed to force the X-Y carriage to follow the motion of the test article suspended by the Z cable. This test is set up similar to the Z-loop error test except that the slew simulator is in the horizontal position. The X-Y loop position error signals and the slew simulator position signal are fed into the strip-chart recorder. The Z-axis force is commanded to some typical test value to ensure tension on the cable. A constant rate equal to the maximum test article rate is commanded to the slew-simulator until the desired amount of travel occurs, and then is shut off. The data recorded will be the X- and Y-loop position error for a ramp position input and the steady-state position error for the time after the simulator is shut off. This data can be used to calculate the torque error applied by the X and Y loops to the test article. This test will be done in each the X and Y direction. The test should be run following ZGTF start-up and after any changes to the X-Y loop compensations.

APPENDIX

VALIDYNE MC1 SYSTEM - MULTICHANNEL MODULAR
TRANSDUCER CONTROL SYSTEM

Validyne

ENGINEERING CORPORATION.

Signal Conditioning for All Types of Transducers
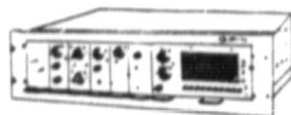
Multi-Channel Modular Transducer Control System

V≡ Validyne
ENGINEERING CORPORATION
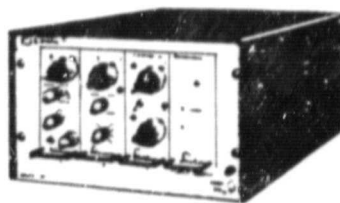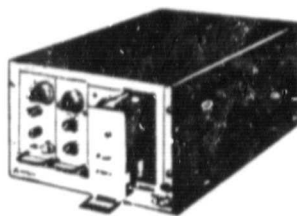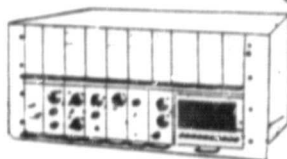
MC1 System

A Multi-Channel Modular Transducer Control System That Can Facilitate Your Data Acquisition Requirements.

- Up to 20 plug-in units per module case
- Operation with Variable Reluctance, Strain Gage, Piezoelectric, Piezoresistive, LVDT and Temperature Transducers
- Conditioners for Frequency and Voltage Inputs
- Selectable Carrier Frequency 400 Hz to 20 kHz
- Short circuit proof
- Low cost per channel

The MC1 System consists of a complete line of Signal Conditioning units housed in compact module cases. Designed to be either rack or surface-mounted, they provide the user with superb flexibility to handle a wide variety of signal conditioning needs.

The signal conditioning requirements of the variable reluctance units have stimulated development of transducer control systems which offer wide usage for all types of transducers and measurement of electrical parameters associated with many physical variables. A stronger capability for data acquisition is now available through the development of signal conversion and digital data handling techniques.

The MC1 module cases provide the necessary DC operating voltage and carrier excitation for the plug-in units and associated transducers. A broad line of signal conditioning plug-in units are available for use with variable reluctance, LVDT, strain gage, piezoelectric, piezoresistive and temperature transducers, voltage and frequency input signals. These are described on the following pages.

The all solid state precision carrier supply is a distortion-free Wien-Bridge oscillator in a closely controlled feedback loop to insure constant voltage and frequency output. Available carrier frequencies from 400 Hz to 20 kHz can be easily changed in the field by means of small plug-in frequency determining boards.

Protection against overload and short circuit of the carrier supply is provided. In the event of an overload or short circuit on the carrier output, the oscillator will shut down and recover automatically when condition is removed.

Validyne maintains its consistently high capability for engineering, design and manufacture of custom electronics and transducers. This is totally in keeping with the level of performance Validyne has achieved ... a

level which meets general instrumentation requirements at a more competitive price.

The MC1 module case is truly multi-channel, housing up to 20 plug-in units and providing the necessary carrier and DC operating voltages for a broad line of plug-in units and associated transducers. The units are available in 20, 10 and 3 channel capacities.
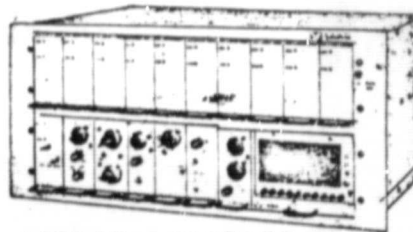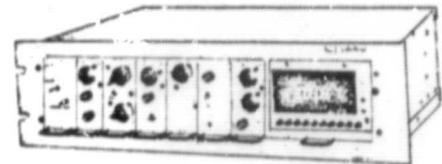
MC1-10 and MC1-20

The MC1-10 Series Module Case provides plug-in capacity for up to 10 plug-in signal conditioning modules and provides the necessary DC operating voltage and carrier excitation both for the modules and their associated transducers. The MC1-20 accommodates up to 20 channels.

The complete line of Validyne manufactured signal conditioning plug-in modules are wholly compatible with the system for use with variable reluctance, LVDT, strain gage, temperature, piezoelectric and piezoresistive transducers, voltage and frequency inputs.

Validyne
ENGINEERING CORPORATION

MC1-3

This is a 3-channel, scaled-down Signal Conditioning System for applications where signal conditioning is to be dedicated to small data acquisition requirements. Typically, the system may be used as peripheral equipment with mini computers. The portability feature of the MC1-3 makes possible many laboratory and field tests, where rapid response to set up requirements is mandatory while restricted to low cost inventory.
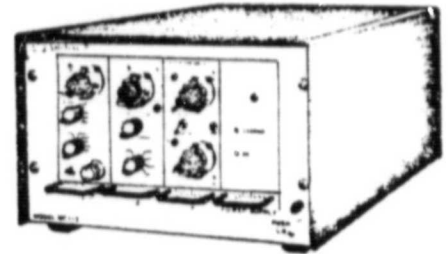
Specifications for MC1-20, MC1-10, MC1-3

Power Input: 105-125V AC, 50-400 Hz Optional 210-250V AC, 50-400 Hz, add -C to model number.

Power Consumption: MC1-10 & -20: 150VA max. MC1-3: 15VA max.

Carrier Supply:
Voltage: 5V rms, sine wave
Power: MC1-10 & -20: 10VA max. MC1-3: 0.75VA max.

Frequency: 3 kHz unless otherwise specified. Optional: 5 kHz, 10 kHz, 20 kHz, and 400 Hz available. Can be changed in field, see "Accessory" page for plug-in assembly P/N 7796

Regulation:	Amplitude	Frequency
Line, 105-130V AC/ 210-250V AC	±0.05%	±0.01%
Load, No load to full load	±0.15%	±0.10%
Temp., 0-160°F	±0.01%/°F	±0.006%/°F

DC Supply: ±15V DC for plug-in units, overload and short-circuit proof.

Electrical Connections:
Transducer Input: WK-4-32S, 1/channel, mating connector WK-4-21C
Output: XLR-3-32S, 2/channel, mating connector XLR-3-11C

Power Connection: MC1-10 & -20: 3-wire socket, rear panel (6' line cord furnished)

MC1-3: 3-wire power cord and plug attached to unit

Size:

MC1-20 — 8¾"h x 19"w x 12"d Standard Rack Mount (22.2cm x 48.2cm x 30.2cm)

MC1-10 — 5¼"h x 19"w x 12"d Standard Rack Mount (13.3cm x 48.2cm x 30.2cm)

MC1-3 — 5-19/32"h x 8½"w x 13¾"d Cabinet (14.9cm x 21.6cm x 34.5cm).

Optional Feature:
MC1-3 — Standard Rack Mount 5-19/32" x 19". Specify MC1-3R

Weight (not including modules):

MC1-20	22 lbs. (10.0 kg)
MC1-10	20 lbs. (9.1 kg)
MC1-3	9 lbs. (4.0 kg)

Validyne
ENGINEERING CORPORATION

MC1 SYSTEM Application Charts

MODULES APPLICATION

APPLICATION	TYPE OF TRANSDUCER	MC1 SIGNAL CONDITIONING PLUG-IN MODULE	TYPES OF MODULES USED
Acceleration, Steady	Variable Reluctance Strain Gage	CD18, CD19, CD90 See Force/Load	Carrier demodulators, dual outputs.
Flow	Differential Pressure Turbine Flowmeter	See Pressure FC62	Carrier demodulators, dual outputs. Frequency-to-voltage converter.
Force/Load	Strain Gage, AC Excitation (see Note 1) Strain Gage, DC Excitation (see Note 2)	CD19, CD90 SG71	Carrier demodulators, dual outputs selectable gain DC strain gage signal conditioner
Position, Linear and Angular	Variable Transformer Potentiometer	CD148, CD18, CD19, CD90 BA112, CD19	Carrier demodulators, dual outputs selectable gain. DC buffer amplifier or carrier demodulator
Pressure	Variable Reluctance Strain Gage, AC Excitation (see Note 1) Strain Gage, DC Excitation (see Note 2) Potentiometer	CD18, CD19 CD19, CD90 PE251 SG71 BA112, CD19	Carrier demodulators, dual output selectable gain. Pressure to voltage/pressure to current converter Strain gage signal conditioner provides DC excitation for strain gage. DC buffer amplifier and carrier demodulator.
RPM	Electro-magnetic or Photocell	FC62 FC236	Frequency to voltage converters.
Temperature	Resistance Thermocouple Thermocouple	PT60 CM196 (see Note 3), CD19, CD90 TC243	Platinum and nickel resistance thermometer signal conditioner. Remote carrier modulator Carrier demodulators high gain. Thermocouple conditioner.
Torque	Strain Gage Rotary Transformer	SG71 CD19, CD90	Strain gage signal conditioner. Carrier demodulator, high gain.
Velocity, Displacement, Vibration	Piezo-Electric Strain Gage Electro-magnetic	PA89 SG71, AM49 AM49	Piezoelectric signal conditioner Strain gage signal conditioner & linear amplifier Linear amplifier with integrators
Vibration	Piezo-Electric Strain Gage	PA89 SG71	Piezoelectric signal conditioners Strain gage signal conditioners

NOTES:
1. AC carrier excitation features low noise and good zero stability, but frequency response limited to 25% of carrier frequency.
2. DC excitation features frequency response to limit of transducer.
3. CM196 is an external accessory mounted near the thermocouple to convert the DC signal to a modulated carrier voltage.

SPECIAL FUNCTION MODULES

APPLICATION	PART NO.	NAME	DESCRIPTION
Alarm	AL64	Alarm Controller Unit	Adjustable HI-LOW Alarm
	AD136	Peak Hold/Auto Zero	Holds peak input signals, provides automatic zero functions.
Analog Multiplexers	MPX255	Analog Multiplexer 10 or 20 Channels	Multiplexes analog output signals of the 10 or 20-channel signal conditioning modules.
	MAD264	Analog Multiplexer, 10 or 20 Channels, with A/D Conversion	Multiplexes the analog output signals of 10 or 20-signal conditioning modules and converts the signal output to digital format.
Arithmetic	MF253	Multifunction Module	Multiplies, divides and performs square-root operations. Internally selectable.
Automotive	FC236	Frequency to Voltage Converter	Converts electrical ignition timing pulses to a DC voltage proportional to RPM

Validyne
ENGINEERING CORPORATION

SPECIAL FUNCTION MODULES (Cont...)

APPLICATION	PART NO.	NAME	DESCRIPTION
Carrier-Demodulator (special purpose)	CD257	Carrier demodulator with Suppression and X10 Gain	Carrier Demodulator with suppression control and X10 gain capabilities
	CD262	Carrier Demodulator with 4 to 20 mA or Square Root, 10V DC output	Carrier demodulator with special outputs
Filters	BPF205	Band Pass Filter	Provides selectable frequencies pass bands from DC to 10 kHz
	LPF162	Ultra Low Pass Filter	Provides low pass filtering 0.1 to 300 second filter time constants
Remote Carrier Modulator	CM196	Remote Carrier Modulator	Provides remote carrier modulation and isolation to low level DC input signals. Optional cold junction compensation for thermocouple inputs.
Null Indicator	NI157	Null Indicator	Provides a visual indication of "R" and "C" balance.
Indicators	PM118	Plug-In Analog Meter	Vertical panel meter. Reads 0 to ±10V DC
	PM204	Plug-In Analog Meter	19-position vertical-scale meter for MC1-10 and MC1-20 systems. Selector switch to display 9 or 19 channels. 10X scale expansion external inputs
	PM212-1	Plug-In Digital Meter	17-position 3½-digit readout for MC1-10 and MC1-20 systems.
	PM212-2	Plug-In Digital Meter	17-position 4½-digit readout for MC1-10 and MC1-20 systems.
Calibration Simulators	TS234	Transducer Simulator	Provides transducer simulation signals for system calibrations and diagnostic testing of carrier demodulators
Temperature	TC243	Thermocouple Amplifier	Provides cold junction compensation and amplification of thermocouple input signals.

MC1 SYSTEM Typical Applications
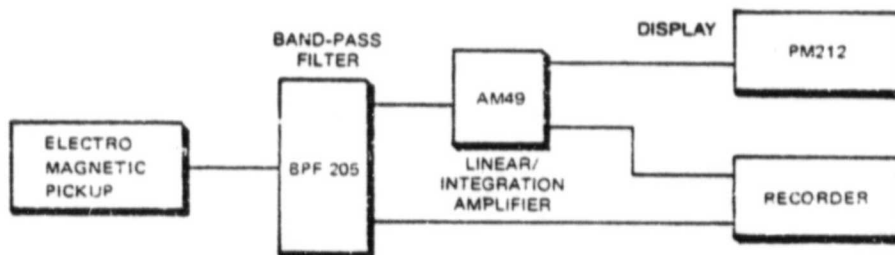
Typical Velocity and Displacement Measuring System
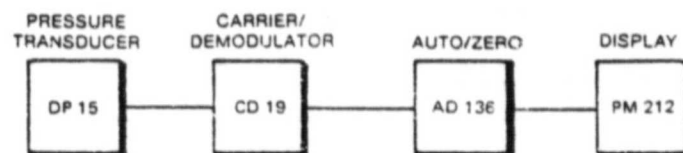
Typical Auto Zero of Residual Pressure System Set-up

Validyne
ENGINEERING CORPORATION

MC1 SYSTEM   Module Index

This numerical index is provided to facilitate module information retrieval. Complete unit information can be found in the appropriate data sheet.

MODEL NO.	NAME	DESCRIPTION
CD18	Carrier Demodulator Dual Output	Demodulates and signal conditions transducer output
CD19	Selectable High Gain Dual Output Carrier Demodulator; Sensitivity from 1 mV/V to 166 mV/V	Operates with full bridge or half bridge transducers — delivers 10V DC output for inputs from 1 mV/V to 166 mV/V
AM49	Linear, Single and Dual Integration Amplifier	Selectable gain linear amplifier with low pass filter
PT60	Resistance Thermometer Conditioning Unit	Indicates resistance of temperature sensor — produces voltage proportional to the input resistance
FC62	Frequency to Voltage Converter	Converts electrical frequency signals between 50 Hz to 50 kHz to a proportional DC voltage
AL64	Alarm Controller Unit	Offers two continuously adjustable set point 0 to ±10V DC
SG71	Signal Conditioner and Power Supply	Provides a short-circuit proof, DC excitation supply for strain gage bridge circuits
PA89	Vibration Monitoring Amplifier	Produces an output proportional to acceleration, velocity or displacement for use with piezoelectric pickups
CD90	Ultra High Gain Dual Output Carrier Demodulator Sensitivity 0.1 mV/V	Provides transducer excitation, amplifies and demodulates output of carrier, excites strain-gage bridges and transducers, LVDT/RVDT
BA112	Buffer Amplifier	Offers a high impedance selection gain differential input for AC and DC signals and provides a low impedance single-ended output
PM118	Plug-In Analog Meter	Vertical Panel Meter. Reads 0 to ±10V DC (Refer to p. 7 for additional information)
AD136	Peak Hold/Auto Zero	Senses and holds a peak input signal without decay until a larger signal is applied or until reset to zero.
CD148	Carrier Demodulator LVDT Conditioner	Demodulates the output of linear variable differential transformer

| MODEL NO.	NAME	DESCRIPTION
LPF162	Ultra Low-Pass Filter	Provides extremely low-pass filtering for other MC1 signal conditioning modules Provides unity voltage gain.
PM204	Plug-In Analog Meter	19-position vertical-scale meter for MC1-10 and MC1-20 systems
BPF205	Band Pass Filter	Provides selectable frequency pass bands from DC to 10 kHz
PM212-1	Plug-In Digital Meter	17-position 3½ digit readout for MC1-10 and MC1-20 systems
PM212-2	Plug-In Digital Meter	17-position 4½-digit readout for MC1-10 and MC1-20 systems
TS234	Transducer Simulator	Provides transducer stimulation signals for system calibrations and diagnostic testing of carrier demodulators
FC236	Frequency to Voltage Converter	Converts electrical ignition timing pulses to a DC voltage proportional to RPM
TC243	Thermocouple Amplifier	Provides cold junction compensation and amplification of thermocouple input signals
PE251	Pressure to Voltage Converter	Provides dual outputs of voltage, square-root function, or 4-20 mA of pressure input
MF253	Multifunction Module	Multiplies, divides and performs square-root operations.
MPX255	Analog Multiplexer 10 or 20 Channels	Multiplexes analog output signals of the 10 or 20 channel signal conditioning modules.
CD257	Carrier Demodulator with Suppression and X10 Gain	Carrier demodulator with suppression control and X10 gain capabilities.
CD262	Carrier Demodulator with 4 to 20 mA or Square Root and 10V DC output	Carrier demodulator with special output capabilities.
MAD264	Analog Multiplexer, 10 or 20 Channels, with A/D Conversion	Multiplexes the analog output signals of 10 or 20 channel signal conditioning modules and converts the signal output to digital format.

Validyne
ENGINEERING CORPORATION

MC1 SYSTEM   Accessories

ACCESSORIES INDEX

MODEL NO.	NAME	DESCRIPTION
MC1-3	MC1 Mating Connector	Set of 9 connectors (Refer to p. 7 for additional information)
MC1-10	MC1 Mating Connector	Set of 30 connectors (Refer to p. 7 for additional information)
MC1-20	MC1 Mating Connector	Set of 60 connectors (Refer to p. 7 for additional information)
7110	Transducer Cable	Standard 10 ft. cable with WK-4-21C on each end (Refer to p. 7 for additional information)
7273	Blank Panel	For empty channel slot (Refer to p. 8 for additional information)
7592	MC1-3 Rack Mount Kit	To mount either one or two MC1-3 cabinet in a standard 19-inch rack (Refer to p. 8 for additional information)
7616-2	Plug-in Module Extender	PC plug-in board with 20-inch cable. PC plug-in board connector at end of cable (Refer to p. 8 for additional information)

MODEL NO.	NAME	DESCRIPTION
7796-X	MC1 Carrier Frequency Determinant	Changes MC1 Module carrier excitation frequency. See table on p. 8 of this brochure for dash number (X) identification. (Refer to p. 8 for additional information)
8050-1	Blank Plug-in Module	Plug-in module with blank PC board. No plating. (Refer to p. 8 for additional information)
8050-2	Blank Plug-in Module	(Same as 8050-1) Complete clad copper-PC board (Refer to p. 8 for additional information)
8542-2	Module Interconnect Cable	2-ft long cable connecting output of XLR3 module to input of another XLR3 module (Refer to p. 8 for additional information)
8573-2	Module Interconnect Cable	2-ft long cable connecting output of XLR3 module to input of a WK-4 module (Refer to p. 7 for additional information)
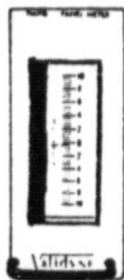
PM118 Plug-in Analog Meter
Consists of a vertical panel meter mounted on a PC plug-in board. Reads 0 to ±10V DC. Connection is made at output connectors on the back panel of the MC1 module case.

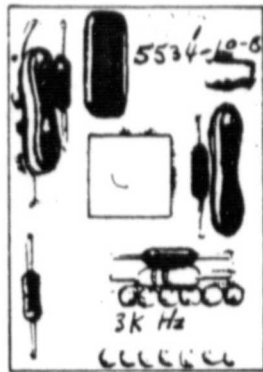**P/N 7592 — MC1-3 Rack Mount Kit**
Designed for mounting either one or two MC1-3 cabinets in a standard 19" relay rack. Takes 5¼ inches of rack space.
For one unit specify (1) each P/N 7592-1 and -2.
For two units specify (2) P/N 7592-1.
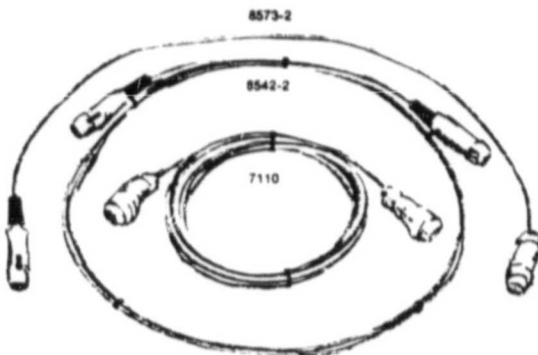
◤Validyne
ENGINEERING CORPORATION

MC1 SYSTEM   Accessories

Alternate Carrier Frequency Accessories

P/N 7796-"X" — MC1 Carrier Frequency Determining Plug-in Assembly
Used to change MC1 module case carrier excitation frequency. See following table for dash numbers that relate to the frequency designation.

DASH NO.		CARRIER FREQUENCY
-1	....	3 kHz
-2	....	5 kHz
-3	....	10 kHz
-4	....	20 kHz
-5	....	400 Hz

P/N 7110 — Transducer Interconnecting Cable
Standard 10-foot cable with WK-4-21C on each end for Validyne Variable Reluctance Transducer input. Specify P/N 7110-10 for standard length. Additional lengths specify footage in dash numbers — e.g., 20-foot cable, P/N 7110-20.

P/N 8542-2 — Connecting Cable
Module interconnecting cable, XLR-3-11C to XLR-3-11C, (output to output) Std. 2 ft.

P/N 8573-2 – Connecting Cable
Module interconnecting cable, WK-4-21C to XLR-3-11C, (input to output) Std. 2 ft.
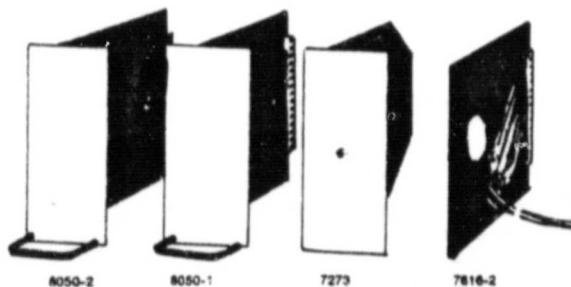
P/N 8050-1 — Blank Plug-in Module
A complete blank plug-in module with blank PC board. PC board contains no plating except for PC connector pads.

P/N 8050-2 — Blank Plug-in Module
A complete blank plug-in module with blank PC board. PC board is copper clad.

P/N 7273 — Blank Panel
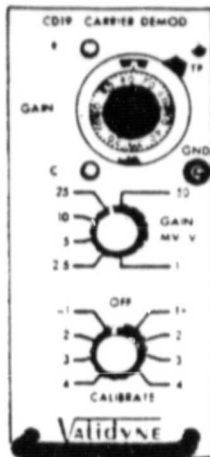The purpose of this panel is to fill in the space of an empty channel.

P/N 7616-2 — Plug-in Module Connection Extender
Permits plug-in modules to be checked or adjustments made outside of the MC1 module case. Accessory consists of a PC plug-in board and a 20-inch cable with a PC board mating connector attached to the end of the cable.

Validyne
ENGINEERING CORPORATION

MC1 SYSTEM

CD19   CARRIER DEMODULATOR

Features

Six selectable gain settings

Selectable calibration points

Four selectable frequency response ranges

3 kHz carrier operation

Adjustable R & C balance controls

Dual output

Specifications

Input Sensitivity: 1 mV/V, 2.5 mV/V, 5 mV/V, 10 mV/V, 25 mV/V and 50 mV/V (switch selected)

Gain Vernier: 0 to 100%, calibrated dial

Bridge Excitation: 5V rms AC, 3 kHz from precision center tapped transformer

Bridge Configuration: 2 & 4 arm variable reluctance & strain gage transducers, LVD transformers and potentiometer transducer

Input Impedance: Single ended, 100K ohms. Differential, 200K ohms

Bridge Balance: Resistive (R), normal 2 mV/V, high 20 mV/V; Capacitive (C) normal 1 mV/V, high 10 mV/V

Output: A: ±10V DC at 10 mA; B: ±5 mV DC at 0.5 mA

Output Impedance: A: 50 ohms; B: 10 ohms

Output Noise: 80 mV p-p with 1 kHz filter; 20 mV p-p with 200 Hz filter; 10 mV p-p with 50 Hz filter; 2 mV p-p with 10 Hz filter

Frequency Response: Selectable 0 to 10, 50, 200 or 1000 Hz, flat ±10%

Linearity: ±0.05% FS

Temperature Range: 0°F to +160°F

Thermal Zero Shift: 0.003%/°F

Thermal Sensitivity Shift: 0.01%/°F

Power Requirements: 5V rms, 3 kHz & ±15V DC supplied by MC1 module case

Description

The CD19 is a high gain, dual output Carrier Demodulator Plug-In Module for use in Validyne Engineering Corporation's MC1 System. The unit is used to provide transducer excitation, and to amplify and demodulate the output of carrier-excited strain-gage bridges and transducers, variable reluctance transducers, potentiometric transducers and linear and rotary variable differential transformers (LVDT/RVDT).

The CD19 will operate with full-bridge or half-bridge transducers delivering 10V DC output for inputs ranging from 1 mV/V to 166 mV/V. A six-position gain switch and a ten-turn vernier gain potentiometer permit the use of inputs up to 166 mV/V.

Screwdriver adjusted "R" and "C" balance controls are provided, with a HI and LOW balance range switch for a 10 to 1 balance range expansion.

A calibration circuit provides availability of four different levels of plus and minus calibration voltages to be injected into the input.

Output frequency response is controlled by a low-pass active filter, and is switch selectable to 10 Hz, 50 Hz, and 200 Hz and 1 kHz.

Options Available

Dash #	Description
-529	A & B outputs 10V DC
-809	"A" output 10V DC "B" output 5V DC
-1155	Bifurcated terminals for R56 & R57
-1268	A & B outputs 5V DC
1309	Output filter 1 Hz, 5 Hz, 20 Hz and 100 Hz
-1312	"A" output 4-20 ma "B" output 10V DC

REPRESENTED BY
QUALTECH, INC
DICK CUNNINGH
610 W. BROADWAY ⸱
TEMPE, AZ. 85281
967-4655

For typical application, see reverse side

Typical Applications
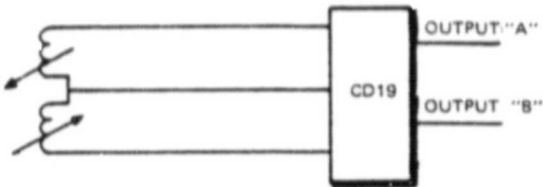
Variable Reluctance
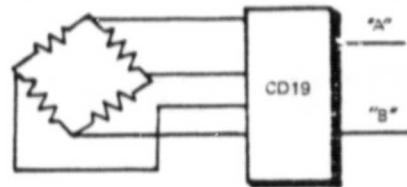
Strain Gage Bridge Carrier Excited

NOTE: CD19 may be operated over 1000 or more feet of cable between it and the transducer.
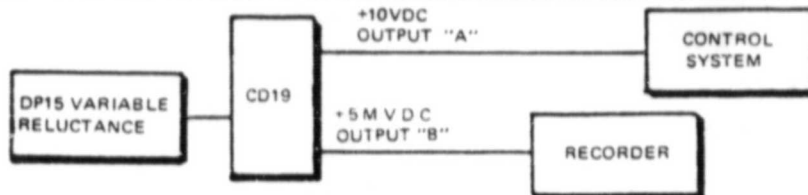
Simple Pressure Measurement and Control System
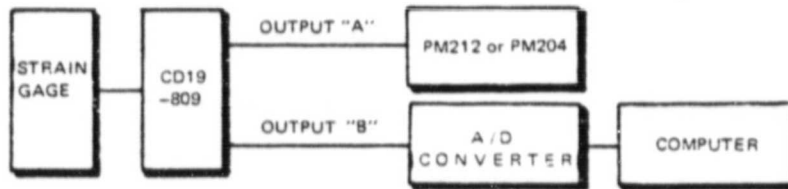
Simple Force/Load Measurement and Control System
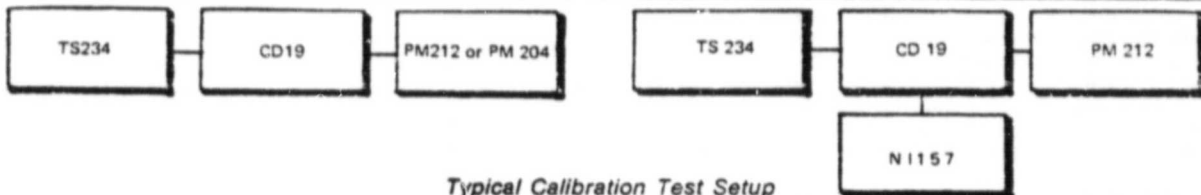
Typical Calibration Test Setup
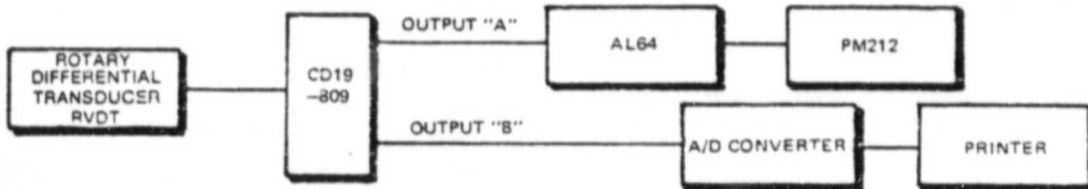
Torque Measurement and Alarm System

Accessories

SERIES D

• SIX COMPONENT
• INTERNAL

STRAIN GAGE
BALANCE
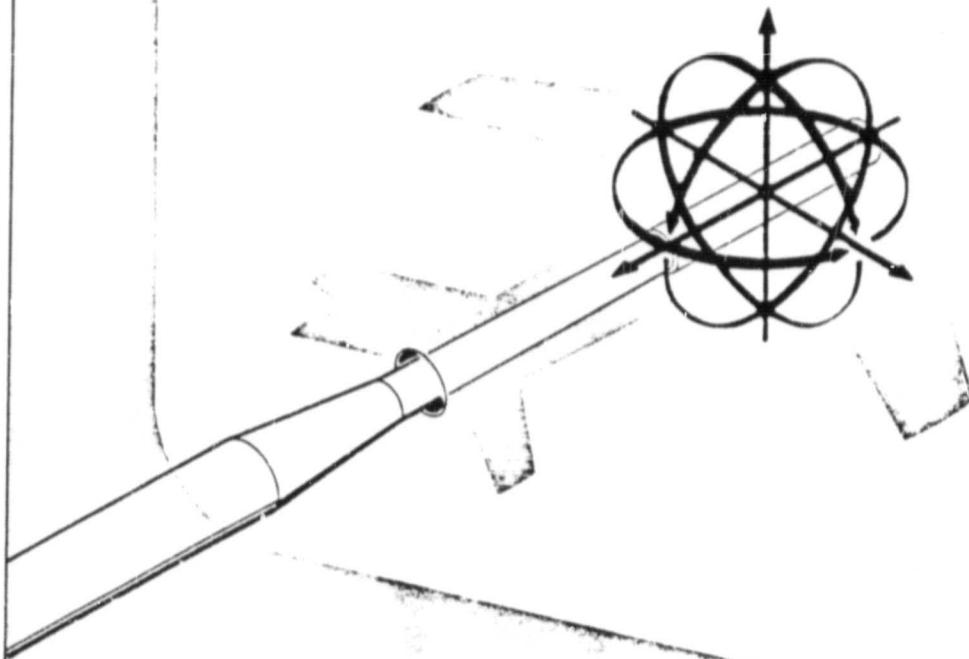
ABLE CORPORATION

GENERAL DESCRIPTION

The Able Corporation Series-D, six component internal strain gage balance is basically of the floating-frame type. The primary frames consist of an inner rod, which fastens to the model support sting, and a cylindrical outer case, which is inserted into and attaches to the model. Forces and moments are resisted by individually removable elements, employing flexure pivots, connected between the inner rod and outer case of the balance.

The six force and moment sensing components of the balance consist of two normal force elements for determination of normal force and pitching moment, two side force elements for determination of side force and yawing moment, a dual axial force element and a dual roll element.

The normal and side force elements are equipped with relaxation members at either end and are arranged to act in roll as a set of crossed ribbon flexures. Similar relaxation members provide compliance in the axial force direction. The rolling moment elements are provided with flexure pivots at either end which are designed to transmit pure rolling moment to the gage section. The dual axial force element is located inside the dual roll element and transmits axial force from the outer case to the inner rod.
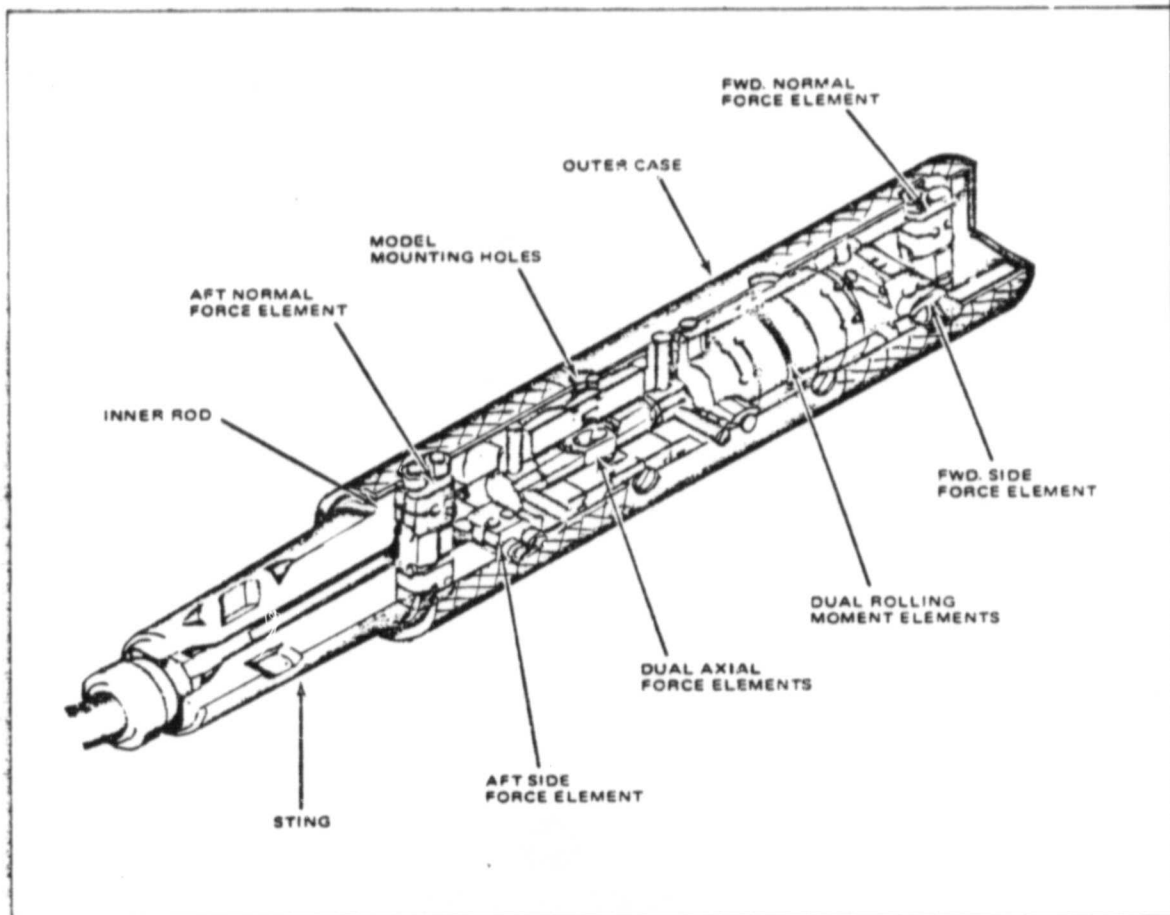
PERFORMANCE

Accuracy – All points from any series of loadings of a single element produce data within ±0.25% of maximum load or ±0.5% of applied load when compared with the best straight line fit. This accuracy is inclusive of all scatter, hysteresis, and non linearity for both plus and minus loads.

Interactions – Percentage interactions on any gage member caused by the application of full design load on any other gage member fall within the following values: Seventy % of the possible first order interactions will be less than or equal to 0.5%. An additional 20% of the first order interactions will be less than or equal to 1.0%. The remaining 10% of the first order interactions will be less than or equal to 3.0%. All interactions in excess of 1.0% will be linear within plus or minus 10% of the interaction output.

The percentage values of the first order interactions may change slightly if specifications require a small diameter balance or a very light or very heavy load range.

Thermal effects – Transient temperature errors in any gage element do not exceed 1.0% of full load output when the sting temperature is constant or changing and the outer case temperature is changing at a rate of 5°F per minute between 60°F and 180°F.

At stabilized temperatures, the error in any gage element does not exceed 0.5% of full load output between 60°F and 180°F.

Sensitivity – Full load output of any gage member is approximately 1 millivolt per volt input.

Gage characteristics – Bridge resistance is 350 ohms for normal and side force elements.

The basic bridge resistance of the rolling moment and axial force elements is 350 ohms. However, these components each operate with two full bridges wired in parallel. Thus the resistance is 175 ohms.

Operating voltage of each element is 6 to 12 volts. Lower voltage is recommended for balances 0.75 inch diameter or less.

PERFORMANCE EVALUATION

Each balance is subjected to a performance evaluation to demonstrate satisfactory operation of all functions. It is expected that a more detailed calibration, tailored to the individual laboratory's needs, will be performed by the user. More complete calibrations can be performed by Able if desired.

TEMPERATURE COMPENSATION PRINCIPLE

The arrangement of axial force elements provides complete mechanical compensation for radial temperature gradients. The two axial force element strain gage bridges are wired to produce a signal when the forces on the two elements are opposite in sign. (This occurs only when an external axial load is applied.) If there is a length increment due to change in temperature added all along the inner rod or outer case, each axial force gage will experience an increment of load having the same sign and the signals will cancel. Thus the sensitivity of axial force to temperature gradients has been significantly reduced.

STRAIN GAGES

All gaged sections, with the exception of rolling moment, are of the bending type employing 4-active foil type, epoxy bonded, 350 ohm strain gages. Rolling moment is resisted by a torque tube to which are bonded similar gages also wired in the form of a 4-active element bridge.

All strain gages are pre-matched in complete bridges for resistance and change in resistance with temperature. Bonding is accomplished using a combination of heat cycling and pneumatically applied pressure. After bonding, the individual bridges are again checked for temperature effects and trimming resistors are added where necessary.

ACCESSORIES

Able Corporation also produces all necessary balance accessories including:

- **Ring and plug gages**—Master gages for balance-to-sting joint.
- **Balance gage**—Exact duplicate of the balance exterior and sting fitting. Center hole permits passage of leads when used in place of a balance.
- **Calibration body**—Loading sleeve used to apply loads for sensitivity and interaction calibration. Includes roll arm, precision circular level and flexures to which weight hangers attach.
- **Calibration rig**—Complete single or multiplane rigs for the application of calibrating loads outside of the tunnel.
- **Calibration weights**—Traceable to National Bureau of Standards are offered in the ranges 2#, 5#, 10#, 25#, 50#, 75# and 100#. Weight tolerance is ±0.1% of the total unit weight. More exacting tolerances are quoted on request.
- **Coolant jackets**—Required for balance operation up to stagnation temperatures of $1,500^\circ$F. Available for all balance sizes and require a minimal diameter increase.
- **Overload stops**—Available for roll and axial force in all balance sizes.

STANDARD PERFORMANCE CALIBRATION PROCEDURE

1. Positive and negative design loads are applied to the balance outer case such that each force and moment element is loaded individually. The load on each element is applied in increments not greater than one-fifth of full design load.

Normal forces and side forces are applied orthogonally to the outer case, and axial force is applied along the axis of the outer case. Rolling moment is applied to the outer case by means of a moment acting in a plane normal to the balance axis.

Each gage output is tabulated and sensitivity calculated for each element in terms of millivolts per volt per pound or millivolts per volt per inch pound for both increasing and decreasing loadings. Interactions are plotted in terms of percent full load output in the member being interacted upon, versus applied load.

2. With the sting taper maintained at approximately 60°F the balance case temperature is increased at a rate of at least 5°F per minute until the balance has reached 180°F. The outer case temperature is then maintained at 180°F until the inner case temperature is stabilized, then the temperature is reduced at least 5°F per minute until the balance is again stabilized at 60°F. The output of all gages and thermocouples are recorded every 2 minutes throughout the run.

A similar test is also performed wherein both the sting taper and balance sleeves are raised simultaneously in temperature to 180°F.

With the balance at approximately 180°F, each component is loaded separately and the sensitivity in millivolts per volt per pound or millivolts per volt per inch pound is calculated.

Prior to assembly, the individual balance elements are subjected to a sudden pressure change from 2 to 60 PSIA and the outputs recorded.

SIZE AND RANGES

Representative standard sizes and ranges of Series D balances are given in the table. The force and moment values shown are based on typical requirements. Other sizes and/or load ranges are available either as new designs or modifications of existing types. There are over 200 standard designs currently available.
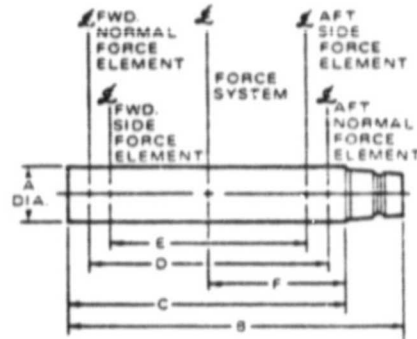
DIMENSION		0.50 MK IV	0.75 MK XLI	1.00 MK XIII	1.25 MK XIV	1.50 MK VI	2.00 MK XXVII	2.50 MK XVII	4.00 MK V
INCHES	A	0.50	0.75	1.00	1.25	1.50	2.00	2.50	4.00
	B	3.34	4.66	6.50	8.25	9.87	11.50	14.43	23.36
	C	2.74	3.83	5.10	6.28	7.23	8.90	11.16	16.75
	D	2.10	3.00	4.30	5.25	6.00	7.25	9.00	14.00
	E	1.70	2.50	3.50	4.25	5.00	6.00	7.50	11.50
	F	1.28	1.80	2.50	3.03	3.60	4.38	5.28	8.05
POUNDS	N_1	75	100	250	650	1000	1500	2500	6000
	N_2	75	100	250	650	1000	1500	2500	6000
	S_1	40	50	150	325	500	800	1250	3000
	S_2	40	50	150	325	500	800	1250	3000
	A	50	30	75	90	150	200	300	500
INCH POUNDS	ROLL	20	100	150	600	1,200	2,000	4,000	12,000
	PITCH	158	300	1075	3,413	6,000	10,875	22,500	84,000
	YAW	68	125	525	1,381	2,500	4,800	9,375	34,500

Price and delivery of these or special balances may be obtained upon request:
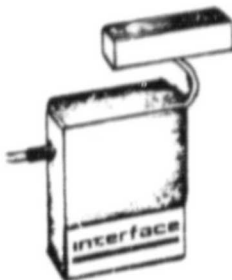
CONTACT APPLICATIONS ENGINEERING
TRANSDUCER PRODUCTS

ABLE CORPORATION
1061 N. Shepard St., Unit K
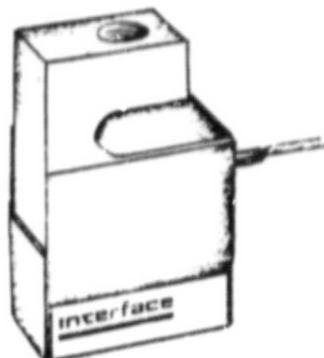Anaheim, CA 92806
Telephone: 714-630-5966

interface
ADVANCED FORCE MEASUREMENT

SUPER-MINI LOAD CELLS

Model SM-25

Designed for Precision Electronic Force Measurement

Model SM-1000

FEATURES

- Ultra Precision
- Excellent Linearity
- High Repeatability
- Thermally Compensated
- Low Moment Sensitivity
- Low Cost
- Easily Installed
- NBS Handbook 44 Sealable

RATED CAPACITIES: 10, 25, 50, 100, 250, 500 and 1000 pounds
(44N, 111N, 222N, 445N, 1112N, 2224N, 4448N)

These ultra precision strain gage load cells are designed expressly for all controlled environment, tension and compression force and weight measuring requirements. Interface's application of proprietary advanced materials technology, in strain gage and flexure design, produces load cells with the highest accuracy in the industry yet priced competitively with lower performance units.

These rugged cells have no moving parts to wear out or get out of adjustment. The specifications listed below illustrate the superior performance of Interface SM Series load cells and are a major factor in their worldwide acceptance in applications such as structural force testing, thrust measurement, steelyard rod conversions (to H-44, PTB and SIM requirements), conveyor scales, check weighers, counting and white scales, tensile testing and engine dynometers.

The Interface optional MR (Moisture Resistant) Super-Mini is now available as a cost effective method of protecting 25 thru 250 lb load cells against the effects of exposure to high humidity (up to 95% RH) and periodic condensation.

For metric applications see Metric Super-Mini Series offering 200N, 500N, 1000N, 2000N and 5000N capacities and metric mounting threads.

SPECIFICATIONS*

Non-Linearity—% Rated Output	±0.03
Hysteresis—% Rated Output	±0.02
Non-Repeatability—% Rated Output	±0.01
Temperature Range, Compensated—°F (−18 to 66°C)	0 to 150
Temperature Range, Operating—°F (−54 to 93°C)	−65 to 200
Temperature Effect on Rated Output—% of Reading/100°F (% of Reading/55.6°C)	±0.08
Temperature Effect on Zero—%Rated Output/100°F (% Rated Output/55.6°C)	±0.08
Temperature Effect on Zero—%Rated Output/100°F (% Rated Output/55.6°C)	±0.12
For Moisture Resistant Models	
**Creep, After 20 Min.—% Rated Output	±0.03
Overload Ratings—% Rated Capacity	
Safe	±150
Ultimate	±500
Nominal Output—mV/V	3
Zero Balance—% Rated Output	±1
Input Resistance—Ohms	350±3.5
Output Resistance—Ohms	350±3.5
Excitation Voltage	
Recommended—VDC	10
Insulation Resistance, Bridge to Case—Megohms	5000

*Per SMA "Load Cell Terminology and Definitions
**Creep specification is determined at rated capacity. Creep performance at reduced loads is proportional to the applied load.
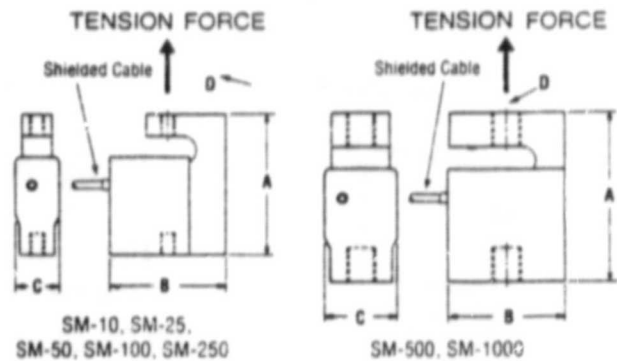
SUPER-MINI LOAD CELLS

INSTALLATION DIMENSIONS

Model		A	B	C	D
SM 10, 25, 50 100, 250	inch	2½	2	¾	¼-28 UNF-2B
	mm	64	51	19	¼ Deep, top & bottom
SM 500, 1000	inch	3	2	1¼	½-20 UNF-2B
	mm	76	51	32	½ Deep, top & bottom

TENSION FORCE

Shielded Cable

SM-10, SM-25, SM-50, SM-100, SM-250

TENSION FORCE

Shielded Cable

SM-500, SM-1000

ELECTRICAL INFORMATION

SM Series is provided with a 4-conductor shielded cable (AWG 28) 5 feet (1.5m) long.

Wiring color code complies with ISA S37.8-1975 "Specifications and Tests for Strain Gage Force Transducers."

RED	EXC
WHT	OUT
BLK	EXC
GRN	-OUT
SHIELD	

TENSION UPSCALE
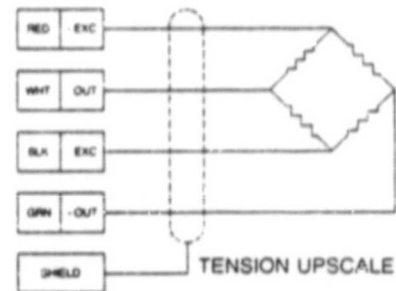
APPLICATION NOTES

1. Super-Mini load cells are designed for controlled environmental applications. In general, they can be used anywhere a readout instrument is used.
2. One diameter thread engagement is desirable—approximately ¼" (6mm) on the 10 through 250 pound ranges and ½" (12mm) on the 500 and 1000 pound units.
3. Moisture Resistant Super-Mini load cells are marked -40. These units are resistant to high humidity conditions up to and including 95% Relative Humidity and periodic exposure to condensation. The design capability is not intended for submerged operation.

4. Jam nuts may be used, however care should be exercised to not apply excessive torque across the load cell. Torque should be reacted against the load cell structure immediately adjacent to the jam nut.

Model	Jam nut torque/inch-pounds
SM-10	5
SM-25	10
SM-50	20
SM-100, 250	40
SM-500, 1000	200

TERMS AND CONDITIONS

1. *Ordering Information:* Super-Minis are ordered by specifying Series (SM) and capacity (10, 25, 50, 100, 250, 500, 1000 pounds). *Example:* SM-100.
2. *Pricing:* Consult your local Interface Representative or the factory for price and delivery.
3. *Terms:* Net 30 days in U.S. dollars, FOB Scottsdale, Arizona U.S.A.
4. *Warranty:* Interface, Inc.'s standard two-year warranty is applicable to the Super-Mini Series load cell. Interface, Inc. certifies that its calibration measurements are traceable to the U.S. National Bureau of Standards (NBS).

Prices and specifications subject to change without notice.

INTERFACE

ADVANCED FORCE MEASUREMENT

INTERFACE, INC. 7401 E. BUTHERUS DR. SCOTTSDALE, ARIZONA 85260 USA (602) 948-5555 TELEX: 668-394

15-238-181 2.5K
Printed in U.S.A.
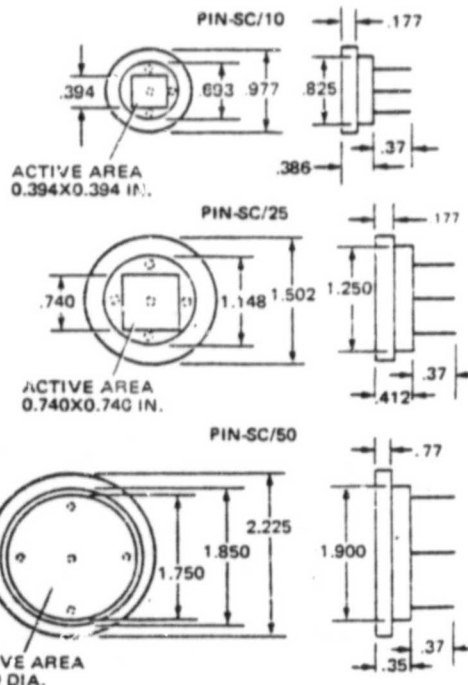
ELECTRICAL CHARACTERISTICS

PARAMETER AND (UNITS)	PIN-SC/10			PIN-SC/25			PIN-SC/50		
	MIN	TYP	MAX	MIN	TYP	MAX	MIN	TYP	MAX
Recommended Mode of Operation	Photoconductive			Photoconductive			Photoconductive		
Spectral Range @ 5% of Peak (nm)	350–1100			350–1100			350–1100		
Responsivity at Peak λ (amps/watt) @ 10V Bias	—	0.35	—	—	0.35	—	—	0.35	—
Uniformity of Response	—	±5%	±15%	—	±5%	±15%	—	±5%	±15%
Position Sensitivity @ Peak λ (amps/watt/cm)	—	0.4	—	—	0.24	—	—	0.14	—
Position ⎫ Central 25%	—	0.5%	3.0%	—	0.5%	3.0%	—	0.5%	3.0%
Linearity* ⎭ Central 75%	—	4.0%	10.0%	—	3.0%	5.0%	—	3.0%	5.0%
Null Point Drift (μm/°C)	—	2	10	—	2	10	—	2	10
NEP @ Peak λ @ 1 kHz (watts/Hz$^{1/2}$)	—	10^{-11}	—	—	10^{-11}	—	—	10^{-10}	—
Dark Current (μa) @ 10V Bias	—	0.5	2.0	—	0.7	7.5	—	3.0	10.0
Breakdown Voltage @ 30 μa (volts)	100	250	—	100	250	—	100	250	—
Source Resistance	N/A Recommended Only for Photoconductive Operation								
Series Resistance (kΩ)	—	5	—	—	5	—	—	5	—
Capacitance (pF) @ 10V Bias	—	490	730	—	1420	2120	—	4800	7300
Rise Time 10%–90% (μs) @ 10V Bias	—	2	—	—	5	—	—	15	—
Fall Time 90%–10% (μs) @ 10V Bias	—	2	—	—	5	—	—	15	—
Recommended Maximum Frequency (kHz) @ 10V Bias	—	10	—	—	2	—	—	1	—
Output Current for 10% Nonlinearity (μa) @ 10V Bias	100	1000	—	100	1000	—	100	1000	—
Approximate Saturation Level (mw/cm²)	—	10	—	—	10	—	—	10	—

*Defined as max. deviation from best straight line over the specified range expressed as a percentage of that range (for a normalized system).
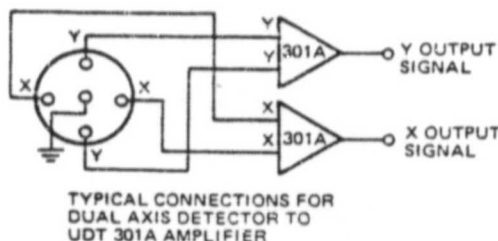
MECHANICAL SPECIFICATIONS

SPECIFICATION	PIN-SC/10	PIN-SC/25	PIN-SC/50
Active Area Total Area (cm²)	1.0	3.5	12.6
Dimensions (in.)	0.394x0.394	0.740x0.740	1.750 Dia.
Package Type	Machined	Machined	Machined
Window	Glass	Glass	Glass
Field of View Full Angle	160°	155°	162°
Temperature Range Operating (°C)	0 to +75	0 to +75	0 to +75
Storage (°C)	–25 to +75	–25 to +75	–25 to +75
Dimension to Active Area (in.)	0.125	0.62	0.05

OUTLINE DIMENSIONS

PIN-SC/10
ACTIVE AREA
0.394X0.394 IN.

PIN-SC/25
ACTIVE AREA
0.740X0.740 IN.

PIN-SC/50
ACTIVE AREA
1.750 DIA.

SCHEMATIC DIAGRAM

Y OUTPUT SIGNAL
X OUTPUT SIGNAL

TYPICAL CONNECTIONS FOR
DUAL AXIS DETECTOR TO
UDT 301A AMPLIFIER

SPECIFICATIONS SUBJECT TO CHANGE WITHOUT NOTICE

D-020-0777

UNITED DETECTOR TECHNOLOGY

The UDT "SC" series detectors are dual axis position sensors that provide X and Y axis position information of a light spot on the detector surface. These devices sense the centroid of the light spot and provide continuous analog output as the light spot moves from null point to the limit of the active area.

These unique devices are unmatched in position sensitivity, resolution and position accuracy. The PIN-SC/10, PIN-SC/25, and PIN-SC/50 are Schottky barrier type PIN photodiodes to provide maximum in performance and reliability with the lowest noise values for large area devices.
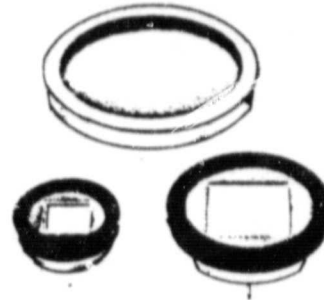
FEATURES:
Position sensitivity to 0.0001 inch
Simultaneous power level and position signal
Position accuracy independent of light spot size
Uncomplicated connection
Electrically variable null point
Adaptable for special applications
Spectral response optimized from 350 to 1150 nm
Position sensitivity for power levels from
  0.5 $\mu w/cm^2$ to 10 mw/cm^2.

APPLICATIONS:
Optical tooling systems
Remote optical alignment
Vibration monitors
Antenna alignment
Structural stress monitors
Medical instrumentation
Machine tool alignment and control

SPECTRAL RESPONSE

SPECTRAL RESPONSE VS TEMPERATURE

CAPACITANCE (pf) VS BIAS VOLTAGE

DARK CURRENT (µA) VS TEMP @ 10 V BIAS